RADIO FREQUENCY IDENTIFICATION FOR THE MEASUREMENT OF OVERHEAD POWER TRANSMISSION LINE CONDUCTOR SAG

BY

TLOTLOLLO SIDWELL HLALELE

SUBMITTED IN ACCORDANCE WITH THE REQUIREMENTS FOR THE DEGREE OF

(MASTER OF TECHNOLOGY)

IN

ELECTRICAL ENGINEERING

AT THE

UNIVERSITY OF SOUTH AFRICA

SUPERVISOR: PROF S DU

17 July 2015

DECLARATION OF OWN WORK

I (……) declare that the dissertation entitled, “Employ radio frequency identification to the measurement of overhead power transmission line conductor sag” is my own work and that all the sources that I have used or quoted have been indicated and acknowledged by means of complete reference.

Signature of student:…… Date:…….

Student number:……

Signature of Supervisor:…… Date:…….

ACKNOWLEDGEMENTS

I would like to express my gratitude to my supervisor Prof. Shengzhi Du for his support, inspiration and encouragement throughout the entire work.

List of Acronyms

AM -amplitude modulation

FM- frequency modulation

JDBC- Java database connector

RFID- radio frequency identification

OHTL -overhead transmission line

GPS- global position system

MRS -Magneto resistive sensors

PLC- power line carrier method

CT- current transformer

VT- voltage transformer

UHF- ultra-high frequency

EMI- electromagnetic interference

NAVSTAR Navigation satellite Timing and ranging

NERSA National Energy regulator South Africa

RMS – Root mean square

PU – Per Unit value

SNR- Signal noise ratio

NF noise figure

RF radio frequency

A cross section area

$A_{pk\text{-}pk}$ peak-to-peak galloping amplitude

CD aerodynamic drag coefficient

CL aerodynamic lift coefficient

Δ- Deflection

γ- Curve fitting factor defined

DGPS Differential Geographical positioning system

ACSR Aluminum conductor steel reinforced

ACSS Aluminum conductor steel supported

SDC Self damping conductor

VR Vibration resistance

AAC All Aluminum conductors

List of Key words

Conductor sag detection

Power quality

Power reliability

Radio frequency identification

RFID radar system

ABSTRACT

This dissertation deals with the challenge of power utility in South Africa which is on proactive detection of fallen power line conductors and real time sagging measurement together with slipping of such conductors. Various methods which are currently used for sag detection were characterized and evaluated to the aim of the research. A mathematical reconstruction done to estimate the lowest point of the conductor in a span is presented. Practical simulations and application of radio frequency identification (RFID) for sag detection is attempted through matlab software. RFID radar system is then analyzed in different modes and found to give precision measurement for sag in real time as opposed to global positioning system (GPS) if one dimension of the tag assumed fixed on the power line. Lastly errors detected on the measurements are corrected using a trainable artificial neural network. A conclusion is made by making recommendations in the advancement of the research.

PROBLEM STATEMENT

In South Africa, electric utilities such as Eskom are under pressure to make optimum use of their existing facilities, of which the high voltage power transmission line is the back bone. The current flowing in the conductors together with the resistance causes losses and local heating, leading to the linear expansion of the conductors. These result to the conductor sagging. Furthermore, proactive detection of fallen power lines and real time sagging measurement is very critical in power transmission. Additional current due to a failure of a parallel route causes more losses and hence more sagging. When too much sagging occurs there is a potential for a dangerous situation to develop or a total failure if they touch the ground. A power utility need to accurately measure both

electric current and line positions in real time, in order to enable the dynamic rating of the power networks.

Factors such as mechanical stress, solar radiation, wind speed, conductor geometry, ice force and ambient temperature causes a problem of torsional motion and the vertical cable deflection, hence more sagging.

HYPOTHESIS

Radio Frequency Identification system (RFID) technology has a potential of giving an accurate conductor sag measurement in real time. With narrow bandwidth which allow it not to interfere with other communication systems at about 915MHz frequency, the angle of arrival measurement can virtually be used in conjunction with range to give a 3D positioning system from predesigned measuring locations to determine conductor sag. Considering a single span of a section for simulations purposes, passive tag attached to a power line can be detected without external power supplied to it. This makes RFID sag detection system cost effective and more accurate.

DERMACATION OF THE FIELD OF STUDY

The study reviewed other techniques which are currently used by Eskom and other power companies for Power line detection. It examined the theory of RFID and its practical application in real time monitoring of conductor sag. Although there is a lot of improvement in RFID, there is still much more work and research to be done considering the high voltage corona discharge.

TABLE OF CONTENTS

CHAPTER 1 INTRODUCTION

CHAPTER 2 LITERATURE REVIEW

CHAPTER 3 THE SYSTEM STRUCTURE DESIGN

CHAPTER 4 ANALYSIS AND RESULTS

CHAPTER 5 CONCLUSION AND DISCUSSION

CHAPTER 1 INTRODUCTION

1.1 A detailed problem statement

Long distance high voltage power lines are very important in electricity power delivery because power stations are normally built far away from power loads. During the transmission process, balance must be constantly maintained to match the power supply and demand. Due to the ongoing electricity needs, existing electrical transmission line performance is also a major concern and a very critical factor. Electric current and line positions are two important parameters to measure transmission lines performance. The electric current flowing in the lines should be measured to avoid overload, phase unbalance and fluctuation. Line positions should be monitored to keep track of the sagging and galloping situations. In this chapter sagging, galloping, power quality and radio frequency identification technology are discussed.

1.1.1 Context of the Problem

1.1.1.1 Conductor sag and voltage sag

Figure 1.1: Illustrate conductor sag and voltage sag phenomenon.

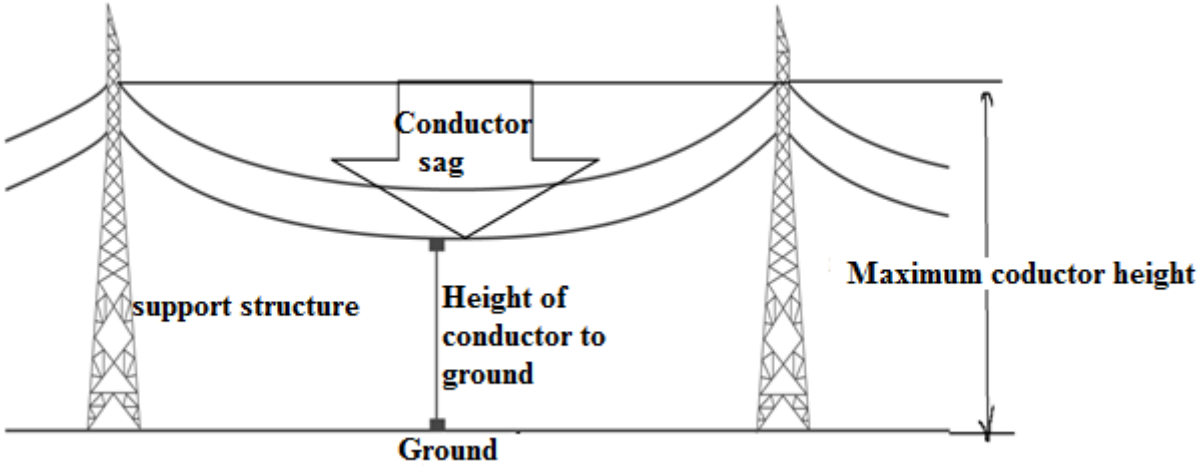

(a) Conductor sag

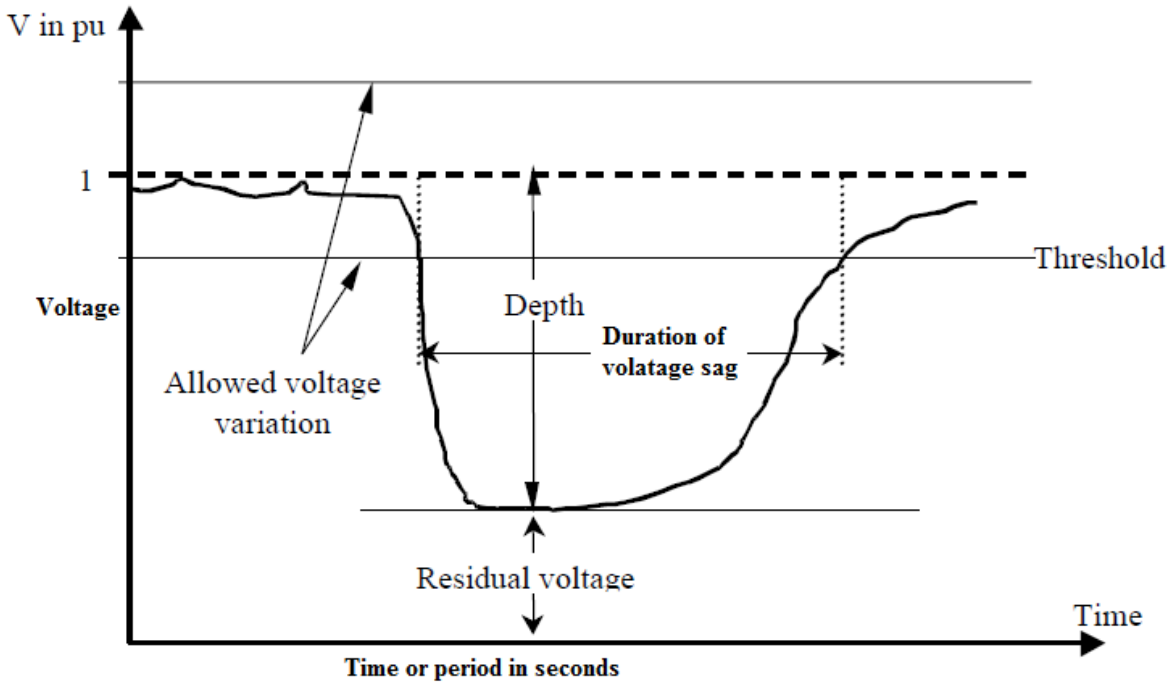

(b) Voltage sag

Figure 1.1 Conductor sag and voltage sag

Conductor sag is the vertical distance between the point at a maximum height where the conductor is joined to the tower and the lowest point of the conductor to the ground. It determines electrical clearances, right of way width, uplift weights, stress and strain, thermal rating. Tension in a form of force, determines structure angle and dead-end wire load. Tension limits determine conductor's system safety factor when calculations are done for design, vibration, and structure cost. Conductors between two transmission towers often suffer sagging phenomenon. It was reported that sagging of a conductor in Figure 1.1 (a) can cause a nonlinear power flow in the power system, which may result in to a sudden reduction in voltage known as voltage sag or voltage dig (IEEE Standard 1159-1995).

According to IEEE Standard 1159-1995 Recommended Practice for Monitoring Electric Power Quality, voltage sag is a decrease in root mean square (RMS) voltage at the power frequency for durations from 0.5cycles to 1 minute, reported as the remaining voltage. Conductor sagging can lower the conductor to an unsafe height above the earth. It can be caused by oscillations which can result into serious transmission problems, such as flashover due to infringed line-to-line clearance, risk of mechanical failure of transmission tower, and excessive loading stress. Efforts have been made to understand this phenomenon better and develop means of protecting the transmission line against this problem, but there is still a challenge of detecting the sag in real time. The low frequency, high amplitude induces vibration on this transmission line conductors as a result, causes serious galloping which result to more sagging.

When the weather is considered, it is valid to interpret galloping as an oscillation of either a single or bundled conductor due to wind force or wind-induced vibration on an iced or wet snow accretion on the conductors. It is also caused by steady crosswind acting upon asymmetrically iced conductor surface. Large amplitude is normally observed on a vertical position depending on the line construction and the oscillation mode excited.

The cost associated with galloping can be due to damaged components which require inspection and repair. It damages the conductor strands which result to a conductor's increase in stress level to a point of breakage and dynamic overload. In the event of this situation, patrolling need to be performed to detect any damage. This requires a helicopter or some sort of physical view, which increase costs and results unplanned maintenance.

The problem of sagging has the impact on system reliability and power quality of service. There may be a losing of customers who are very sensitive to power quality. There can also be a swinging of the suspension points longitudinally to the power line which is likely caused by the variation in

tension; that could accompany galloping and act to couple the galloping motions in adjacent spans, resulting to a more dangerous sagging phenomenon.

By constantly tracking the conductor motion, with the distance from this lowest point to the ground, sag could be proactively measured or determined.

1.1.2 Research gap (power quality concept)

In modern electrical power systems, electricity is produced at generating stations, transmitted through a high voltage network, and finally distributed to consumers. Due to the rapid increase in power demand, electrical power systems have been developed extensively during the 21st century, resulting in today's power industry probably being the largest and most complex industry in the world. Electricity is one of the key elements of any economy, industrialized society or country. A modern power system should provide reliable and uninterrupted services to its customers at a rated voltage and frequency within constrained variation limits. If the supply quality suffers a reduction and is outside those constrained limits, sensitive equipment might trip, and any motors connected on the system might stall. The electrical system should not only be able to provide cheap, safe and secure energy to the consumer, but also to compensate for the continually changing load demand. During that process the quality of power could be distorted by faults on the system, or by the switching of heavy loads within the customer facilities.

Reliability and power quality are terms believed to interpret the power system stability. Several research groups work on these subjects around the world. Reliability should be interpreted as the continuity of the electrical supply. This term is well comprehended; however there is no unanimity about the meaning of the term power quality. According to the Standard IEEE 1100(Std 11, 1999) power quality is the concept of powering and grounding electronic equipment in a manner suitable

to the operation of that equipment and compatible with the remise wiring and other connected equipment. This definition considers electronic equipment only. In this research we find that not only electronic equipment is subject to power failure and the power quality should be explained considering critical infrastructure such as transmission line; such that it is the performance of a transmission line towards the load supplied and the response of the load towards the transmission line. Therefore conductor sag has to be monitored and detected in real-time, to enable the power utilities do dynamic rating of the power networks, monitor the condition of the line.

1.2 Research objective and questions

1.2.1 The objectives of this study

Analyze the feasibility of Radio Frequency Identification (RFID) technique to perform high voltage conductor sag measurement. Unlike other techniques found in the literature, this new method does not need any external energy supply and considers a measurement of signal from the tags attached on the transmission line to the ground position in 3D.

1.2.2 Research questions

i. How to use RFID technology to improve the real-time transmission line monitoring process?
ii. How to estimate the 3D position of tags attached to transmission lines from locations of ground?
iii. How to estimate the lowest point of the sag given the position of tag detected?

1.3 Approach

We use a systematic research method to view the problem, theoretical analysis and simulations are used to formulate the solution. Comparison with GPS method is used to show the advantage of the proposed method.

1.4 Research goal

The goal is to implement RFID real-time conductor sag detection for effective monitoring of power utility. This method will determine the conductor sag proactively in real-time and enable the power utilities to dynamically rate the power networks.

1.4.1 Research contribution

Design and implementation of a practical system of RFID real time conductor sag detection and monitoring. Our research output adds value into the new designs of transmission and distribution network dynamic rating, by relating RFID-SAG to a transmission line rating at initial design stage.

1. 5 Study overview

By viewing factors affecting the power system performance, the conductor sagging phenomenon is considered to be an important factor of the performance of a power system transmission line. The study reveals the importance of sag detection and introduces the RFID-SAG monitoring system. This system consists of a reader, antennas, passive and active tags. By formulating this system the dissertation helps on better understanding of a real world RFID system commonly used. In our method, we adapt the RFID radar system for long range precise measurement for sag detection of power transmission lines. Because passive tags have long life span they are used in the monitoring system. The radar system has several requirements for efficient operation. These include a controllable read zone for a reader and a tag. For every tag within the reader zone, a

reader has 100% read-rate and 0% read-rate outside the reader zone. Particular attention is paid to insensitive performance of the system to the following factors:

i. Physical orientation of a tag,

ii. The nature of the object on which the tag is placed,

iii. The environment in which the system is deployed,

iv. Communication of multiple tags with the reader in a collision-free manner and the time for reading a fixed number of tags.

Having these characteristics, the practical application of RFID real-time sag detection problem is illustrated in the Figure 1.2.

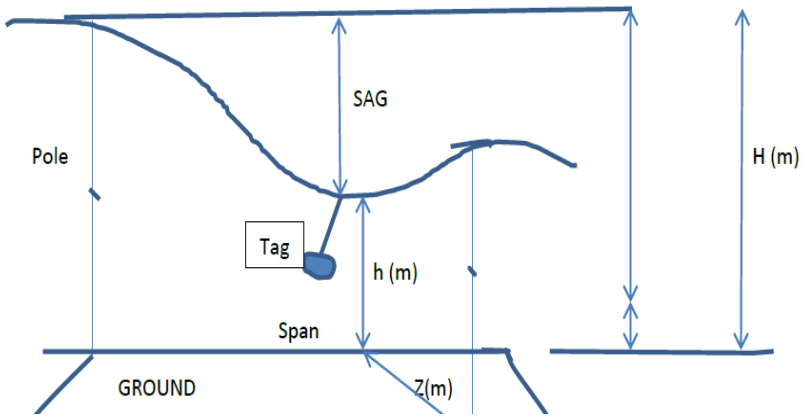

Figure 1.2: A tagged sagging conductor using passive tag

It must be noted that the system structure and the tags used in this research does not have ISO standard.

1.6 Dissertation outline

Chapter 1: Introduction

This dissertation is organized and documented in five chapters. Chapter one introduces the general background of the work and the rest of the dissertation is as follows:

Chapter 2: Literature Review

In this chapter, the general findings related to the topic and theories are summarized. The arguments are made and therefore the gap to initiate the research on RFID is illustrated. Different methods that are currently used by power utilities including power line carrier method which is used by Eskom, state owned company (SOC) limited, South Africa to detect power line sag are discussed. The literature is characterized and evaluated to find the real phenomenon behind the sag and identify the impact on power system reliability and power quality. The syntheses of new technologies which are at simulation stage in particular such as Global Positioning System (GPS) are also viewed and drawbacks are given. Advantages of RFID sag detection method over the current methods are addressed.

Chapter 3: System structure

The main aim of this chapter is to present the state of power transmission line sag detection and how RFID contribute in real-time measurement of the sag (conductor vertical position). RFID-Radar system is presented as an effective technology for power line sag detection in real-time. The performance of passive ultra-high frequency (UHF) RFID system in practice is given and the strength of radar system for long range measurement is analyzed. Our radar system is evaluated under different weather conditions, with its read rate, electromagnetic interference and corona effect on the tag performance.

Chapter 4: Analysis and Results

The data obtained from the radar system is presented in this chapter. The result of sag detection is analyzed to show the performance of the proposed monitoring system.

Chapter 5: Conclusion and Discussion

The findings are discussed and conclusion is made in this chapter. The tag sensitivity on metal conductor object is better off seen from 8mm than that of a free space. Tag reflection from the surface of a wooden object is not bigger in such that it requires greater power for tag that is close to the surface. The graphical representation of result shows that active tags which are battery assisted have shown to give more precision and better range than passive tags.

CHAPTER 2 LITERATURE REVIEW

2.1 Introduction of this chapter

In this chapter the phenomenon of sagging and galloping is discussed in details and explanations are given based on previous theories and practical historical events. Power quality problem due to conductor sag is also detailed. Current methods used to measure conductor sag are presented and the radio frequency identification theory and its advantages in transmission line sag detection are addressed.

2.2 Transmission line sagging

Overhead transmission lines for transport of high-voltage electricity are cables made of aluminum alloy, suspended between high towers in the countryside. One cable of several kilometers between two anchoring towers and carried by several towers in a row is called a section. The part of a section that is suspended between two towers is called a span. As the cable is connected to the

towers by a freely movable suspension string or isolator, the dynamical motion of neighboring spans are coupled. In wintertime when the cable is covered by snow or ice, the cables are vulnerable to large scale vertical vibration in combination with a torsional vibration sustained by steady cross winds. This aero-elastic instability is known as galloping. For high enough amplitudes neighboring conductors may get close enough for the air-insulation to break down, causing a short-circuit and structural damage to the cables. It is known from observations that even a small wind force is sufficient to maintain a galloping vibration (Rienstra S.W., 1988 pp. 133-134).

The transmission line might have length extension of a line conductor caused by many factors such as overheating due to excessive current loading, wind vibration; ice force and etcetera. The length extension results in the increase of sagging.

2.2.1 Power quality disturbances

It is important to define the performance of a power system and discuss the power quality incidences on utility system for customer satisfaction and economic impact.

As discussed in the first chapter, conductor sag might result into voltage sag and possibly a power disturbance. This can also be seen as an interruption which is defined as a 0.9pu reduction in voltage magnitude for a period less than one minute. An interruption is characterized by the duration as the magnitude while transient is an increase of RMS voltage for longer than one minute. Typically the voltage magnitude is 1 to 1.2V per -unit which is caused by switching off the large load from the system, energizing a capacitor bank, poor tap settings on the transformer or inadequate voltage regulation (Amin, S.M and Wollenberg, B.F., 2002). Overvoltage's can be caused by equipment damage and failure. Harmonic issues are caused by the increasing power electronic devices like variable speed drives and inverters, which increases the harmonic distortion

in the power system. The presence of harmonics in the system could also cause several unwanted effects in the system including excessive transformer heating or overloading and failure of power factor correcting capacitors, therefore it is related to transmission line sagging. The maximum total harmonic distortion which is acceptable on the utility system is 5% at 2.3 to 69kV, 2.5% at 69 to 138kV and 1.5% at higher than 138kV voltage levels (IEEE Std. 1250, 1995).

Voltage imbalance is normally caused by unequal distribution of loads amongst the three phases. At three phase distribution level, unsymmetrical loads at industrial units and un-transposed lines can result in voltage imbalance. Voltage imbalance is of extreme importance for three phase equipment such as transformers, motors and rectifiers, for which it results in overheating due to a high negative sequence current flowing into the equipment. The asymmetry can also have an adverse effect on the performance of converters, as it results in the production of harmonics.

2.2.2 Determination of sag

The energized conductors of transmission and distribution lines must be constructed in such a way that the possibility of their potential to touch ground is regularly tracked. Overhead conductors, however elongate with time, temperature and tension, thereby changing their original positions after installation. Despite the effects of weather and loading on a line, the conductors must remain at safe distances from buildings, objects, and people or vehicles passing beneath the line at all times. To ensure this safety, the shape of the terrain along the right of way, the height and lateral position of the conductor support point, and the position of the conductor between support points under all wind, ice, and temperature conditions must be known (Douglass D.A and Trash R., 2013 pp14-2). The shape of the catenary changes with conductor temperature, ice and wind loading, and time. To ensure adequate vertical and horizontal clearance under all weather and electrical loadings, and to ensure that the breaking strength of the conductor is not exceed, the behavior of

the conductor catenary towards the consumer, under all conditions must be known before the line is designed. The future behavior of the conductor towards the external forces is determined through calculations commonly referred to as sag-tension calculations.

Sag tension calculations predict the behavior of conductor based on recommended tension limits under varying loading conditions. These tension limits specify certain percentages of the conductors rated breaking strength that is not to be exceeded upon installation or during the life of the line. These conditions, along with the elastic and permanent elongation properties of the conductor, provide the basis for determining the amount of resulting sag during installation and long-term operation of the line. Accurately determined initial sag limits are essential in the line design process, to enable dynamic rating of the networks. According to (SANS10280/NRS 041-1:2008), conductors current ratings can be determined by either assuming the worst case cooling conditions using deterministic method or by assessing the risk of an unsafe condition arising that is probabilistic method. For deterministic ratings the weather assumptions is in accordance with guide of weather parameter selection for overhead conductor rating given by (Cigre, brochure 299). These include the following:

Table 1: Weather parameter selection

Weather assumption	**Parameter value**
Wind speed perpendicular to line	$0.6m/s$
Absorptivity and emissivity	0.8
Solar radiation	$1000w/m^2$
Ambient temperature	40℃

Although this parameters are followed from the initial design stage of transmission networks, extreme weather conditions have been experience dramatically recently in South Africa and the

factors are unknown. This could escalate the sag and eventually the poor power system performance and instability.

Final sags and tensions depend on initial installed sags and tensions and on proper handling during installation. The final sag shape of conductors is used to select support point heights and span lengths so that the minimum clearances will be maintained over the life of the line. If the conductor is damaged or the initial sags are incorrect, the line clearance may be violated or the conductor may break during heavy ice or wind loading (Douglass D.A. and Trash R., 2013 pp14-2).

2.2.3 Level Spans

The shape of a catenary is a function of the conductor weight per unit length, w, the horizontal component of tension, H, span length, S, and the maximum sag of the conductor D. Conductor sag and span length are illustrated in Figure 2.1 for a level span. The exact catenary equation uses hyperbolic functions. Relative to the low point of the catenary curve shown in Figure 2.1, the height of the conductor, $y(x)$, above this low point is given by the following equation (Ramon R., 1987 pp. 851-856):

$$y(x) = \frac{H}{w}\cosh\left(\left(\frac{w}{H}x\right) - 1\right) = \frac{w(x^2)}{2H} \tag{2.1}$$

For a level span, the low point is in the center, and the sag, D, is found by

$$D = \frac{H}{w}\left(\cosh\left(\frac{ws}{2H}\right) - 1\right) = \frac{w(S^2)}{8H} \tag{2.2}$$

At the end of the level span, the conductor tension, T, is equal to the horizontal component plus the conductor weight per unit length, w, multiplied by the sag, D as shown in the equation below:

$$T = H + wD \tag{2.3}$$

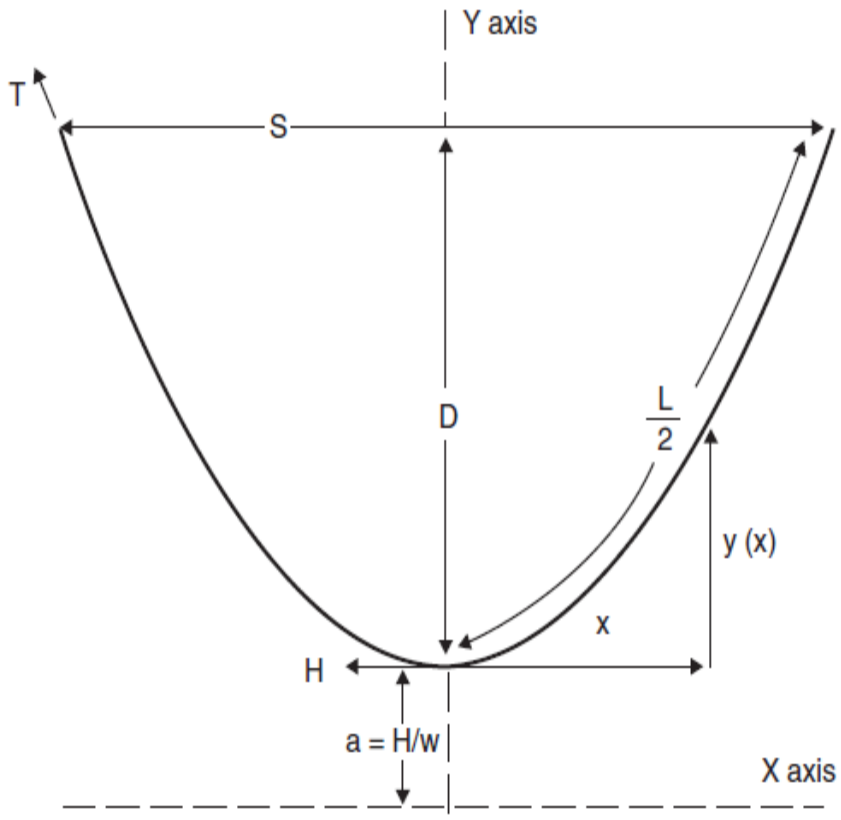

Figure. 2.1 The catenary curve for level spans (Rienstra S.W., 1988 pp. 133-134)

2.2.4 Conductor length

Conductor length from the low point of the catenary from either direction of the sag can be obtained as follows:

$$L(x) = \left(\frac{H}{w} SINH(\frac{Sw}{2H})\right) = S\left(1 + \frac{x^2(w)^2}{6H^2}\right) \quad (2.4)$$

For a level span, the conductor length corresponding to $x = \frac{S}{2}$ be the half of the total conductor length and the total length L, is:

$$L = \left(\frac{2H}{w}\right) SINH\left(\frac{Sw}{2H}\right) = S\left(1 + \frac{x^2(w^2)}{24H^2}\right) \quad (2.5)$$

The parabolic equation for conductor length can also be expressed as a function of sag, D, by substitution of the sag parabolic equation, giving:

$$L = S + \frac{8D^2}{3S} \quad (2.6)$$

A conductor should have a slack to avoid high stress level. This Slack is the difference between the conductor length, L, and the span length S. The parabolic equations for slack may be found by combining the preceding parabolic equations for conductor length L, and sag D (Rienstra S.W., 1988 pp. 133-134).

$$L - S = S^3\left(\frac{w^2}{24H^2}\right) = D^2\left(\frac{8}{3S}\right) \quad (2.7)$$

The slack of the conductor in a span can contribute to the changes in conductor sag.

Such that sag $D\ is$:

$$D = \sqrt{\frac{3S(L-S)}{8}} \quad (2.8)$$

For inclined spans: they may be analyzed using essentially the same equations that are used for level spans. The catenary equation for the conductor height above the low point in the span is the same. However the span is considered to be consisting of two separate sections, on to the right of the low point and the other to the left of the low point. The shape of the catenary relative to the low point is unaffected by the difference in suspension point of elevation. In each direction from the low point, the conductor elevation, relative to the low point is given by:

$$y(x) = \frac{H}{w} cosh\left(\left(\frac{w}{H}x\right) - 1\right) = \frac{wx^2}{2H} \tag{2.9}$$

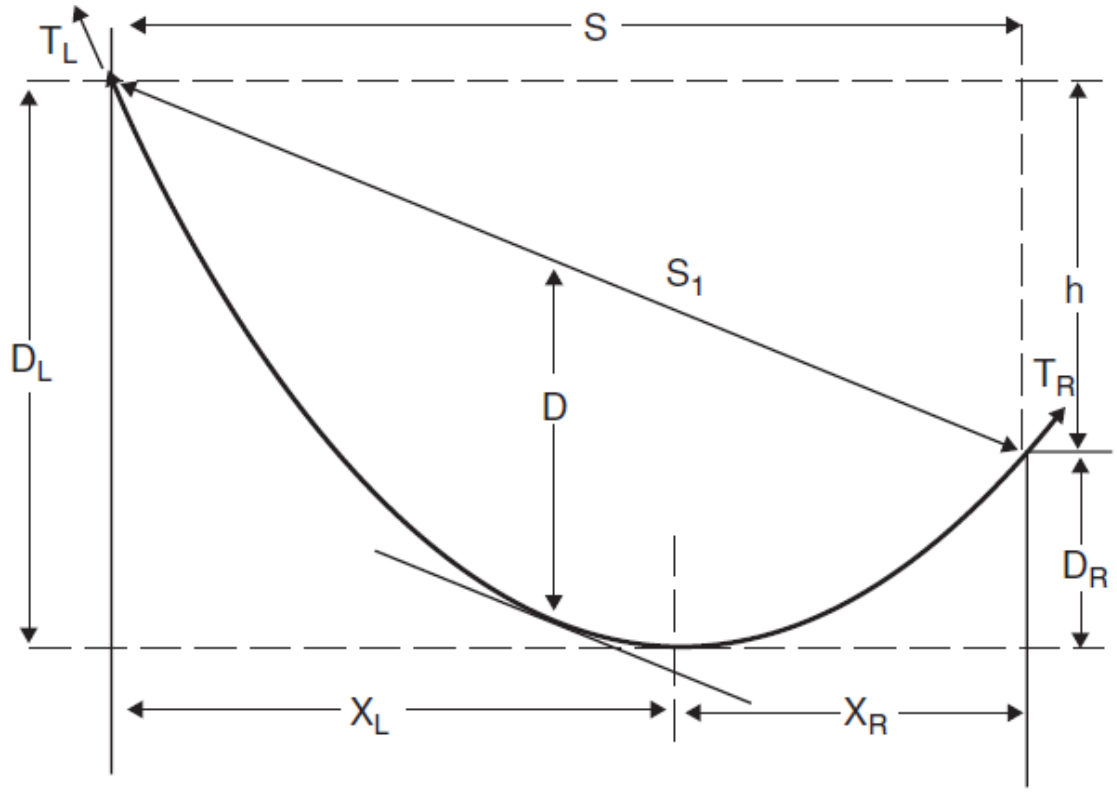

Figure 2.2: shows the inclined catenary (Rienstra S.W., 1988 pp. 133-134)

The horizontal distance XL from the left support point to the low point in the catenary is

$$XL = \frac{S}{2}\left(1 + \frac{h}{4D}\right) \tag{2.10}$$

The horizontal distance, XR from the right support point to the low point of the catenary is:

$$Xr = \frac{S}{2}\left(1 - \frac{h}{4D}\right) \tag{2.11}$$

From the inclined catenary span $S1$ is the straight-line distance between support points, S, horizontal distance between supports, h, vertical distance between support points, D, the sag measured vertically from a line through the points of conductor support to a line tangent to the conductor.

The midpoint sag D is approximately equal to the sag in a horizontal span equal to the length to the inclined span, knowing the horizontal distance from the low point to the support in each direction, the preceding equations for $y(x), L, D\ and\ T$ can be applied to each side of the inclined span, S1. Knowing the horizontal distance from the low point to the support point in each direction, the preceding equations for $y(x), L, D, and\ T$ can be applied to each side of the inclined span. The total length in the inclined span is equal to the sum of the lengths in XR and XL sub-span sections (Ramon G., 1987 pp. 851-856).

$$L = S + \ (X_R^3 + X_L^3)\left(\frac{w^2}{6H^2}\right) \tag{2.12}$$

In each sub-span, the sap is relative to the corresponding support point elevation

$$D_R = \ wx_R^2 * \frac{1}{2H} \tag{2.13}$$

$$D_L = \ wx_L^2 * \frac{1}{2H} \tag{2.14}$$

Where DR and DL is the sag on the right and on the left.

One of the important factors in designing the transmission network is considering the ice and wind conductor loads. During incidents of heavy ice or wind loads, the conductor catenary tension increases dramatically along with the loads on the angle and dead-end structures. Both the conductor and its supports can fail unless high-tension conditions are considered in the line design. The loads must be accounted for in the line design process so they do not have a detrimental effect on the line. Ice in the overhead conductor may take several forms such as rime ice, wet snow and glaze ice. The impact of low density ice formation is usually considered in the design of line sections at high altitudes. The formation of ice on the overhead conductors has the following influence on line design; that is the maximum vertical conductor loads that structures and foundations must withstand, in combination with simultaneous wind loads; ice loads also determine the maximum transvers loads on structures (Alexis Polycarpou, 2011).

The sag permanent increase in due time in regions of heavy ice loads may be due to ice loadings. Ice loads for use in designing lines are normally derived on the basis of past climate experience and weather conditions, national energy regulations code of practice and the historical weather data. Mean recurrence intervals for heavy ice loadings should be the function of local conditions along various routings. Hence considering the dynamic climate changes in the initial stage is vital. The current transmission networks are not guaranteed for climate changes in Africa.

2.2.5 Wind loadings on overhead lines

They influence line design in a number of ways: that is the maximum span between structures may be determined by the need for horizontal clearance to the edge of right of way during moderate winds, the maximum transverse loads for tangent and small angle suspension structures are often determined by infrequent high wind speed loadings and permanent increases in conductor sag may

be determined by wind loading in areas of light ice (Olsen R.G. and Edwards K.S., 2002 pp.1142-1152).

2.2.6 Maximum Conductor Tension

It is the tension of the conductor allowable to conductor's rated breaking strength. Transmission lines under wind or ice loading experience high level tension which result into Aeolian vibration and unsafe levels. Under everyday conditions, tension limits should be specified to control the vibration. Aeolian vibration levels, and thus appropriate unloaded tension limits, vary with the type of conductor, the terrain, span length, and the use of dampers. Special conductors such as ACSS SDC and VR bring about high self-damping properties and may be installed to the full limits. The conductor length depends on span and sag and is not directly dependent on conductor tension, weight or temperature (Dale Douglass, Paul Springer, IEEE Technical brochure, 2013).

2.2.7 Thermal Elongation

Increase in temperature causes an increase in length and sag and decreases the tension. Concentric-lay stranded conductors, particularly non-homogenous conductors such as ACSR, are not inextensible. Rather, they exhibit quite complex elastic behavior. Initial loading of conductors results in elongation behavior substantially different from that caused by loading many years later. Also high tension levels caused by heavy ice and wind loads cause a permanent increase in conductor length, affecting subsequent elongation under various conditions. ACSR and AAC conductors elongates with increasing conductor temperature (DA Douglass and Ridley Trash 2013 pp.14-2).

(Muhr *et al* 2005 pp.14) presents the results of a study of elongation mechanism of an overhead conductor, which shows that the deflection of the tension insulators affects the sag behavior of the

close-by spans. In the rod distribution of a flat overhead line symmetric, the deflection of the suspension insulators was negligible and had no significant effect on the sag calculation. The deflection of the suspension insulators is not negligible when the rod distribution is asymmetric. The span with the largest distance between the rods will sag much more than the smaller spans (Olsen R.G. and Edwards K.S., 2002). The elongation of the overhead conductor reduces this safety distance. The main point of the calculations is that the deflection of the suspension insulators affects the sag and the phase to earth clearance significant by asymmetrical rod distribution. The elongation of the overhead conductors caused by everyday stress leads to an increasing of the sag. During the planning and construction lower sag than necessary gives a safety distance to the regulation clearance. With sag verification of aged overhead lines by measurement or calculation, the reliability of the overhead line can be improved. Depending on the system voltage and the object type, the minimum phase to earth clearance can be assured (Thomas G., 2002).

The common practice is to assume that power line conductors are straight horizontal wires of infinite length. In fact, they are periodic catenaries, the sag of which depends on individual characteristics of the line and on environmental conditions. Consideration of catenaries effects in the literature is scarce, since most often they are assumed to be negligible. Whenever analysis of the power line is concentrated on phenomena in close proximity to the conductors, the straight wire approximation must be critically reviewed (Ramon G., 1987).

2.2.8 The occurrence of galloping to sag

2.2.8.1 Types of motions

(Anjo K., *et al* 1974) indicate that conductor motions can be large enough to cause flashovers between adjacent phases, especially when the phases are above each other. The vertical motion may result from a combination of two or three loop modes. The swinging of the suspension points

longitudinally to the line, referred to above, are caused by the variation in tension that can accompany galloping, and they act to couple the galloping motions in adjacent spans.

When the spans are on quasi fixed supports, such as in many lower voltage distribution lines, the motions are commonly in the two-loop mode but with very high amplitudes (several times the sag observed), in such severe cases tension changes, despite the two loops mode, can be quite high. The amplitudes are again similar to each other in the different spans, due to feed-through at the supports, which can occur because this class of line is frequently supported on wood poles with cross arms, which allow some longitudinal support point movement (Admirat P., *et al* 1988). In addition to causing flash over's between phases, galloping can lead in to agitation of sag phenomenon which could damage the structures due to twisting of the wood cross arms and poles accompanying synchronous motions of the phases.

(Chadha J., 1974b) shows that the common designs of overhead transmission lines are short line sections between dead-ends. Linear analysis of the motions calculation shows that for the modes at 0.386 and 0.403Hz, there is only small variation in tension during galloping. This is because when one span is at its upwards extreme of motion, there is another span at the downward extreme. The variations in the arc length of the two spans compensate each other by means of swinging of the suspension support between them.

2.2.8.2 Factors influencing a transmission line galloping

i. Ice accretion type and shape (eccentricity, weight, and aerodynamic properties)
ii. Sagging Conditions (effect on vertical frequencies)
iii. Wind velocity (with limited effects of turbulence and orientation as detailed)

iv. Conductor self-damping (vertical, torsion) in the low frequency range (including span end-effects)

v. Span lengths (including all spans of a section) and section length

vi. Longitudinal stiffness at attachment point on tension tower

vii. Yoke plate assembly (tension and suspension tower)

viii. Number of sub conductors and their arrangement

ix. Sub conductors spacing

x. Ration vertical frequency for each mod in the presence of wind

2.2.8.3 A view of Overhead line aerodynamics

When the shear center in the case of a conductor is viewed, the forces and moments acting at a known location need to be considered. This requires the introduction of an aerodynamic pitching moment about the new location. The evaluation of lift, drag and pitching moment is usually done in a wind tunnel on a fixed, rigid cylinder on which the ice shape has been reproduced (Gartshore I.S., 1973). The evaluation of such forces and moments on a fixed wind tunnel model rather than a moving one is still a concern.

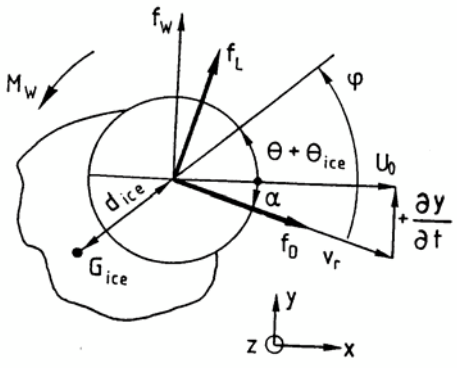

Figure 2.3: Aerodynamic characteristic of an iced conductor (Gartshore I.S., 1973)

The conductor, subject to a wind, U_0, is shown at a time, t, during vertical torsional motion. Aerodynamic forces, f_L, and f_D, and moment, M_W, act at the shear Centre.

The conductor is assumed to move vertically upwards with a positive vertical speed. The initial ice position is $\Theta_{ice\ and}$ Θ is the actual rotation of the conductor φ is the angle of attack and is positive anticlockwise. The drag force, f_D, is oriented in the direction of the relative wind speed, v_r (the combination of U_0 and the conductor's vertical speed). The lift force, f_L, is perpendicular to the drag force and positive upwards. The pitching moment is positive anticlockwise. We believe that the analysis on the forces acting upon the conductor helps in the dynamic rating of future transmission networks. It therefore important to carefully consider every cause of motion in the conductor that leads to conductor sagging dangerous situation.

Looking at the stability conditions or (reduced amplitude), the conductor self-damping, ice position and ice aerodynamic are very complex to estimate. This complicates the parameter line predictions for voltage rating or temperature, stress and young's modulus elasticity. Reference (Gurung C.B., *et al* 2002) shows that the bundle moment of inertia plays a major role in the instability criterion. The bundle conductor moment of inertia's main contributors are the sub conductor mass and bundle diameter, which is an important factor for galloping and sagging. Most of the time, the diameter of the bundle is fixed by other considerations such as corona effect and manufacturer standardization. However there are some exceptions. In theory an increased bundle moment of inertia decreases the risk of instability. However the same cannot be said concerning the amplitude, if instability criterion remains violated. An increase in sub conductor spacing increases both the moment of inertia of the bundle and its torsional stiffness. In the absence of any anti-galloping device however, these two increases unfortunately compensate each other so that the effect on torsional frequency is insignificant (Halsan K.A., *et al* 1998).

2.2.8.3.1 Conductor Self-damping

The amplitudes of galloping that actually occur are determined by energy balance between the net energy supplied through aerodynamic action, including effects of aerodynamic dampers and mechanical dissipation in the galloping system. Mechanical dissipation mainly arises from self-damping in conductors, hysteresis at span support, and damper (Harvard D.G., 1996). For transverse vibration, self-damping is small but the highest Aeolian frequencies, and negligible at galloping frequencies. Basically Elastic solid cannot dissipate more energy during a loading-unloading cycle than is stored in it at the time of maximum loading (Harvard D.G., 1997). It is common to refer to the loss coefficient of a solid, $\eta = \frac{D}{2\Pi U}$ Where D is the energy actually dissipated in a full cycle and U is the maximum stored energy of strain (Hoerner S.F., 1965). Dynamic loads resulting from galloping have been viewed as indicated by (Halsan K.A., *et al* 1998) the maximum dynamic loads are of the order of 1.2 times the static value at dead-ends and 1.7 times the static value at suspensions (Hillier R. and Cherry R.J., 1981). In areas subjected to ice loads, suspension insulators everyday loads are normally very low compared to their tensile strength; the ratio being of the order of one to nine. Consequently, the effect of galloping cyclic loads is normally of no consequence. (Harvard D.G., 1978) indicates that on distribution lines where pin type insulators are used, tie wire failures due to sagging happen occasionally. Where clamp-top insulators are used, cement failure of the porcelain insulators due to the bending moment applied on it during sagging has also been observed. Damage on insulators during the sagging phenomenon is mostly occurring in the transmission lines when insulator string is being clashed on the tower arm (Harvard D.G., 1984). However these damages are not related to a fatigue phenomenon.

There are several methods and devices which are being used to detect the sag of a transmission

line which is discussed in section 2.3.

2.3 Different Methods used to measure conductor sag

2.3.1 Current transformers (CTs)

They are typically used for current measurement. However, they are expensive and limited by their magnetic core characteristic and narrow bandwidth (Glorver B. and Bhatt H., 2003). The CTs performance under distorted conditions is usually characterized by means of the frequency response test. The method uses an excitation waveform (primary current) that consists of one harmonic current, with adjustable amplitude and phase shift, superimposed on the fundamental current. The measurement of harmonic current phasor is characterized by two basic errors (Glorver B. and Bhatt H., 2003):

The *h-order* harmonic rations error:

$$\%e_h = \frac{KI_{sh} - I_{ph}}{I_{ph}} . 100 \tag{2.15}$$

Where: $K = Ns/Np$ is the nominal transformer ratio (Ns and Np are the secondary and primary number of turns, correspondingly); Ish and Iph are the rms values of the secondary and primary number of turns respectively); Ish and Iph are the rms values of the secondary and primary h-order harmonic currents.

The *h-order* harmonic phase angle error:

$$\varepsilon_h = \alpha_{sh} - \alpha_{ph} \tag{2.16}$$

Where: α_{sh} and α_{ph} are the secondary and primary harmonic current phase angles in degrees, respectively. These indexes were used to characterize two current transformers excited by a non-sinusoidal current (Glorver B. and Bhatt H., 2003). Basically Current transformers measures the flow of current in a conductor not the position of the conductor, therefore cannot detect sag. There are some existing devices that can directly or indirectly measure sag of transmission lines.

2.3.2 Power Line Carrier Method (PLC)

It determines average overhead conductor height variations by correlating sag with measured variations in the amplitude of signals propagating between PLC stations (Mensah C., 2011). The PLC-SAG technique is fundamentally based on the theory of natural modes supported by multi-conductor transmission lines. PLC system Provide a highly reliable infrastructure for the transmission and reception of data, speech and protection signals between stations.

2.3.2.1 PLC Attenuation Sensitivity and Height Variation

Attenuation of the PLC signal is due to two major contributions: that is attenuation due to the transmission line, including the effect of ground resistivity; which is complex and requires the rigorous theoretical analysis of modal propagation on multi-conductor transmission lines and attenuation due to the coupling system, is simple to compute.

With outer-to-outer phase coupling, the signal level is sensitive to variations in line height. The PLC-SAG technique makes use of this phenomenon to remotely monitor the average height movement of the OHTL (Cataliotti *et al*., 2008).

2.3.2.2 PLC based on the Modal theory

The voltage propagation is referred at the product of impedance and admittance matrices given by

$$P = ZY \tag{2.17}$$

The voltage propagation matrix is determined in terms of its eigenvalue matrix λ and eigenvectors E_v such that

$$P = E_v \;\; E_v^{-1}\,\lambda \tag{2.18}$$

The eigenvectors are determined by the fixed, physical geometry of the transmission line. The eigenvalues describe the variable or dynamic characteristics of the solution. The modal of the system is constructed from the eigenvector columns, and is fixed by the transmission lines physical geometry. For a horizontal transmission line, the columns of the Clarke matrix give a good approximation of the natural modes (Wernich V. and Arthur B., 2008).

$$\begin{bmatrix} \frac{1}{2} & 1 & 1 \\ -1 & 0 & 1 \\ \frac{1}{2} & -1 & 1 \end{bmatrix} = M \tag{2.19}$$

Mode 1 is defined by the first column and is the mode with the lowest attenuation. Mode 2, the differential mode, is defined by column 2 and it propagates with a lower phase velocity and higher attenuation than mode 1. It makes a significant contribution to the total received signal. Mode 3 is the common mode and is heavily attenuated due to ground losses and can be neglected. Relative amplitudes of the modes, which are excited on transmission line, are determined by the voltage excitation vector applied to the line by PLC coupling configuration.

$$m = \frac{\partial y}{\partial t^2} + mg \tag{2.20}$$

Eigenvalues of the propagation Matrix describe the dynamic characteristics of the different natural modes of the system. Thus the attenuation and phase retardation of modes are associated with the eigenvalues (Wernich V. and Arthur B., 2008).

The horizontal transmission line can be determined in terms of the voltage on phase NV_{pN} as given by the following matrix;

$$\begin{bmatrix} e^{-\gamma 1x} & 0 & 0 \\ 0 & e^{-\gamma 2x} & 0 \\ 0 & 0 & e^{-\gamma 3x} \end{bmatrix} E_v \; E_V^{-1} \begin{bmatrix} V_{p1} \\ V_{p2} \\ V_{p3} \end{bmatrix} = \; V_x \qquad (2.21)$$

Where $e^{-\gamma 3x}$ is the scalar factor, E_v is the sending end voltage

This is not accurate as conductors swing differently in different conditions more specifically when we consider the wind induced vibrations. Although this method is currently used by ESKOM South Africa, it is clear that advancements are needed in order to obtain measurements in real time. This method can only obtain the sag through average calculation of signal amplitudes.

2.3.3 Power donut

It is an instrument platform for remote monitoring of overhead transmission lines, powered directly from the conductor electric field (Xignlong Z. and Jiping S., 2002). This instrument performs measurements of voltage, current, conductor temperature and the angle of inclination.

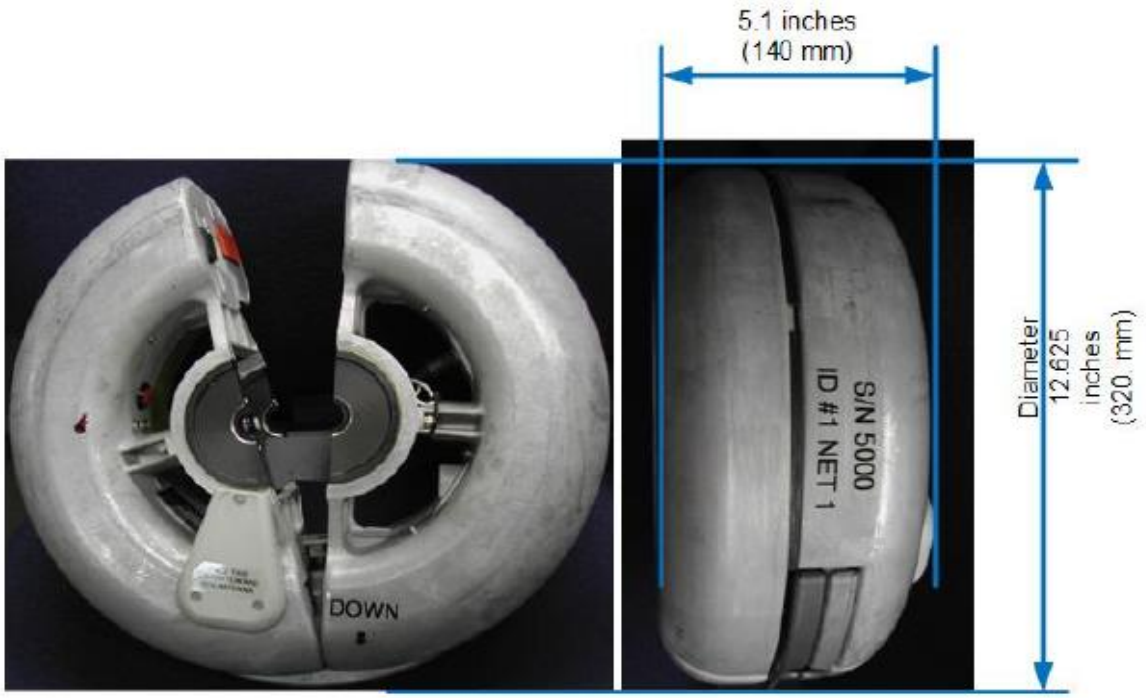

Figure 2.4: Power donut temperature sensor (Fish L., 2006)

It is installed on live conductor wires. However, this device measures the conductor surface temperature rather than the core temperature for calculating sag.

Giving the standard heat flow as $local\ heat\ flow$.

$$(Q) = -k\nabla T \tag{2.22a}$$

Where k is the material conductivity and ∇T is the temperature gradient. It is not always true that K should be treated as the constant. The thermal conductivity of a material varies with temperature; the variation can be small over a significant range of temperatures for some common materials. In anisotropic material, the thermal conductivity typically varies with orientation; where k is represented by a second-order tensor. In nonuniform material, k varies with spatial location (Xignlong Z. and Jiping S., 2002).

According to Fourier's law of heat conduction, local heat flow in x direction is such that;

$$q_x = -k\frac{dT}{dx} \quad (2.22b)$$

Where k is the thermal conductivity (W/m°C). Q is the vector quantity and can have x, y and z components. Therefore the heat transfer in a power transmission line conductor cannot determine the vertical movement of the conductor in real time. However it can help in the dynamic design of the line rating at initial stage.

In addition, this platform is very expensive and its installation requires working with live wires is more risky.

2.3.4 Global Positioning System

Application of the global positioning system (GPS), based on a constellation of 24 satellites, which uses the Navigation satellite Timing and Ranging (NAVSTAR) developed, launched, and maintained by the United States government (Thomas G., 2002).

It is a worldwide navigation and positioning resource for both military (i.e., precise positioning service) and civilian (i.e., standard positioning service) applications. This method relies on accurate time-pulsed radio signals in the order of nanoseconds from high altitude Earth orbiting satellites of about 11 000 nautical miles, with the satellites acting as precise reference points. These signals are transmitted on two carrier frequencies known as the L1 and L2 frequencies. The L1 carrier is 1.5754GHz and carries a pseudo-random code (PRC) and the status message of the satellites. There exist two pseudorandom codes: the coarse acquisition (C/A) and the precise (P) codes. The L2 carrier is 1.2276GHz and is used for the more precise military PRC. The signals from four or more satellites are received by a specially designed GPS receiver, and the following simultaneous equations are solved (Thomas G., 2002):

$$\left(X_{sk} - X_{rj}\right)2 + (Y_{sk} - Y_{rj})^2 + (Z_{sk} - Z_{rj})^2 = (R_k - dT) \quad (2.23)$$

$$K = 1, 2 \ldots \text{N}\ k = 1,2, \ldots., n\ n \geq 4 \quad (2.24)$$

Where ($X_{sk,}Y_{sk}$, $and\ Z_{sk}$) represents the kth satellite position ($X_{rj}\, Y_{rj}, Z_{rj}$) denotes the unknown jth receiver position $R_k$denotes the range to kth satellite, and dT is the unknown receiver clock bias converted to distance. This gives the longitude and latitude of the receiver (i.e., defectively x and y), the altitude of the receiver (effectively z), and the time that the measurement was made t. interestingly, the GPS transmission is made at low power level (the signal strength at the point of reception is about -90 to -120dBm). At this power level, the SNR is very low at the surface of the Earth. The attenuation of the noise is accomplished by averaging the received signal. The noise is averaged and a distinctively coded signal appears as an output. The averaging processes, as well as the solution of (1) are the main time limiting processes that determine how often a GPS measurement can be made (Fish L., 2006).

There is a potential in this technology, although there are some errors contributing to estimates. The differential GPS is generally used in order to decrease the selective availability errors. This mode consists of the base and the rover. The main disadvantage of the DGPS is the requirements of a second GPS receiver and corresponding communication equipment between the base and rover instruments. It is costly, and its performance in a HV environment is unreliable.

The accuracy of the direct instrumentation of overhead power line conductor sag measurement is about 19.6 cm range and 70% of the time. In the implementation of this technology, the phenomenon of the corona discharge in a transmission line conductor is a challenge in that it creates potentially intolerable conditions for radio reception in the 930MHz and 1.5 GHz frequency bands (Edelsein A., 2007).

This method relies on accurate time-pulsed radio signals in the order of nanoseconds from high altitude Earth orbiting satellites of about 11 000 nautical miles, with the satellites acting as precise reference points. This technique is promising; however the challenge such as electromagnetic interference (EMI) from the phase conductors is questionable.

2.3.5 Image processing based on camera

It is a costly technique and its installation requires contact with phase conductors for placing the targets. In image processing an edge is the boundary between an object and its background appearance. This represents the frontier for single objects. If the edges of image objects are identified with precision all objects can be located and their properties such as area, perimeter and shape can be calculated. Edge detection is an essential tool for image processing technology. There are two advanced and optimized edge detector in image processing, namely canny edge detectors and infinite symmetric exponential filter (Martin A and Tosunoglu S., 2002). These detectors follow different algorithms such that for canny edge detection, it is represented as follows:

- Read the image I.
- Convolve a 1D Gaussian mask with I.
- Create a 1Dmask for the first derivative of the Gaussian in the x and y directions.
- Convolve I with G along the rows to obtain I_X, and down the columns to obtain I_Y.
- Convolve I_X with G_X to have I_X', and I_Y with G_Y to have I_Y'.
- Find the magnitude of the result at each pixel

$$M(x,y) = \sqrt{I_x^{'}(x,y)^2 + I_y^{'}(x,y)^2} \qquad (2.25)$$

Infinite Symmetric Exponential Filter uses another optimization function to find the edge in an

image this function can be written as:

$$C_N^2 = \frac{4\int_0^\infty f^2(x)dx.\int_0^\infty f'^2(x)dx}{f^4(0)} \tag{2.26}$$

The function C_N is minimizing with an optimal smoothing filter for an edge detector, which result into an infinite symmetric exponential filter, as follows;

$$f(x) = \frac{p}{2}e^{-p|x|},\ f(x,y) = a.e^{-p(|x|+|y|)} \tag{2.27}$$

The filter in the infinite symmetric exponential filter edge detector is presented as one dimensional recursive filter. By presuming the 2D-filter function real and continuous, it is given by;

$$f[i,j] = \frac{(1-b)b^{|x|+|y|}}{1+b} \tag{2.28}$$

In some instances, image processing technique, uses automatic image analysis technique for extracting information from the line insulators. This concerns the detection of snow overage on insulators on the line and the detection of swing angles of insulators with respect to the vertical position. It must be clear that no real-time detection of the actual transmission line is made by this technique; hence it cannot be translated or linked to real time dynamic rating of the line.

2.3.6 Electro-magnetic Coupling Method

Electromagnetic Coupling Method is based on the magnetic field surrounding the conductor (Olsen R.G. and Edward K.S., 2002). For different line configurations, the grounded wire position and the sag calculation need to be modified. Also, Electro Magnetic Interference from nearby transmission lines cannot be neglected.

2.3.7 A Mathematical approach

When we review the position of a stretched conductor, such that the position vector $X(l,t) = (X(l,t), Y(l,t))$ with corresponding tension vector $T(l,t) = T(l,t)\,(cos\psi, sin\psi)$, where ψ is the positively oriented angle between the cable tangent and the horizontal. The tension vector is tangent to the cable because of the assumed negligible bending stiffness. The conductor element stretched under tension is represented as follows (Olsen R.G and Edward K.S., 2002):

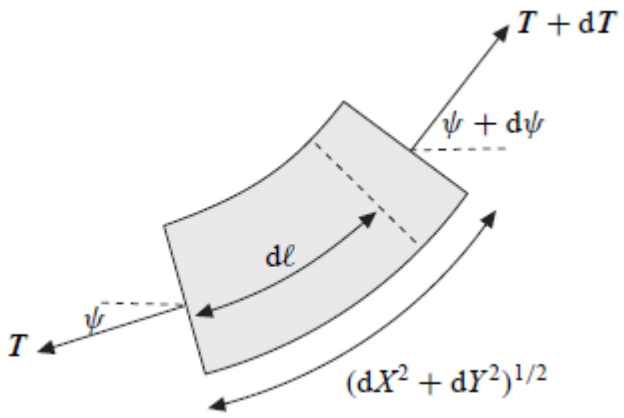

Figure 2.5: conductor element under tension stretch (Olsen R.G and Edward K.S., 2002)

Now considering a small cable element, dl. Due to gravity, cable tension, and inertial forces, this element is stretched however the mass remain the same. A conductor element is elongated in proportion to tension, according to Hooke's law, such that:

$$\left(dX^2 + dY^2\right)^{\frac{1}{2}} = \left(1 + \frac{T}{EA}\right) dl.\text{A} \tag{2.29}$$

According to a Newton's law, the internal tension and the external gravity forces are in equilibrium with the inertial forces, such that;

$$dT = \left(ge_y + \frac{d^2y}{dx^2}\right) m\, dl \tag{2.30}$$

$$\frac{\partial X}{\partial l} = \left(1 + \frac{T}{EA}\right)\cos\psi, \frac{\partial Y}{\partial l} = \left(1 + \frac{T}{EA}\right)\sin\psi, \tag{2.31}$$

The equation result in the limit $dl \xrightarrow{yields} 0$ are given by

$$\frac{\partial}{\partial l}\left(\frac{T}{1 + \frac{T}{EA}}\frac{\partial X}{\partial l}\right) = m\frac{\partial^2 X}{\partial t^2}, \tag{2.32}$$

$$\frac{\partial}{\partial l}\left(\frac{T}{1 + \frac{T}{EA}}\frac{\partial Y}{\partial l}\right) = m\frac{\partial^2 Y}{\partial t^2} + mg, \tag{2.33}$$

$$\left(\frac{\partial X}{\partial l}\right)^2+\left(\frac{\partial Y}{\partial l}\right)^2=\left(1+\frac{T}{EA}\right)^2. \tag{2.34}$$

For the boundary and coupling conditions in the Figure 2.6,

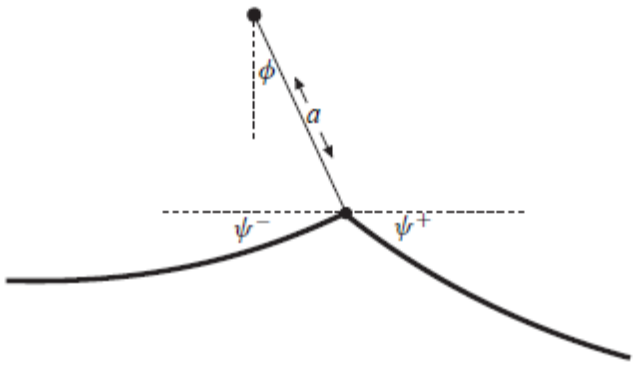

Figure 2.6: Boundary and coupling conditions (Olsen R.G and Edward K.S., 2002)

$L = 0\ and\ L = NL$ For a fixed support

$$X=0, Y=0, (l=0), \tag{2.35}$$

$$X=0, Y=0, (l=0), \tag{2.36}$$

At suspension string:

$$[X]_{l=nL-}^{l=nL+}=0, \tag{2.37}$$

$$(X-nS)^2+(Y-a)^2=a^2, \tag{2.38}$$

$$[T\cos(\phi-\psi)]_{l=nL-}^{l=nL+}=0. \tag{2.39}$$

Where ϕ is the angle of the supension string

The mathematical approach help us to understand the problem of sag more and the behavior of the transmission line under galloping conditions. Hence it only help us to reduce various problem parameters in to a single clear problem phenomenon.

2.3.8 Magneto Resistive Sensors

Magneto resistive *(MR) sensors* were recently applied for sag measurement. It calculates the current flow and line positions from the magnetic field emanated from the phase conductors (Eldelstein A., 2007). Provided the sensitivity of the magnetic sensors is sufficient, the electric and spatial information of the overhead line can be found by inverse calculation from the magnetic field measured at the ground level. However the accuracy of this technique is questionable. Factors such as multiple power conductors, bundle conductors and image current due to a conducting ground have to be taken in to consideration.

2.3.9 Autonomous Robot Technique

Autonomous robot technique based on simulations uses energy from the line and run along the conductor while making the inspection. The energy absorbed by the robot comes from the line, producing an increment in the line impedance and therefore, a voltage drop in the point of the line where the robot is located during the inspection (Graham H., 2008). The stability and reliability of this technique is questionable as the magnetic field emanated from the conductors always vary and the storage of such. This system also requires more number of turns in the secondary side of the current transformer to increase the power transmission to the system, therefore need the large ration transformers. This is an expensive method.

2.4 Background of RFID

RFID technology has been around since World War II (1948), where it was used to help solders to identify fighter plane. Although it was a crude vision and tags were very big in size. This technology uses radio waves to automatically identify objects and alternatively provides a means of storing data and retrieving data, through electromagnetic waves transmission to RF compatible integrated circuit. The major applications of RFID extended to various industries in recent years; including farm produce tracing, vehicle identification, entrance guards, and trade control (Bouc M. *et al*., 2010). RFID may be seen as the next logical step in the progression of tracking system and sensor networks because of technological advances in several fields. As we introduced this technology in chapter one of the dissertation, we continue to detail the explanation of key operational parameters that affect RFID performance in terms of range and throughput. We then look at the scalability and security later.

2.4.1 The key parameters of RFID

The key parameters that affect range and data rate are interdependent as shown in the depend encygraph of Figure 6. In this figure, the parameters and decision choices that the designers/users of RFID system have control over are shown within the hexagons (Bouc M. *et al.*, 2010).These parameters include operating frequency, transmit power, bandwidth, digital modulation encoding, and maximum tolerable bit error rate (BER).The key operational parameters that are affected by those design parameters include operating distance (range) and system throughput (proportional to data-rate). These operational parameters are shown within the rectangles of Figure 2.7.

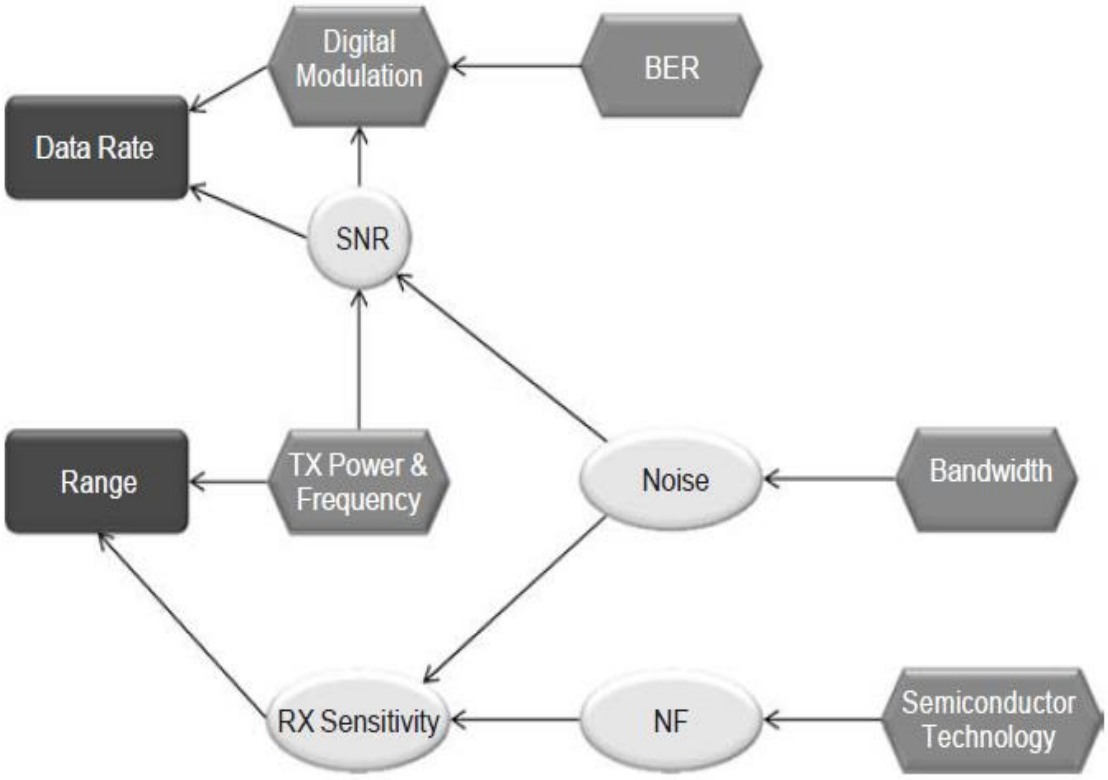

Figure 2.7: Key operational parameters and design trade-off (Bouc M. et al., 2010).

The oval objects in Figure 6, are intermediate factors that are influenced by one or more design parameters. They include signal-to-noise ratio (SNR), noise level, receiver sensitivity, and noise figure (NF). For example, the amount of "noise" at the input of a receiver is strongly dependent on the bandwidth of the receiver. Noise figure is a measure of degradation of the signal to noise ratio, caused by components in the RF signal chain. NF depends on the type of semiconductor technology and determines how much the noise at the input of the receiver is amplified relative to the signal before arriving at the demodulator. The specific parameter combination and their values ultimately determine the type of the tag. Although there is large number of possible parameter permutations, the type of tag can be categorized by the type of communications link (near-field or far-field), the method of tag transmission (emission or reflection), and the type of

power supply (battery or energy harvesting). The far-field begins where the wave impedance quickly settles towards the free-space impedance value of 377 ohms (Marrocco G., 2008).

For electrically small antennas, this distance is given by

$$R_{NF} = \frac{\lambda}{2\pi}. \tag{2.40}$$

The distance is essentially the radius of the near-field region around an antenna, and is less than one foot for popular commercial UHF RFID system that operate in the 915MHz band. Passive tags transmit data by reflecting power from the interrogator. This is also referred to as a backscatter modulation for systems that operate in the far-field, and load modulation for systems that operate in the near-field. Passive tags harvest energy from the interrogator instead of using a battery. While an active UHF tags, make use of an on-board battery for the power needed to emit a modulated RF signal that encodes the data (Marrocco G., 2008).

The most commonly utilized frequencies for both active and passive RFID operation are at or near 125 kHz, 13.65 MHz, 315 MHz, 433.92 MHz, 915 MHz, 2.45GHz, and 5.8GHz. Systems operating in bands below 70MHz tend to operate in the near-field with inductively coupled coil wire antennas because far-field antennas at those frequencies would be impractically large. The majority of standards prescribe passive UHF RFID operation in the region between 860MHz and 960MHz because of its favorable output power and RF energy harvesting characteristics (Bridgelall R., 1999).

Although passive tags are seen as cheaper because of not using the external power supply as opposed to active tags, there are also constraints when it comes to sensitivity. (Bridgelall R., 1999) shows that the lower the power a tag requires for activation and signal decoding, the greater its

operating distance from the interrogator. Figure 2.8, illustrates this relationship for a selected sub-set of system type that operates under various regulatory allocations.

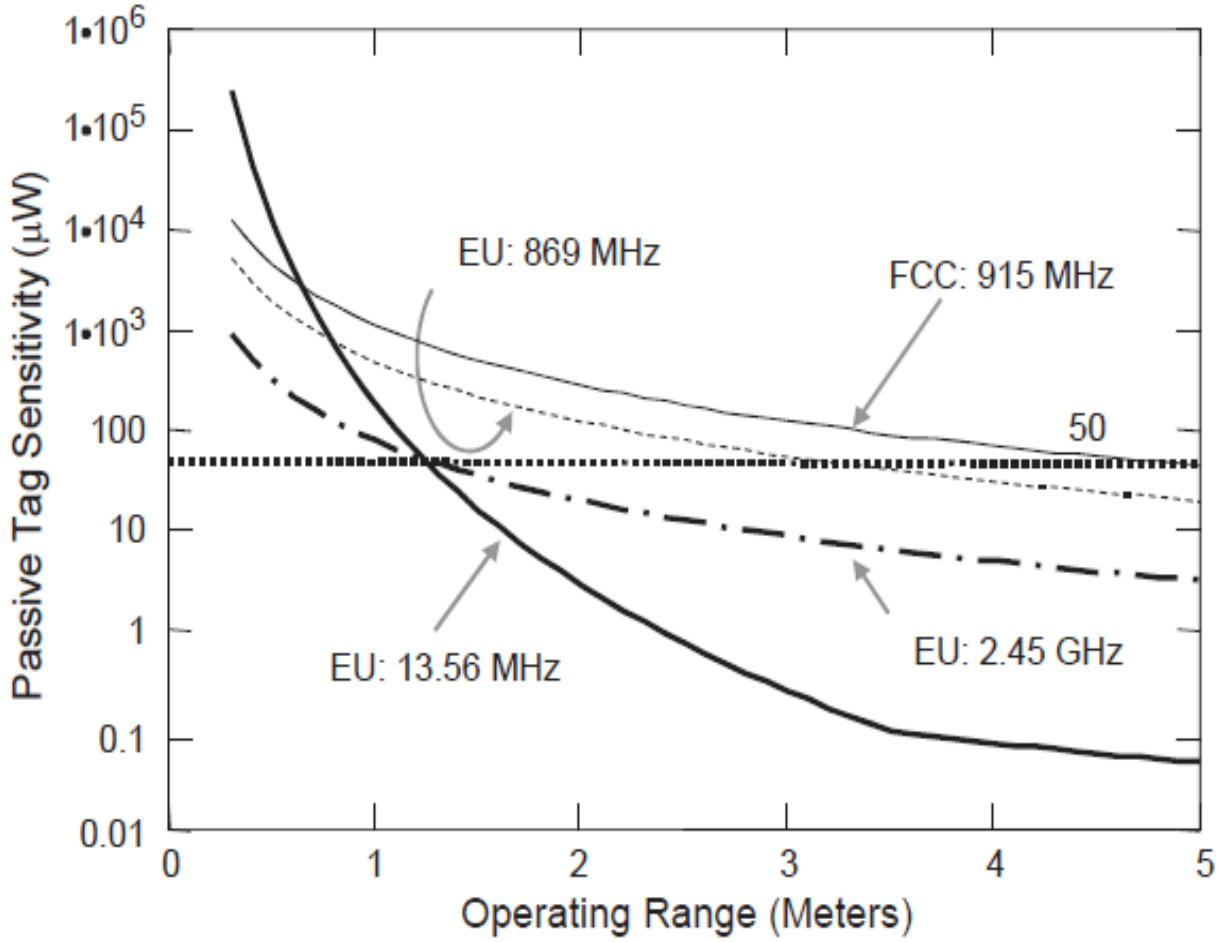

Figure 2.8: Effect of sensitivity on range (Bridgelall R., 1999).

This Figure 2.8 shows that an EU compliant tag operating at 868MHz requires 50 micro watts to energize and decode a signal will respond from an unobstructed distance of about3.25meters, under ideal conditions. The same tag can respond from an unobstructed distance of about 5meters if the tags sensitivity improves to 20 microwatts. Signal power diminishes as the inverse square of the distance ($1/\mathbf{r}^2$) in the far-field, and as the inverse sixth power of the distance ($1/\mathbf{r}^6$) *in* the near-field. Therefore, near-field tags will operate at a significantly reduced distance from far-field

tags of the same sensitivity.

Active tags have the advantage of longer range as opposed to passive and can continuously report back to the reader without waiting for the energy from the reader. Passive tags receivers consist of signal envelope detectors constructed from passive diodes or an equivalent construction. Such detect a signal only when the input signal is sufficiently strong to overcome the passive diode detector forward bias threshold (Mandal S. and Sarpeshkar R., 2007). Active tags utilize the on-board battery to bias active rectification circuits, which substantially lowers this forward bias threshold. The sensitivity difference can be significantly greater than 100dB. A lower UHF operating frequency is preferred because of the more favorable energy capture characteristics of a longer wavelength. The *Fries* far-field transmission formula for unobstructed narrowband propagation gives;

$$P_{i\_tag} = P_s\left(\frac{\lambda^2}{4\pi r}\right).T\psi ri \tag{2.41}$$

Such that the amount of signal power that the tag receives, $\mathbf{P_{i\_tag}}$ proportional to the wavelength λ squared. $\mathbf{P_S}$ is the power supplied by the interrogator, r is the operating distance, $\mathbf{T}$ is the interrogator antenna gain, and $\psi\mathbf{ri}$ is the tag's antenna sub-system gain when I is absorbing energy.

2.4.2 Constraints on Interrogator Sensitivity for Passive UHF Tags

The interrogator signal received from a backscattering passive UHF tag decreases with free-spaced is represented as follows (Mandal S. and Sarpeshkar R., 2007):

$$P_B = P_s\left(\frac{\lambda^4}{4\pi r}\right).T^2\psi ro \tag{2.42}$$

That is, the amount of signal power ($P_{B\,\mathbf{received}}$) by the interrogator decreases at the rate of $1/\mathbf{r}^4$ for passive UHF systems. $\mathbf{P_S}$ is the power generated from the interrogator and delivered to the antenna, **r** is the operating range, **T** is the interrogator antenna gain, and $\psi_{\mathbf{ro}}$ is the tag antenna subsystem gain when it is reflecting energy, including any transmission losses. In an optimized design, the interrogator decoding sensitivity should be at least $\mathbf{P_B}$ when the tag is at its maximum operating distance. Solving for **r** in the first equation and setting $P_{tag}=P_{tag\_sens}$ gives the maximum powering range $\mathbf{r_{max}}$ as a function of the tag's decoding sensitivity as follows (Mandal S. and Sarpeshkar R., 2007):

$$r_{\max} = \left(\frac{\lambda}{4\pi}\right).\left(\frac{P_{sT\psi ri}}{P_{tag\_sens}}\right) \tag{2.43}$$

Substituting equation above in to the first equation and setting $P_B=P_{I\_sens}$ to maintain maximum range gives the required interrogator sensitivity as a function of the tag sensitivity gives (Mandal S. and Sarpeshkar R., 2007) ;

$$_{I\_sens} = \left(\frac{P^2_{tag\_sens\psi ro}}{P_{s\psi^2 ri}}\right) \tag{2.44}$$

Even though interrogators can radiate a relatively large signal for powering passive tags, the available backscatter signal ($\mathbf{P_B}$) from passive tags is still the order of magnitude less than a low-power signal ($\mathbf{P_I}$) arriving from a typical active tag from the same distance. For example, from **equation 2.43**, a four Watt EIRP(~36dB) signal transmitted from an FCC compliant interrogator operating at 915MHz will become approximately 3 microwatts (-25.27dBm) after

travelling a distance of 30 meters in free space. A battery-powered backscatter tags will reflect a portion of the tree microwatts towards the interrogator. In comparison, a low power active tag in the same band will typically transmit 1 mill watt (0dBm) of signal, which is over 300 times more powerful than the signal backscattered from a passive tag (Smith A.A., 1998). This means that an interrogator with the same sensitivity can also decode the active tag's response at a lower distance. With all other parameters unchanged, increasing range means either increasing the average signal power transmitted or increasing the receiver sensitivity. However, regulatory rules limit the transmitted power, and the receiver noise figure bounds its sensitivity. The theoretical noise floor is a function of bandwidth and temperature (Smith A.A., 1998).

It is clear that the power consumption of the passive tag is very important to consider when designing the tag, this should go with the size of the tag as well. Advancement in polymer electronic for fabrication of the tag is required.

For practical implementations, transmission power, noise figure, and bandwidth affect key application level considerations such as power consumption, cost, and size. Increasing antenna gain in order to increase the receive signal strength tends to increase the size of the antenna. Higher antenna gain also favors transmission or reception in one direction over others. Whistle lower gain antennas must be used if the application requires Omni-directional performance. A lower noise figure amplifier increases sensitivity but also tends to demand more power or require a more expensive semi-conductor technology (Gray P.R. *et al* 2001).

If we need more output power from the interrogator, it means we need to put additional heat sinks, and increase their size because interrogator's power consumption will increase. Therefore when designing RFID system factors such as bandwidth, size, range, power consumption and cost should be taken into consideration.

2.4.3 The System Throughput

Given a data exchange protocol, the amount of bandwidth per channel that an interrogator can legally transmit is directly proportional to the maximum achievable data rate of a specified modulation scheme. Interrogators select an available channel from the sub-divided frequency band by utilizing traditional narrow-band multiple access techniques such as frequency hopping or carrier sensing (Charles M. and Farhad A., 2008).

According to wireless network standards such as (IEEE 802.11b) and (IEEE 802.15.4), digital modulation schemes such as FSK, PSK, and QSPK are used to transmit a higher data rate within the same channel bandwidth (Misic J., 2009). However the majority of RFID systems with low power consumption utilize ASK modulation for forward and reverse bias mode link.

2.4.4 Data Modulation

The achievable bit rate is a direct function of the bandwidth occupied, bit encoding scheme (Skalar B., 1988). Once allotted a fixed bandwidth, the maximum bit rate achievable depends on the spectral efficiency of the selected bit-encoding scheme. All passive tags and most of the active tags utilize non-coherent ASK modulation and demodulation because their implementation inherently requires low-power, which result in a low cost. It is also possible to utilize a sub-carrier modulation type such as FSK and PSK along with ASK. FSK sub-carrier modulation is achieved by manipulating the ASK modulation speed in a data stream to encode binary digits.

2.4.5 Channel Sharing

Interrogators designed for use with passive tags must transmit sufficient power to energize tags

and consequently do not utilize multiple access techniques such as Direct-Sequence- Spread-Spectrum (DSSS) or Ultra-Wide-Band (UWB) that spread energy across a wide spectral region using relatively short time period signals. Rather, multiple access techniques that require channel hopping are used because the tag can collect energy from a non-modulated carrier using a simple diode rectifier front-end. Consequently, interrogators for passive tags are limited to time-sharing or activity-based media access (MAC) protocols. They either randomly select a channel and occupy it for fixed duration before moving on to another, or wait until a channel becomes vacant before transmitting. Standards have dubbed the former method as frequency hopping (FH) and the latter a Listen-Before-Talk (LBT). FH with a randomized hopping pattern is a requirement for UHF transmission levels greater than 125 milli-watts under FCC regulated domains. The intention is to spread the power averaged across the band over specified duration. Interrogators must also hop at a rate such that the average time transmitting in anyone channel is less than 400 milliseconds over any 20-second period (Kern C., 1999).

The new designs of RFID system should be able to use a smaller band and read multiple tags without any communication interference.

2.4.6 Interrogator Interference

When interrogators operate simultaneously within a few channels of each other, they produce interfering signals that affect the operation of both tags and interrogators (reader) within range. The impact on broadband back-scatter tags is more significant than for narrow-band active tags. The mixing of a carrier from the desired interrogator with a carrier from another nearby interrogator causes interference. Nonlinearities from practical RF amplifiers and mixers produce signal components called inter-modulation products that appear within the receiver bandwidth and can distort the tag data signal. The C1G2 standard defines a “dense reader environment” as one where as many interrogators are operating as there are channels allocated in the band (Karthaus U.

and Fischer M., 2003).

The net effect from any interference is a reduced system throughput. It means that adding a second interrogator does not necessarily double the through-put of tags identified per unit interval of time. Interference of the tag to interrogate produce the corrupt signal and therefore bad output.

2.4.7 Tag interference

(Karthaus U. and Fischer M., 2003), insists that increasing the number of available channels in a band may increase aggregate throughput for active tags but not necessarily for passive tags. The reason for this is that passive tags have fixed broadband receivers that listen to the entire band. Unlike active tags, passive tags cannot dynamically hop to another vacant channel to establish an isolated link with an interrogator. They simultaneously receive and integrate signals within range from all interrogators transmitting anywhere in the band. Under certain circumstances, adding a low pass filter to the tag's baseband receiver circuit may partially mitigate this issue.

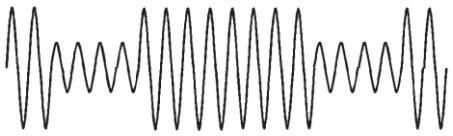

(a) Carrier modulated signal received without interferer (demodulated data signal)

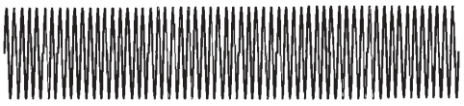

(b) Interfering carrier in another channel- (demodulated data signal)

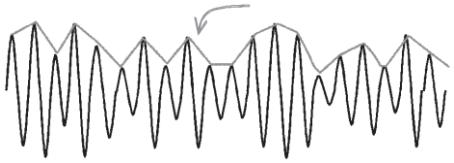

(c) Corrupted data signal

Figure2.8: Signal from the tag interference (Karthaus U. and Fischer M., 2003).

Like any other communications systems, RFID mostly rely on the electromagnetic waves to function. Factors such as signal interference from or to the tag, and antenna to transmit inquiry energy to the tag and sense modulated responses from tags should be considered when implementing the RFID.

An analytical approach for probabilistic predictions of voltage sags in Power transmission networks is proposed by Lim (Lim, Y. S., 2002). The probability density is the function of the voltage sag caused by tensile forces in the transmission network. It is not easy to practically apply such in real transmission network.

2.4.8 Conclusion

The read rate or read accuracy for each tag is defined as the percentage of time a reader is able to correctly read the tag's identity. For the ideal system if a reader sends out name (N) queries to a population of tags that are all within its well-denied read zone, it receives N responses from each of the tags containing their respective identity. Furthermore if a reader sends out N queries to a population of tags that are all outside its read zone, it will receive no response. In an ideal system, this holds true for multiple readers with overlapping read zones, that is, if multiple readers send out N queries to a population of tags that are simultaneously in the read-zone of all the querying

readers, and then each of the readers will receive N responses from each of the tags containing the respective tag identity. As mentioned in the above characterization, the behavior of the ideal system is unaffected by factors such as orientation, environment and relative motion.

There are challenges in any technology as long as it uses electromagnetic waves. RFID has some challenges that need more attention and improvement. This includes power management on tags and privacy, when we focus on symmetric RFID tags. The prevailing passive tags which we believe could be useful on sag detection cannot be 100 percent secured according to the reviewed theory. Although RFID has the potential to improve the real-time measurements, object identification, the technology has not been tested under high density field such as high voltage transmission line, extreme weather conditions, different conducting and non-conducting objects, excitation systems and prime movers. It is the aim to find the strength of this technology, particularly for sag detection of high voltage transmission lines. To do this we adopt the radar system in chapter three for long range precision measurement and perform analysis.

CHAPTER 3 THE SYSTEM STRUCTURE

3.1 Transmission line performance and sag detection: A mathematical reconstruction

When designing power transmission line, different factors are considered at an early stage including the allowable amount of conductor sag at specific environments. In determining the sag we also consider factors such as temperature, ice coating and corona discharge. The normal static vision of power transmission line is presented by the span length l, conductor length L, conductor weight W, the tensile strength T, and the maximum arrow D, as follows:

$$L = l \cong l\left(1 + \frac{Wl^2}{24T}\right) \tag{3.1}$$

$$D = \frac{Wl^2}{8T} \tag{3.2}$$

A differential equation for the curve to derive the equation for the position of the tag is used. For equally supported spans shown in Figure 3.1, the tag position is estimated as follows.

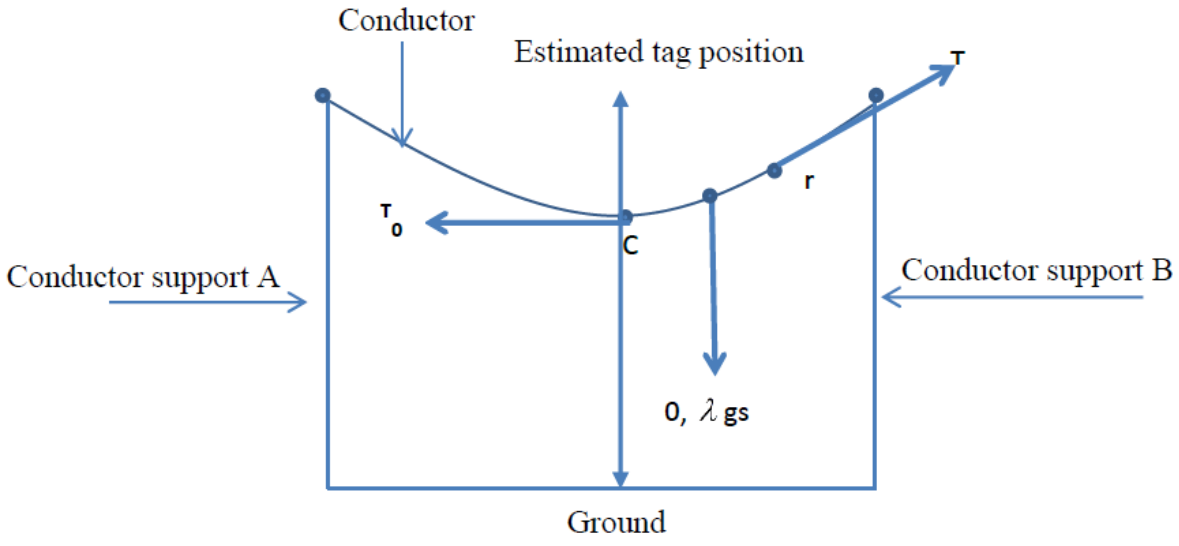

(a): Transmission line span

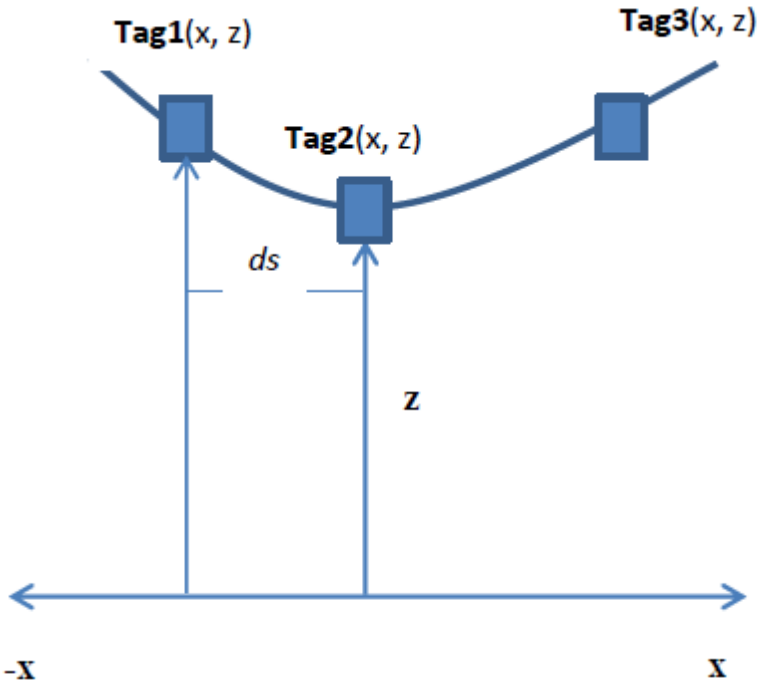

(b) Tags on the transmission line

Figure 3.1: Equally supported transmission line span

From Figure 3.1 (a), considering a single span the midpoint position is ***C*** as the conductor is assumed steady. Let ***C*** be the lowest point on the conductor, called the *vertex* of the catenary and measure the parameter length of the conductor ***S*** from the lowest point of the conductor ***C***. Assume the position vector **r** is to the right of ***C*** since the other case is implied by symmetry. The forces acting on the section of the conductor from ***C*** to **r** are the tension of the conductor at ***C***, the tension of the conductor at **r**, and the weight of the conductor. The tension at **c** is tangent to the curve at ***C*** and is therefore horizontal, and it pulls the section to the left so it can be written as $(-T_0, 0)$ where T_0 is the magnitude of the force. The tension at **r** appears parallel to the curve at **r** and pulls the section to the right, so it may be written as $T = (T\cos\varphi, T\sin\varphi)$, where T is the magnitude of the

force and φ is the angle between the curve at **r** and the *x*-axis. Finally, the weight of the conductor is represented by $(0, -\lambda gs)$ where λ is the mass per unit length, g is the acceleration of gravity and s is the length of conductor between ***C*** and **r**. The path of the conductor route is presented by a parametric equation of a curve through the equation expressing the coordinates of the point of the curve;

$$r = (x, y) = (x(s), y(s)) \tag{3.3}$$

$$\frac{dr}{ds} = u \qquad \text{Where} \quad u \text{ is a unit tangent vector} \tag{3.4}$$

Since our conductor is assumed to be equilibrium

$$T\cos\varphi = T_0 \tag{3.5}$$

$$T\sin\varphi = \lambda gp \tag{3.6}$$

$$\frac{dy}{dx} = \tan\varphi = \frac{\lambda gs}{T_0} \tag{3.7}$$

Putting a as,

$$a = \frac{T_0}{\lambda g} \tag{3.8}$$

Bearing in mind that the conductor weight is equal in magnitude as the tension at point ***C*** $(0, \lambda gs)$. It is simpler to define the curve by,

$$\frac{dy}{dx} = \frac{s}{a} \tag{3.9}$$

Solving the differential equation above, the arc length is determined by,

$$\frac{ds}{dx} = \sqrt{\frac{dx^2 + dy^2}{dx^2}} = \sqrt{1 + \left(\frac{dy}{dx}\right)^2} = \frac{\sqrt{(a+s)^2}}{a} \tag{3.10}$$

Then

$$\frac{dx}{ds} = \frac{1}{\frac{ds}{dx}} = \frac{a}{\sqrt{a^2 + s^2}} \tag{3.11}$$

$$\frac{dy}{ds} = \frac{\frac{dy}{dx}}{\frac{ds}{dx}} = \frac{s}{\sqrt{a^2 + s^2}} \tag{3.12}$$

Integrating this equation gives,

$$y = \sqrt{a^2 + s^2} + \beta \tag{3.13}$$

Where β is an integral constant

If $\beta = 0$ then,

$$y = \sqrt{a^2 + s^2}, y^2 = a^2 + s^2 \tag{3.14}$$

The integral expression of $\frac{dx}{ds}$ is given by,

$$x = a \times \sinh^{-1}(\frac{s}{a}) + \alpha \tag{3.15}$$

Where α is an integral constant

The integral of $\frac{dx}{ds}$ is

$$x = a \times \sinh^{-1}(\frac{s}{a}), s = a \times \sinh(\frac{x}{a}) \tag{3.16}$$

Shifting the y-axis position the angle $\alpha = 0$,

$$x = a \times \sinh^{-1}(\frac{s}{a}), s = a \times \sinh(\frac{x}{a}) \tag{3.17}$$

Considering the temperature effect which escalates the stress σ, of the conductor, the thermal expansion is noted, in that

$$\frac{ds}{dx}=\sqrt{1+\left(\frac{dy}{dx}\right)^2}=\sqrt{1+\left(\frac{Ws}{T_o}\right)^2}\,or,dx=\frac{dq}{\sqrt{\frac{w^2q^2}{T_0^{\,2}}+1}} \tag{3.18}$$

Where s is the arc length in this case and other parameters remain unchanged. When integrating both sides we find that,

$$\int dx=\int\left(\frac{ds}{\sqrt{\frac{W^2s^2}{T_0^{\,2}}+1}}\right) \tag{3.19}$$

$$\therefore x=\left(\frac{T_0}{W}\right)sih^{-1}\left(\frac{Ws}{T_0}\right)+C \tag{3.20}$$

Assuming the conductor becomes elastic due to the sigma factor then we have the linear elastic such that $\sigma=E\varepsilon$. Where σ is the stress, E is the constant of modulus elasticity and ε is the strain. If S is the length then,

$$S=y\left(1+\frac{T}{E}\right)p \tag{3.21}$$

In this case p is the natural length of a section of a conductor, T becomes the tension applied and E the constant then,

$$\frac{ds}{dp}=\left(1+\frac{T}{E}\right)y \tag{3.22}$$

So the elastic conductor curve can be derived from the vertical tension T and the horizontal tension T_0 such that for unchanged length we say,

$$T\cos\varphi=T_0 \tag{3.23}$$

$$T\sin\varphi=\lambda_0 gp \tag{3.24}$$

Where λ_0 is the mass per unit length of the conductor without tension and g is the gravitational acceleration.

Re-writing this formulae

$$\frac{dy}{dx} = \tan\varphi = \frac{\lambda_0 gp}{T_0} \tag{3.25}$$

$$and, T = \sqrt{T_0^2 + (\lambda gp)^2}$$

The mass of the conductor, in nature is denoted as λ_0 .

Let

$$a = \frac{T_0}{\lambda_0 g} \tag{3.26}$$

Then

$$\frac{dy}{dx} = \tan\varphi = \frac{p}{a}, T = \frac{T_0}{a}\sqrt{a^2 + p^2} \tag{3.27}$$

Since

$$\frac{dy}{ds} = \sin\varphi = \frac{\lambda_0 gp}{T}, \tag{3.28}$$

$$\frac{dx}{ds} = \cos\varphi = \frac{T_0}{T} \tag{3.29}$$

Evaluating in terms of natural length

$$\frac{dx}{dp} = \frac{T_0}{T}\frac{ds}{dp} = \frac{a}{\sqrt{a^2 + p^2}}\left(1 + \frac{T_0}{E}\right) \tag{3.30}$$

And substituting (3.26) to (3.31) we have,

$$\frac{dy}{dp} = \frac{ds}{dp}\left(\frac{\lambda_0 gp}{T}\right) = \frac{T_0 p}{a}\left\{\frac{1}{T} + \frac{1}{E}\right\} = \frac{p}{\sqrt{a^2 + p^2}} + \frac{T_0 p}{Ea} \tag{3.31}$$

Integrating $\frac{dy}{dp}$, to obtain x and y we obtain,

$$x = a \times \sinh^{-1}\left(\frac{p}{a}\right) + \left(\frac{T_0}{E}\, p\right) + \alpha \tag{3.32}$$

And

$$y = \sqrt{\left(a^2 + p^2\right)} + \frac{T_0}{2E_a}\, p^2 \tag{3.33}$$

When considering the wind pressure q and the conductor with the ice weight w_i, the size of the conductor thickness t. We can have the resultant force acting on the line W, where;

$$W = \sqrt{q^2 + (W + W_t)^2} \tag{3.34}$$

The tensile strength during the construction and the tensile strength in adverse conditions T_c are also taken into account then, and could be found as follows;

$$T^3 + T^2\left\{E_a\left(at + \frac{W^2 l^2}{24T_c^2}\right) - T_c\right\} - \frac{W^2 l^2 E_a}{24} = 0 \tag{3.35}$$

Assuming the length of the cable is X at Figure 3.1 (b) as it lies between two points (x, z) and $(-x, z)$. The height of the cable can be determined from the point of its potential energy as it lies on the xz plane. With $(z > 0)$ and $X > 2x$ satisfy the inequality. Assuming that dm is the mass, dV be the potential energy, λ mass density per unit length, g the gravitational velocity and ds the arc length.

$$dV = (dm)gz = (\lambda ds)gz \tag{3.36}$$

$$ds = \sqrt{(1+(z')^2)}dx \tag{3.37}$$

$$V = \int_{-x}^{x} dV = \lambda g \int_{-x}^{x} y\sqrt{(1+(z')^2)}dx,\ z' = \frac{dz}{dx} \tag{3.38}$$

If $z = z(x)$ and boundary conditions are set from $z(-x) = h$ to $z(x) = h$. Letting λ to be the multiplier parameter then it follows that,

$$f = f(x, z, z') = \lambda gz\sqrt{(1+(z')^2} + \lambda\sqrt{(1+(z')^2)} \tag{3.39}$$

$$\frac{d}{dx}\left(\frac{\partial f}{\partial z'}\right) - \frac{\partial f}{\partial z} = 0, \Rightarrow \frac{d}{dx}\left[\frac{\lambda gzz' + \lambda z'}{\sqrt{(1+(z')^2)}}\right] - \lambda g\sqrt{(1+(z')^2)} = 0 \tag{3.40}$$

The variable x is independent and therefore letting α to be a constant in this case,

$$\alpha = (\lambda gz + \lambda)\left[\frac{(z')^2}{\sqrt{(1+(z')^2)}} - \sqrt{(1+(z')^2)}\right] \tag{3.41}$$

Solving for z'

$$(z')^2 = \frac{(\lambda gz + \lambda)^2}{\alpha^2} - 1 \tag{3.42}$$

Changing the variables

$$\lambda gz + \lambda = \alpha u \tag{3.43}$$

$$\frac{du}{\sqrt{u^2 - 1}} = \frac{\lambda g}{\alpha}dx \tag{3.44}$$

Integrating the above equation we have,

$$In(u + \sqrt{u^2 - 1}) = \frac{\lambda g}{\alpha}x + c \tag{3.45}$$

Where c is the constant of integration. In simplifying the algebraic equation (3.45), substitute the constant c as;

$$c = -\frac{\lambda g}{\alpha}\beta \quad \text{where,} \quad \beta = \frac{\alpha c}{\lambda g} \tag{3.46}$$

β is a new constant

$$u = \frac{\lambda g z + \lambda}{\alpha} = \cosh\left[\frac{\lambda g(x-\beta)}{\alpha}\right] \tag{3.47}$$

Therefore the height of the tag can be represented by

$$z = z(x) = -\frac{\lambda}{\lambda g} + \frac{\alpha}{\lambda g}\cosh\left[\frac{\lambda g(x-\beta)}{\alpha}\right] \tag{3.48}$$

Where

$$X = \int_{-x}^{x}\sqrt{(1+(z')^2)}dx = \int_{-x}^{x}\cosh\left(\frac{\lambda g x}{\alpha}\right)dx = \frac{2\alpha}{\lambda g}\sinh\left(\frac{\lambda g x}{\alpha}\right) \tag{3.49}$$

These estimations are aimed to improve the efficiency usage of high voltage transmission line by using RFID sag monitoring system. The target is to promptly providing the grid operators with the conductor ground clearance. When all these parameters for power transmission line are examined, a particular attention is on how RFID system performs under environmental factors. We first look at the operation of the system and attempted to locate it in an equal or unequal spans of transmission line.

To do this, firstly data obtained from 132 KV line tension and current parameters at Lesotho Electricity Corporation (LEC) was used in the depicted Figure 3.2, and used to view the rate of change of conductor sag. The derived mathematical model is then used to generate Figure 3.3 and demonstrate the variation of conductor sag for different times of three day period from 01 April 2015 to May 2015. There is a very complex correlation that is exhibited between conductor sag and current loading due to variable temperature conditions.

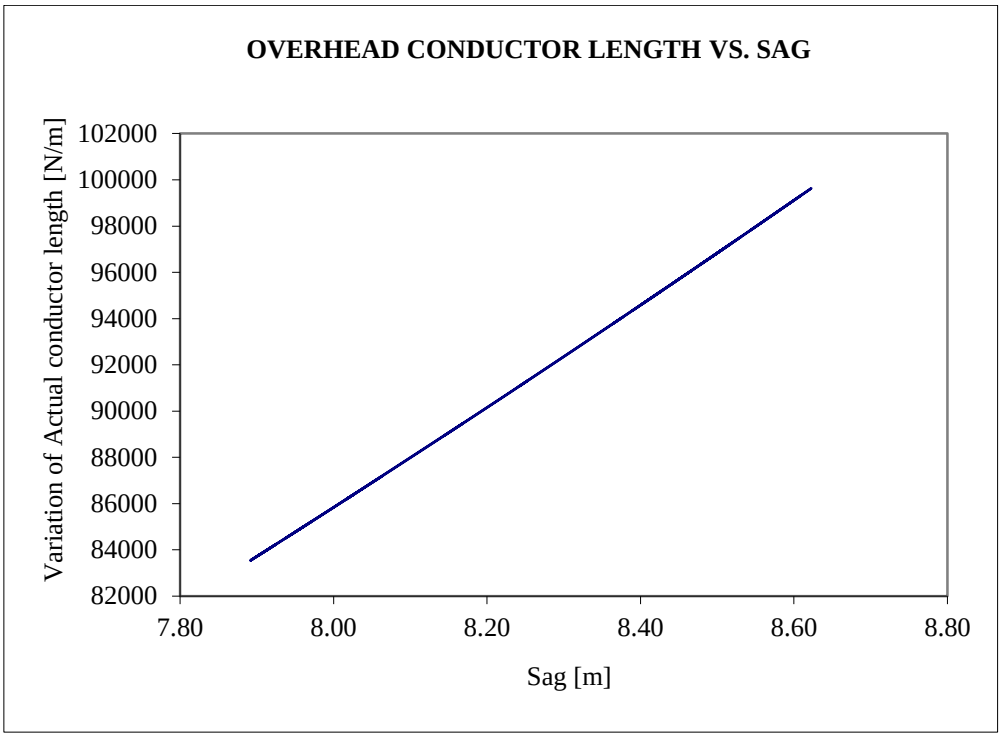

Figure 3.2: Rate of change of conductor length with maxima sag using 123KV line LEC data.

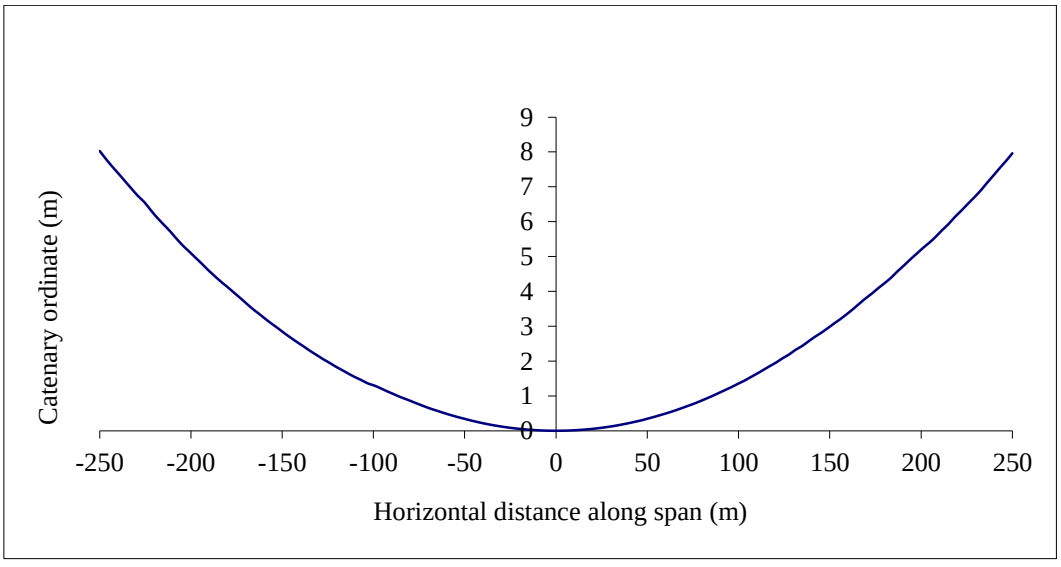

Figure 3.3: Catenary of LEC 132 KV line

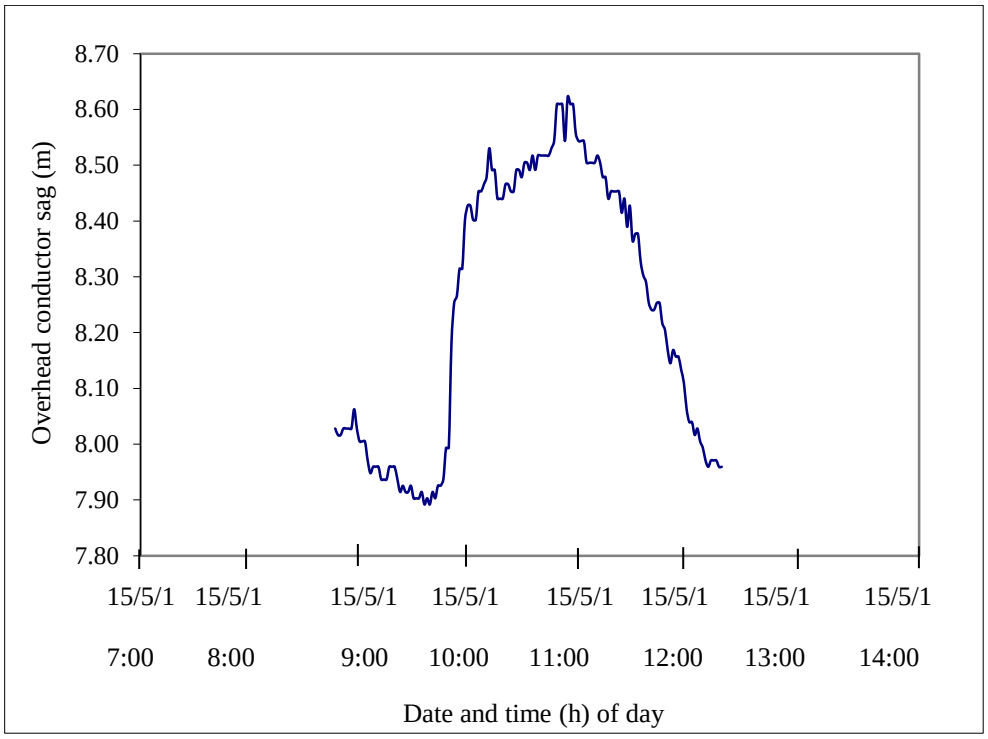

Figure 3.4: Variation of conductor sag due to variation in temperature loading

Correlation that is exhibited between conductor sag and current loading due to variable temperature conditions.

3.1.1 A GPS application for conductor sag in comparison with the proposed RFID

The effective use of a Differential GPS is based on the idea that if a GPS base station receiver is fixed at a known location, it can be used to determine exactly what errors the satellite data contains. The Differential GPS measurement of overhead HV conductor position is a more direct measurement technique. This is concluded because direct measurement of conductor position involves no intermediate models, assumptions or calculations so to speak. There are several potential disadvantages of the proposed Differential GPS method which are mentioned in chapter

two of literature review. Figure 3.4 demonstrate a tried simulation of a GPS method with a base and rover attached to the transmission line.

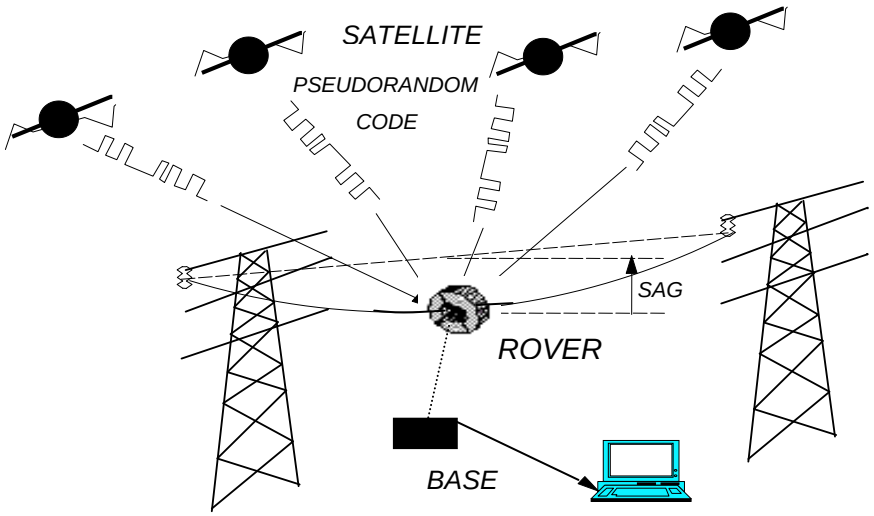

Figure 3.4: DGPS line diagram

The hypothesized advantage of RFID passive tags is that they should transmit and receive signal without external power source required. Whereas the GPS need a power supply and use a rover and receiver. A simplified block diagram of a DGPS is depicted in Figure 3.5. Assuming the DGPS in stationery position. The DGPS measured results show the weak altitude signal measurement hence the improvement of accuracy a necessity.

It can be concluded that some delays or unsteady performance of DGPS is or can be caused by environmental factors hence delay cause DGPS accuracy to deteriorate as distance increase between ground as a reference point and receivers.

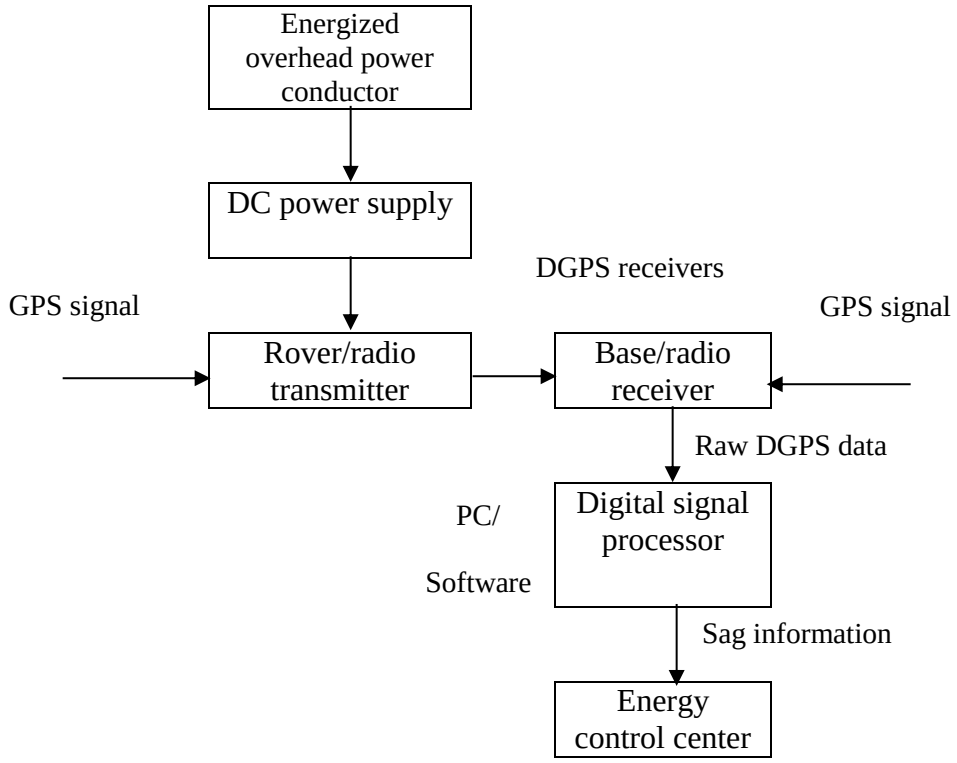

Figure 4.5: A block diagram of DGPS Conductor Sag measurement.

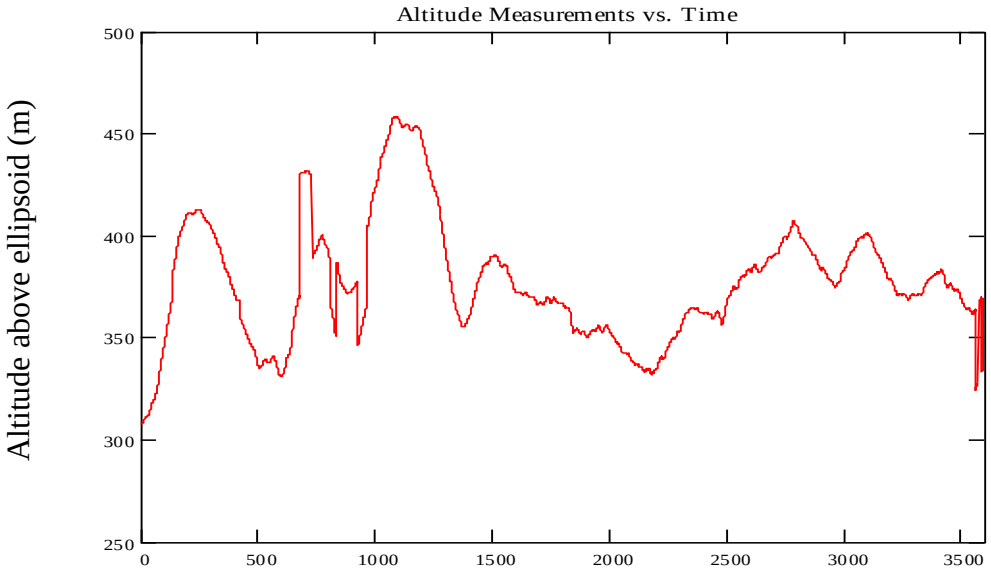

Figure 4.6: DGPS vertical measurement 01

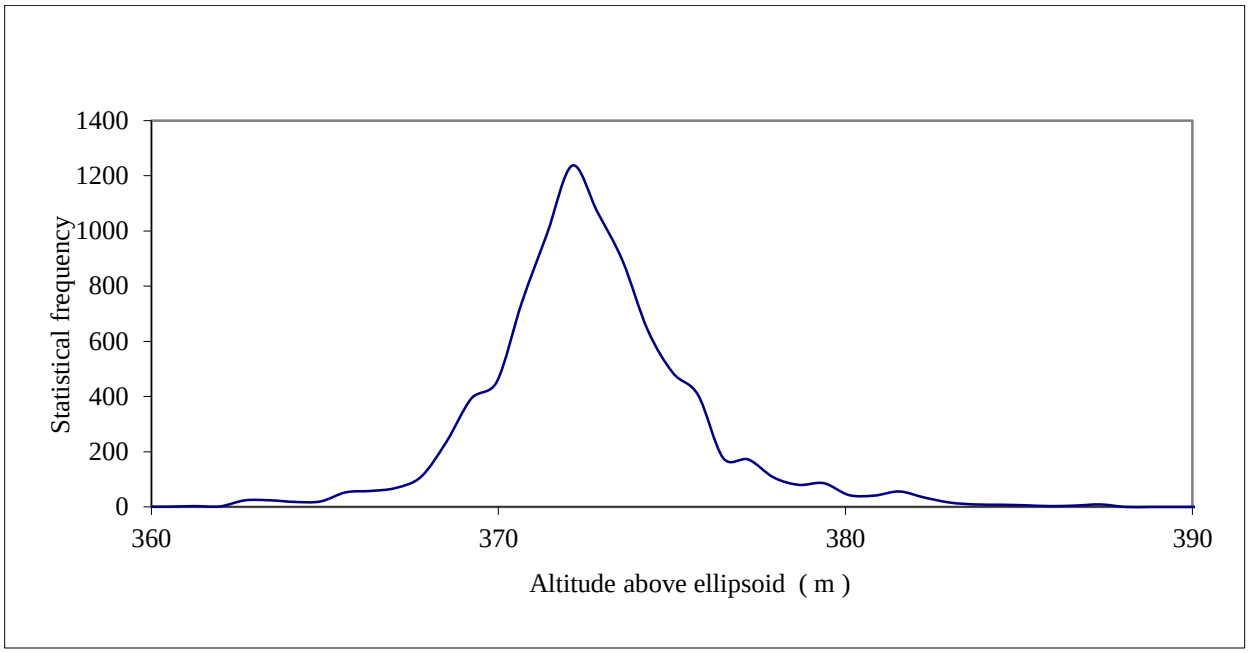

Figure 4.7: DGPS vertical measurement distribution 02

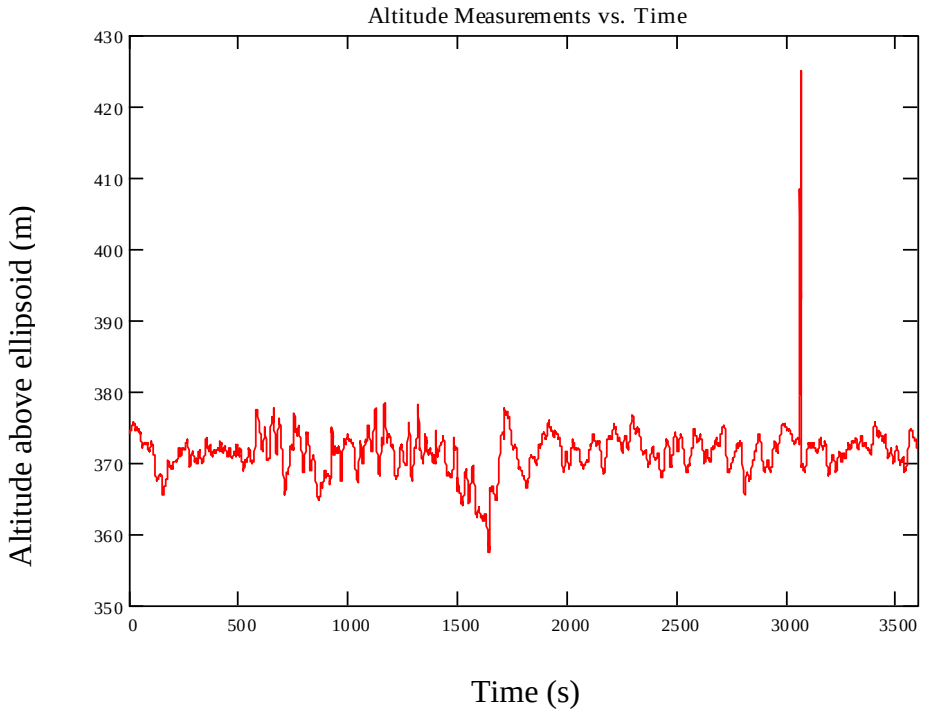

Figure 4.8: DGPS vertical (z) measurement 03

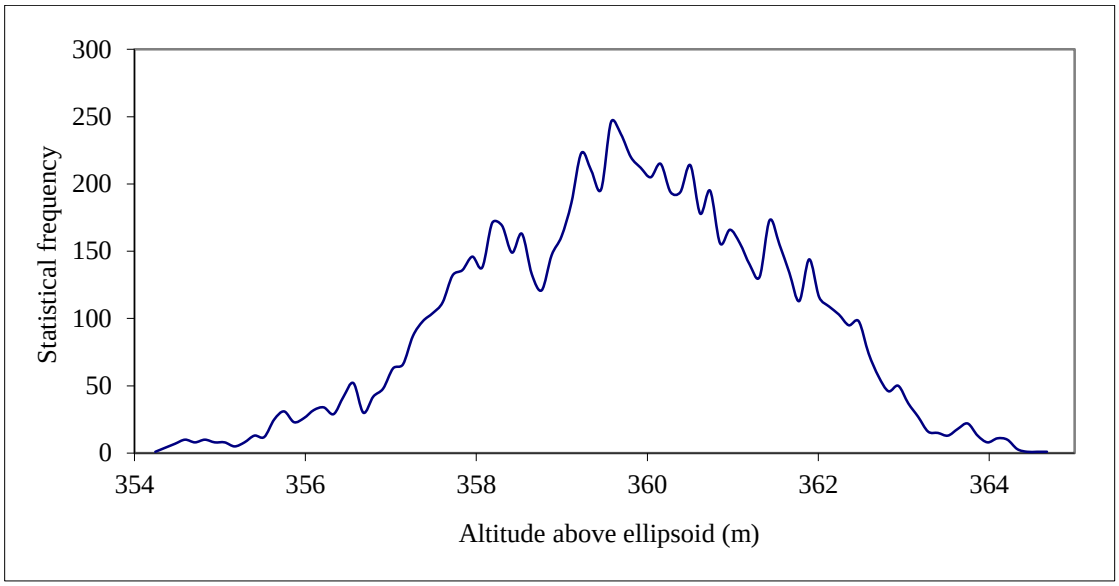

Figure 4.9: Vertical Height of DGPS measurement 04

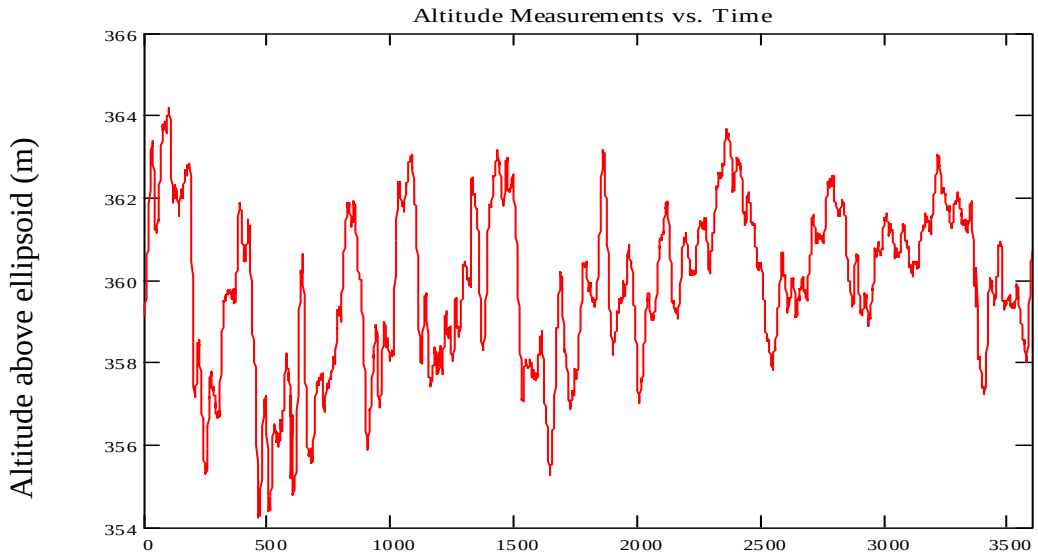

Figure 4.10: DGPS vertical (*z*) measurements 05

3.2 RFID sag detection and monitoring system

RFID sag detection system consist of two parts namely radar (reader) and a tag. The operating frequencies are classified into two which is Ultra High Frequency (UHF) 915 MHz and Microwave 2.4 GHz. For UHF the read range can read up until 40m whereas in microwave can read up to 1m because of its sensitivity to the environment. As mentioned on the theory, RFID tags can be classified in to active tag (battery assisted) and passive tag (without battery). In this dissertation passive tag is adopted. The radar sends the electromagnetic waves first to wake up tags, and then transmit the modulated wave to command the tag. It then absorbs power from the field generated by the radar and utilizes it to energize microchip circuitry. Radar will then transmit continuous wave while the passive tag backscatters the information. The operating modes of radar detection system can be divided into three parts that is to identify any new tag in its zone, locks on to the signal from the tag to determine its position and track the movement of the tag in the its zone.

The detection system assumes a tag attached to the power line. The tag has a unique 9 digit number. For example BCBBB0005 ID linked to a database and data transferred through link encoding. The class 1 and Generation 2 protocol used, binary data from radar to tag is encoded as pulse interval encoding of the low amplitude pulse. Data-0 is encoded by a 1/8 T_0 pulse width modulation, data-1 is encoded by 3/8 T_0 width modulation.

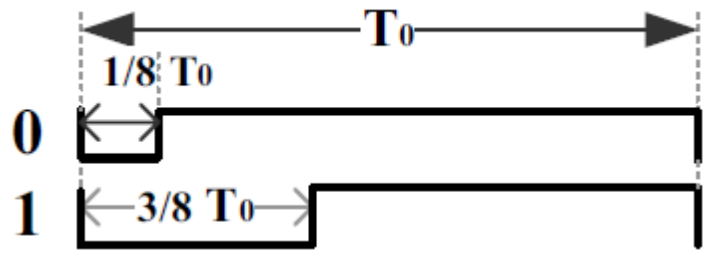

Figure 3.11: Class 1 Forward link pulse interval encoding

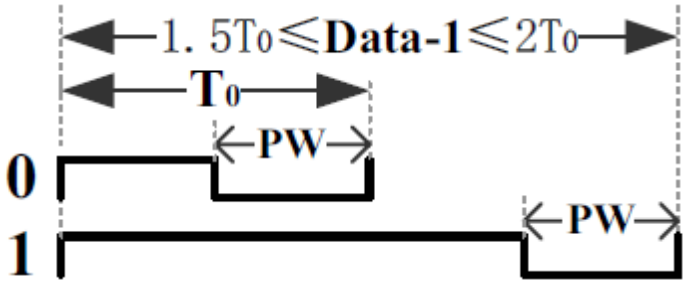

Figure 3.12: Generation 2 forward link pulse interval encoding

The duration of data-0 is T_0; the duration of data-1 is between 1.5 T_0 and 2 T_0. In class 1 protocol radar talk to tag via the amplitude shift keying modulation from 30% to 100% depth. While in Gen 2 protocol radar have to use double-sideband amplitude shift keying (DSB-ASK), single side amplitude shift keying or phase reversal amplitude shift keying and the 80% to 100% modulation depth.

Example of data linked to database

Time	Tag ID	Distance
22:45:08	BCBBB0005	19.2 m
22:45:08	BCBBB5002	0.5 m
22:45:08	BCBBB0026	31.6m
22:45:09	BCBBB0004	15.5m
22:45:09	BCBBB0002	3.1 m
22:45:09	BBBBB0000	8.8 m

Table 3.1: Example of data linked to database

3.2.1 Structure design of the monitoring system

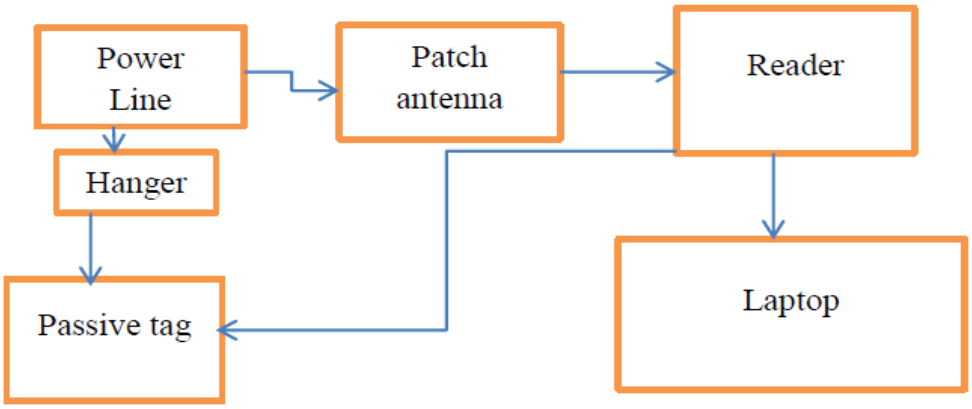

Figure 3.2: Block diagram of RFID sag detection system

Referring to Figure 3.2, the system operates at UHF frequency band allocated for RFID. It uses electric coupled propagation properties to transfer energy from the reader to the transponder and from the transponder back to the reader. The radar system measures the path length for signals travelling from the transponder to the reader to determine range. On comparing signals arriving at two identical receivers with close spaced antennas, the reader determines the angle of arrival of the signal from the transponder and the direction of that transponder from the reader. The system use three identical high gain patch antennas operating with horizontal polarisation. The line diagram in Figure 3.3 depicts the structure of a single span considered when designing the system.

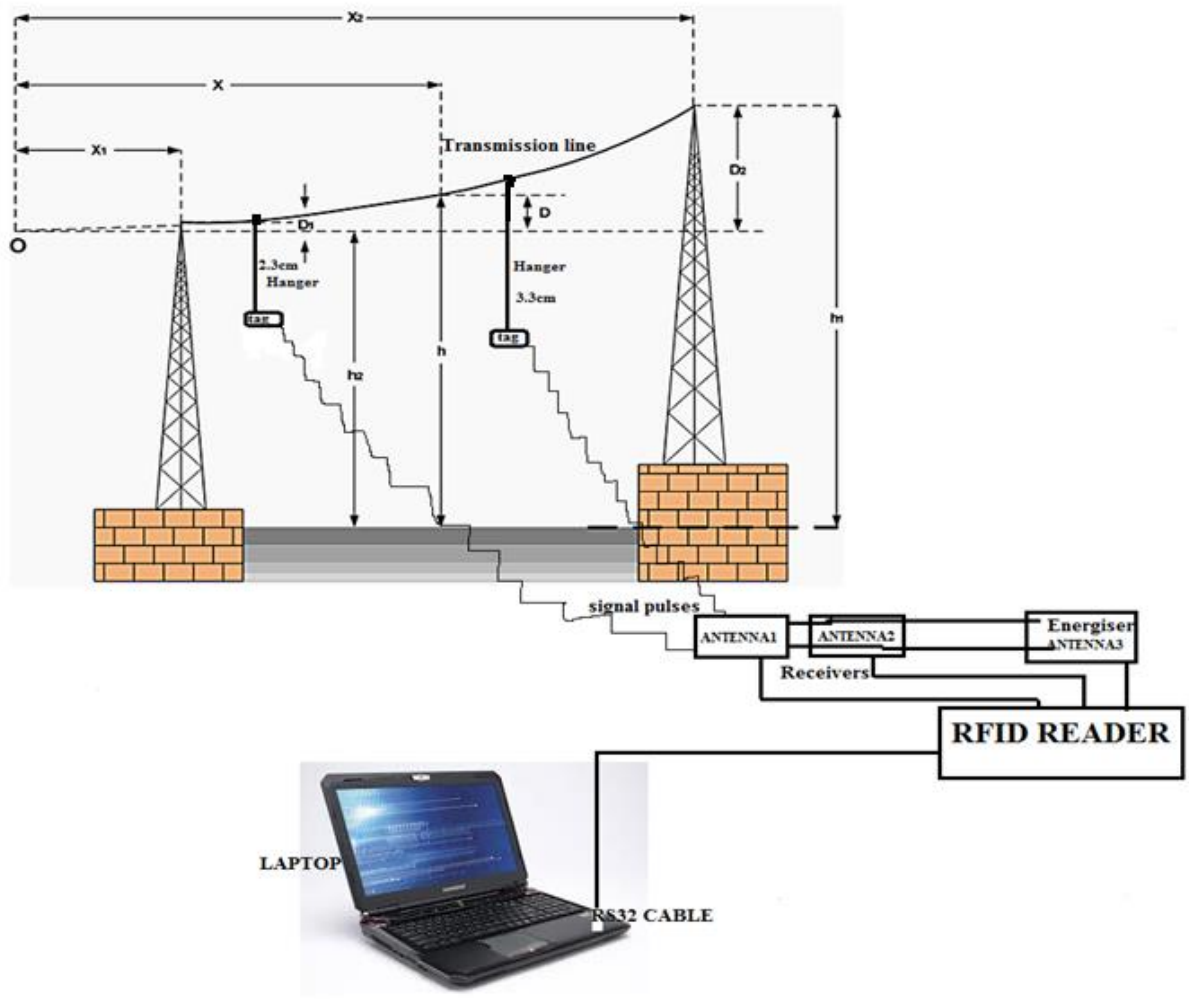

Figure 3.3: single line diagram for unequal supports with RFID sag detection system

3.2.1.1 Capacitance of transmission line

In high frequency circuits and long distance transmission lines capacitance **C** is actually proportional to the charging current drawn from the field of the line. This is an important factor when sag detection is done with RFID tag. Other variables such as inductance **L**, Voltage **V** contribute to the nature of response which will be received from the tag. As a result the more voltage applied to the line the more charge will be seen on the capacitor, which is predicted to be one of the constraints in RFID tag performance.

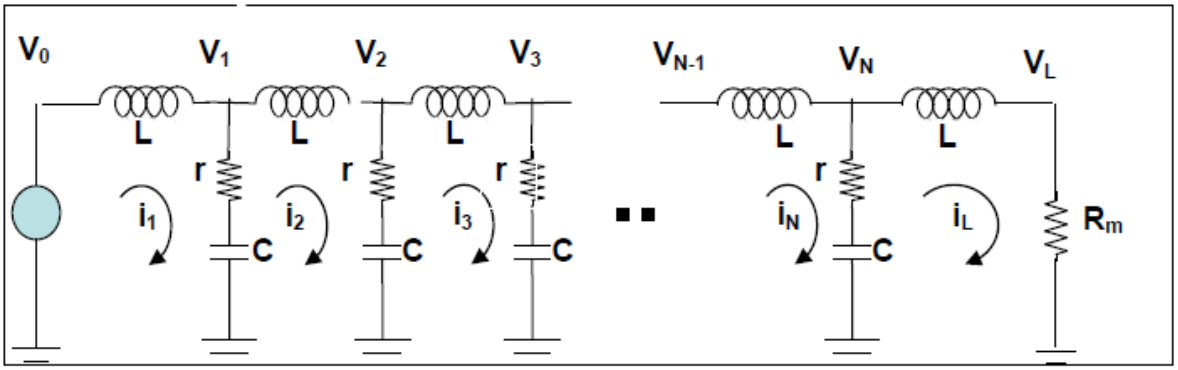

Figure 3.4: Transmission line circuit

This relationship is predicted that charge will be proportionally to the voltage applied to the conductor as seen by blue and the charge by red.

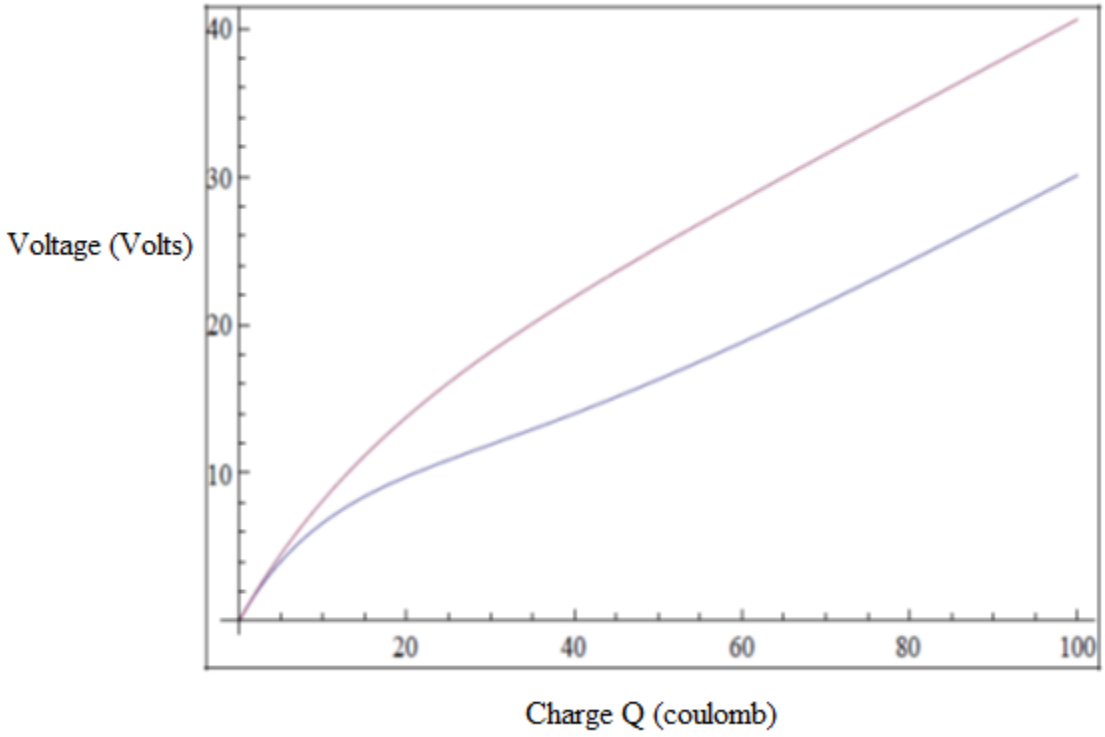

Figure 3.5: Capacitance charge voltage response

3.2.2 Principle of the monitoring system

One of the antennas is used for providing the energy field whereas the other two are used to receive the weak signals for the receiver. The spacing of the receiver antennas is important for calculating the angle of arrival. These antennas are 31 cm apart and the energising antenna 54cm from the right receive antenna. It must be mentioned that two antennas work as sensors and the third antenna work as an energiser which is mounted at the right.

The energising antenna is on the right behind the array and towards its direction of radiation so as to complement the function of energy signal such that;

$$E_f = \int_{-\infty}^{\infty} |f(t)|^2 \, dt < \infty \tag{3.50}$$

While the receive antennas are the centre antenna and the left hand antenna. Because the operation principle of energizer antenna uses the function of energy signals it can be represented by the signal expansion using a series of basic functions ($\varphi_n(t)$) because the response of a linear system to a complex periodic signal can be found by linear superposition of the responses of simpler inputs. Let τ be the time interval and C_n the coefficient expansion, then,

$$\int_{t_1}^{t_1+\tau} \varphi_m(t) f(t) dt = \sum_{n=0}^{\infty} c_n \int_{t_1}^{t_1+\tau} \varphi_m(t) \varphi_n(t) dt \tag{3.51}$$

The RFID radar is set to make two measurements on each signal received from each transponder in its receiving zone - namely a range measurement and an angle of arrival. Taking the range measurement with narrow bandwidth, the performance of the system will make this an outstanding unique RFID instrument for sag detection. The system uses the same transponders that are used by conventional RFID readers allowing RFID radar to monitor the same transponder simultaneously.

Light and radio waves travel at the speed of light, namely 300 000 000 meters per second. RFID systems need to operate in a crowded RF spectrum, where other RFID systems, cell phones, radio

stations and other communication users have to share the available radio spectrum. RFID-radar uses just 10 kilohertz of bandwidth to operate, meaning we are able to detect time differences only as small as 0.1 milliseconds, or 0.0001 seconds. In this time the radio wave will travel 30 kilometers, or 30 000 meters or 3 000 000 centimeters; yet the radar is able to determine the range of the transponder based on its received transmission to an accuracy of a few centimeters, or nearly 1 million times better than its basic time measuring properties. If conventional military radar approach is employed and expecting to get centimeter precision, then the time of flight measurement has to be done in the precision of 0.3pico seconds (.3*10-12) which would use 300GHz spectrum. RFID radar pays for this million times improvement in the timing accuracy of the basic system by taking a longer time to determine the exact position. As a result it is well suited to static situations where transponders are relatively stationary like suspended on the overhead transmission line for sag detection. However developments are in progress to address the accurate tracking of movement by adapting some of the principles of operation. The angle of arrival measurement is virtually instantaneous and used in conjunction with range from a single measuring location.

The system measures range by calculating the distance a signal from the transponder has travelled to the reader. To acquire correct measurement the reader determines delays through the antennas and time to travel through the cables and the amplifiers. The delay of the signals from the stick tags is slightly different from that of the claymore tags hence the stick tags are very good in calibrating. They have the same radiation pattern as a dipole but with the battery assistance for power usage.

The radar is able to resolve angles based on the 31cm spacing of the receive antennas of the negative 30 degrees to positive 30 degrees. Should it happen that the transponder is beyond those

angles, that particular tag will be read and displayed with the negative angle. For the tag moving from the left to right at 10 degrees per reading, the angles are displayed as follows:

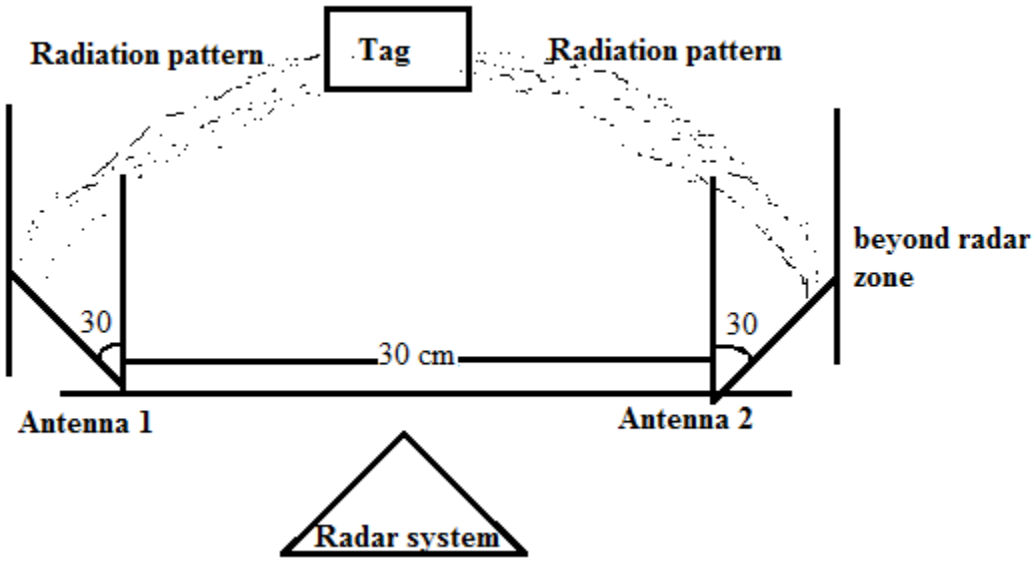

Figure 3.5 Radar angle positioning in degrees

- ✓ -30 degrees
- ✓ -20 degrees
- ✓ -10 degrees
- ✓ 0 degrees
- ✓ 10 degrees
- ✓ 20 degrees
- ✓ 30 degrees
- ✓ -20 degrees ALIASED
- ✓ -10 degrees ALIASED

The hanger used to suspend a tag from the transmission line under 11KV is a non-conductor strain insulator. This is suspended about 2.3cm below the midpoint of the span. The midpoint of the span where the sag is at lower point is determined by the sag equation;

$$D = \frac{wl^2}{8T} \tag{3.52}$$

The D value is regarded as the lowest point caused by the weight of the conductor. For equal spans this becomes the target point of the tag placement which is within the reader zone.

3.2.3 Selection of tags

A common tag implementation consists of an electronic microchip that stores data and executes the tag's functionality, an antenna that performs the function of receiving and transmitting RF energy, a tag powering circuit that utilizes the RF power from the reader to power up the microchip, and substrate into which the whole tag is built upon. The tag integrated circuit controls the tag operations according to the reader's commands and the communication protocol. Tag antenna receives readers continuous wave (CW) during the readers powering up phase. The tag powering up circuit rectifies this CW signal from the reader and further delivers it to its integrated circuit (IC). Powering up phase of the reader transmission is followed by the command transmission phase in which modulated RF is sent by the reader as command signal. The powered up tag IC executes the reader's command. After the reader has transmitted its command, it again starts to broadcast a continuous field again which the tag will modulate and backscatter again as its response to the reader's command. The modulation then is produced by switching the tag's antenna matching. The Figure 3.6 shows the communication principle of tag to reader.

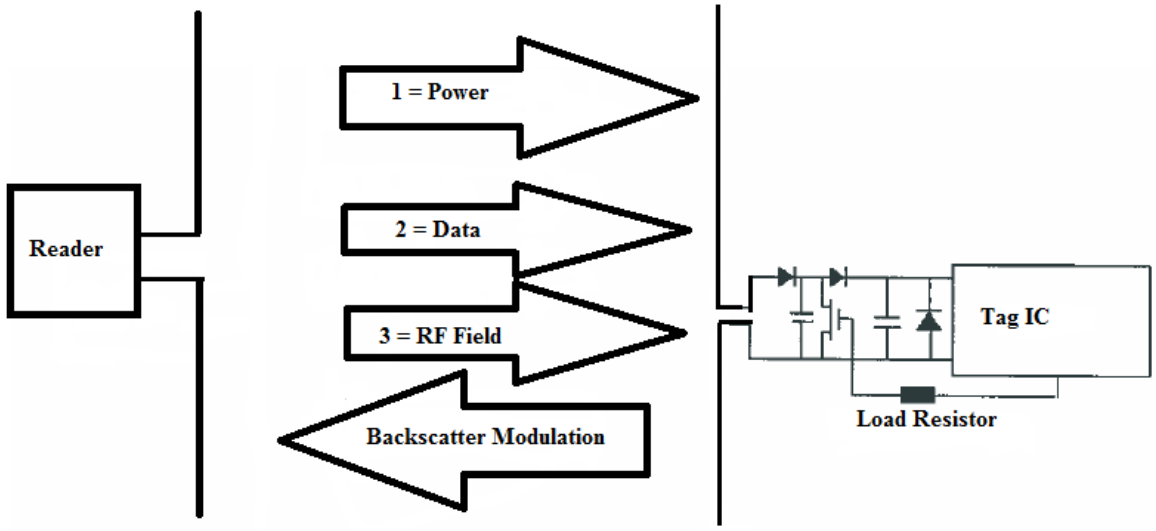

Figure 3.6: communication principle of a tag

The communication of tag, as response of the tag to the reader's query identity (ID) command depends on whether reader is operating in global scroll or inventory mode. The query ID command format from the reader depends upon these modes and depending upon which format is used in the reader data field, the tag response will take one of the two possible forms. The global scroll command is intended to identify one tag at a time and the tag response to this command is generated in the form of tags identification code in the wheel, which includes both the tag' electronic product code (EPC). In case of inventory mode of the reader goes through all possible code combinations with the minimum number of readings using an anti-collision algorithm. Each reply of the tags includes a 15bit part of its EPC defined in the reader's command code. Passive transponders are in a form of credit card sized offering the range up to 18m. Battery assistant does not operate on the dedicated frequency. They operate over the frequency range of 100 MHz, and allow many types of radar systems to determine their range at the same instant, even if radars are operating on slightly different frequencies. These transponders do not radiate any energy and are not transmitter type of devices.

Claymore types are active tags since they are battery assisted. They are generally mounted on a large piece of plastic and are made to be attached to a large item, such as a container. They use the nearness of the large item as part of the antennas to focus additional energy onto the sensitive part of the antenna and in doing so, is thereby increasing the range. These transponders have a direction of radiation marked on the transponder. The advantage of active tags is that they provide longer read range and can perform other functions apart from the reader's request, although they are costly.

Stick type transponders and credit card type transponders radiate energy equally around the center longitudinal axis. These are passive tags which have an advantage of not requiring any external power source like active tags. In the dissertation credit card passive are used to test the system operation in different conditions. Clay more and stick tags are used to determine the precision measurement and detection errors.

3.2.4 Backscattering of the system

The major components of a backscattering passive system are readers, tags and an application host. RFID radar mainly comprises of a set of antenna, a radio interface, a control unit and a powering unit. The antenna performs the function of transmitting and receiving the electromagnetic energy used for communication and powering the tags, within its range in that a signal transmitted is finite average power, P. For signal $F(t)$ at time interval from $t1$ to $t2$.

$$P = \frac{1}{(t_2 - t_1)} \int_{t1}^{t_2} \left| f(t) \right|^2 dt. \tag{3.53}$$

It satisfies that

$$0 < \lim_{T \to \infty} \frac{1}{T} \int_{-\frac{T}{2}}^{\frac{T}{2}} \left| f(t) \right|^2 dt < \infty \tag{3.54}$$

The radio interface performs the job of detection, modulation, and demodulation of the RF signal. The control unit executes the communication protocol with the tags and interprets the data received from the tags. In performing all the above-mentioned functionalities, the reader communicates with the tags within range as directed by the application host and reports the results to the host.

3.2.5 Interference problem

Passive UHF RFID system operates by a very steady manner of energizing signal which is received by the tag, converted to direct current (DC) power which powers the tag. This is a carrier wave signal that has minimal modulation and causes virtually no interference to the system on frequencies adjacent to the operating one. As the data from the tag to the reader sent back by backscattering modulation in such that antenna impedance of the tag is altered by the data to be transmitted, causing differing amounts of energy to be reflected by the tag back to the reader. This in most cases result the data to be reflected at virtually the same frequency as the energizing field and therefore cannot be detected to any other equipment that the reader provide the energy field. As the energy from the transmitter leaves the antenna it travels away at the speed of light, in various directions at instant. The Figure 3.7 presents area surface of 1m and 2m of antenna sphere.

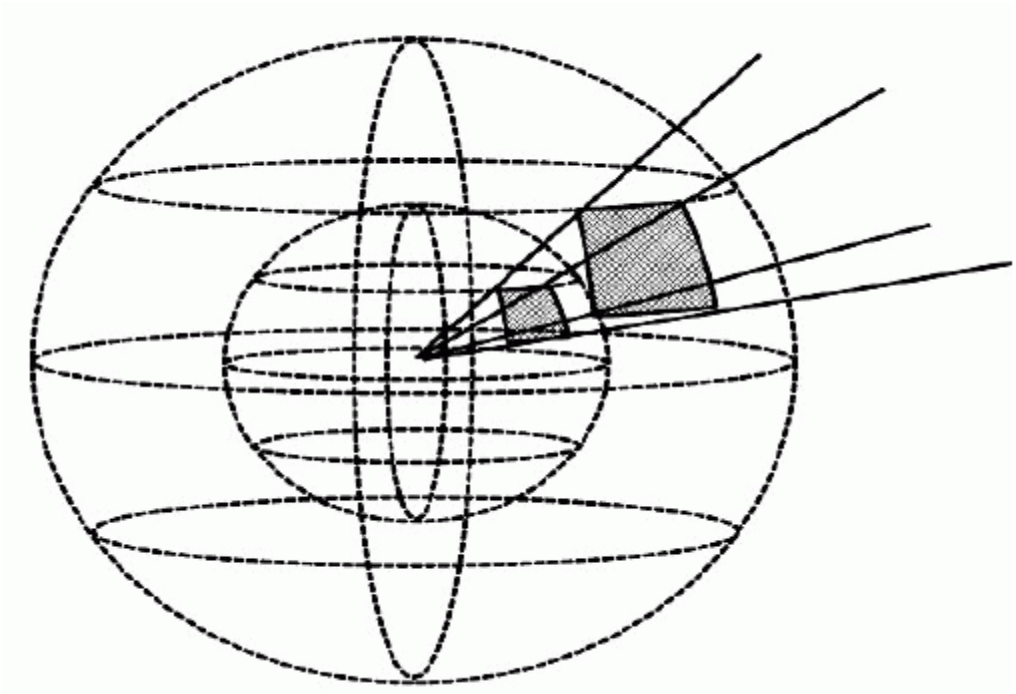

Figure 3.7: Area surface of the antenna sphere

The bigger shaded area marked in the Figure 3.7 is the surface area of the cell on 2m sphere and the other small shaded area is the surface area of a cell on a 1m antenna sphere. By the time the energy gets 1m away from the antenna, the Power density P_D will be as follows:

$$P_D = \frac{P_T}{4\pi r^2} \tag{3.55}$$

Where P_T power transmitter and r is the sphere radius of 1meter.

Compared to the old historic tags or transponders systems, UHF tags operate over ranges that are doubling the wavelength of their operating frequency. The Figure 3.8 shows signals arriving at a point without any shifting phase difference.

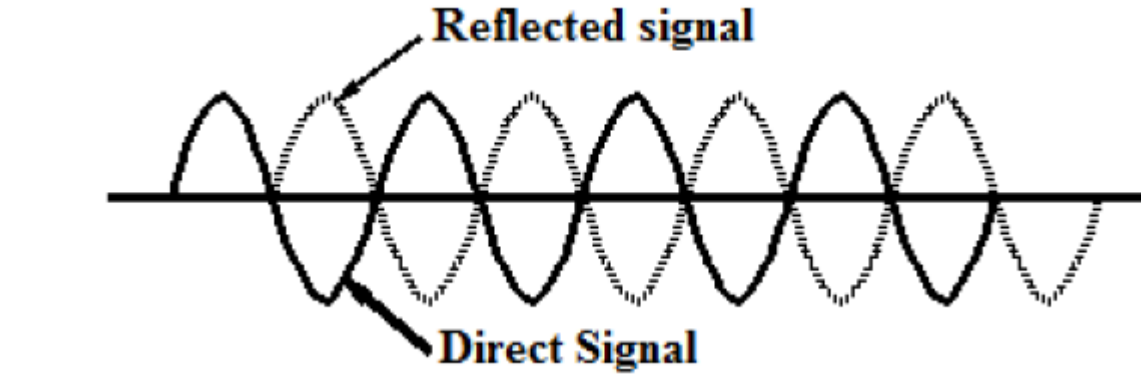

(a)

(b)

Figure 3.8: Signals arriving in an in-phase manner

Figure 3.8(a) depicts direct and reflected signal in an in-phase manner, and Figure 3.8(b) is the vector sum of the direct and reflected signal. In a situation where signals from the energizing antenna arrives at a point directly and a signal bounces off a reflecting surface and travels the same distance with an additional half wavelengths, the resulting zone can have no energy despite it being close to the antenna. The zones are only a few centimeters wide and by just moving the tag or the energizer antenna, or chanting the angle of the antenna to weaken the reflected signal somehow rectifies the problem. This is illustrated in Figure 3.9.

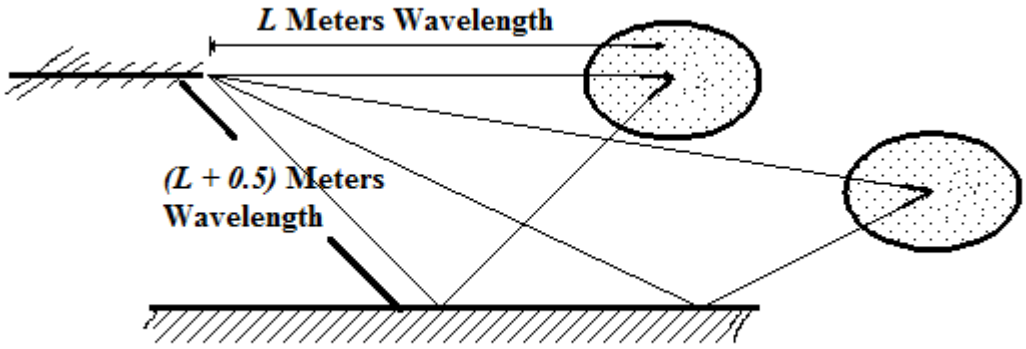

Figure 3.9: The shifting of the energizer angle

The same situation can possible be seen in a case of signal back from the tag to the sensing antenna. For this phenomenon to occur a good reflecting surface is needed. In the scenario where the tag and the reader are moving relative to each other, the hole problem is not significant as even though it might be in few times where the tag is in holes, with relative motion which will cause the location of the holes to move and power will be restored to the tag.

3.2.6 Effect of mounting the antenna

As the antennas radiates and receive electromagnetic energy into the air. The property of the resulting signal is polarization. Here in Figure 3.10, we illustrate two polarizations examined in our antenna study.

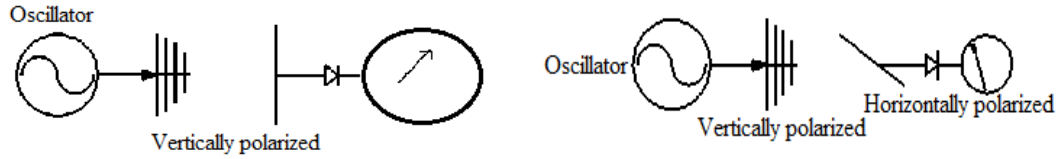

(a) (b)

Figure 3.10: Vertically and horizontally polarized antenna

In order for the tag to receive energy and send it back in a form of signal to the sensor antenna, all the three antennas which were connected horizontally need to be operating on the same polarization. When one of the antennas has the wrong polarization, more especially the energizer antenna and the tag antenna, no energy is transferred to the tag and therefore resulting the system the non-operating. This illustration is depicted in Figure 3.10 (b).

The amount of energy available to a tag varies with the range from the energizer antenna. The antenna on the tag collects the radio frequency energy that falls on around the tag. As the range increase from the energizing antenna the area of the sphere centered on the energizing antenna increases as shown in Figure 3.11.

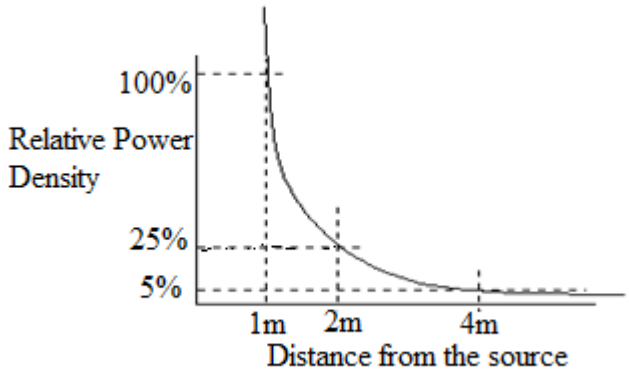

Figure 3.11: The variation of the amount of energy in the antennas

A tag within 4m range will only collect 5 percent of the energy collected by a tag at 1m. It is clear that a tag needs to operate at a very low power to give a better range and have a wide operating

voltage to allow it to work close to energizer antenna. It can be conclude that at a very close range a tag might overload and stop working.

3.2.7 Effect of attaching the tag on the conducting or non-conducting material

The tags used in the proposed system, credit type passive tags are used which can read up until 18meters range. When UHF radio wave is travelling through medium and encounter a surface of a different material that is large compared to the wavelength of the radio wave, some of the energy is reflected at the interface and some is transmitted through the new medium. Whenever the radio signal travelling through medium encounters an object with a different dielectric constant, it causes some of the energy to reflect therefore thwarting it not to reach the intended tag. The objects are to be sizable compared to the wavelength of the signal (32cm at 915MHz) for the impact to be notable. The reflection from the items such as wood, paper, cement, and ceramic is similar to the reflections got from the conducting materials such as steel conductor or water. The sensitivity of the tag for a dipole type antenna, operating at 915MHz, would be $132cm^2$.

3.2.7.1 Effect of attaching the tag on the conducting material

At the surface of the metal where the signal that travel through the air meets the metal conductor, the signal is reflected from the metal back towards the reader and this signal has the opposite phase angle to the incoming signal which then cancels the incoming signal at the surface. A few millimeters away from the metal conductor a signal exists and can initiate a talk with the tag. The Figure 3.12 shows the impact of mounting the tag at a small distance away from the metal conductor, using some spacing material that has a dielectric constant similar to air.

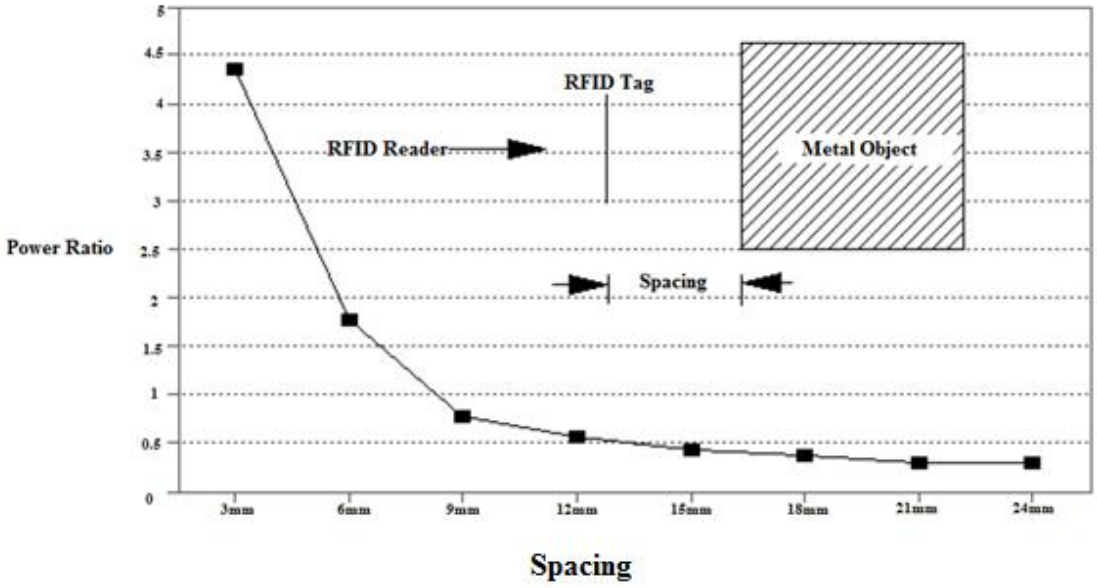

Figure 3.12: RFID tag performance on a metal conductor [19]

On the y-axis, the value "1" refers to the power needed to operate the tag at the same distance if it was mounted in the medium air environment. From the graph, it can be seen that with a 3mm air layer between the tag and the surface of the metal, a tag designed to operate on 1milliwatt in free space will need 4.3milliwatts in that situation of a metal to operate. Keeping the same operating range, the reader power could be increased by 4.3 fold or if the reader power is kept constant the operating range will decrease by 48percent. From 8mm onwards the sensitivity is better-off than that of free space giving additional range by the lowering the reader power. At 15mm a tag that needed 1milliwatt in free space would need only 0.5 milliwatt if mounted on this metal surface.

3.2.7.2 A tag attached on the wood

Non-conducting materials such as wood and paper seem to have impact on the operating of the tag when the sensitivity of that material is considerable to the wavelength of the signal. In the case of

these materials, the reflection from the surface is not so bigger in such that it require much greater power for the tag that is close to the surface and at some instance at further distances, they do not give sensitivities that are much better than that which we achieve in free space. This performance is shown on Figure 3.13.

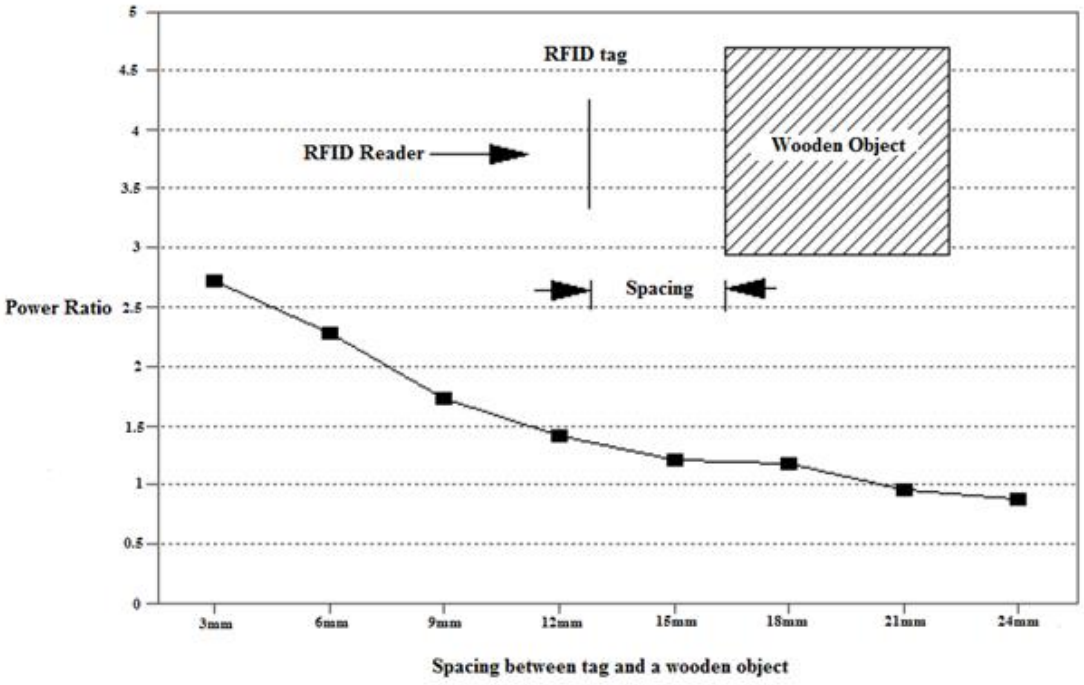

Figure 3.13: Tag performance on the wooden object [19]

3.2.7.3 Mounting a tag on a wet body

It is imperative also to examine whether the blood flow in human body, which is also an electrical path to the ground, could possibly have the impact on tag performance. This needs a further study in future. However Figure 3.14 shows a graph that depicts a performance.

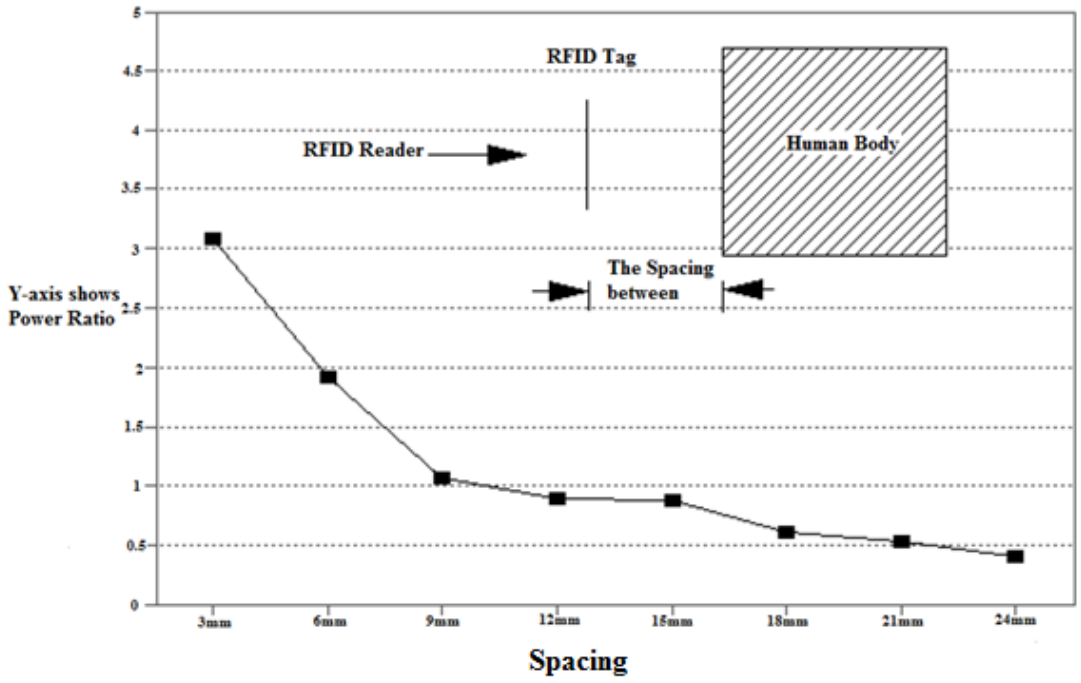

Figure 3.14: RFID tag performance on a human body [19]

Figure 3.14 show that the high water content body or flesh which is close to the tag impacts the operation of the tag. Hot sweating bodies kill the RF signals close to the skin.

3.2.7.5 Tag on the paper

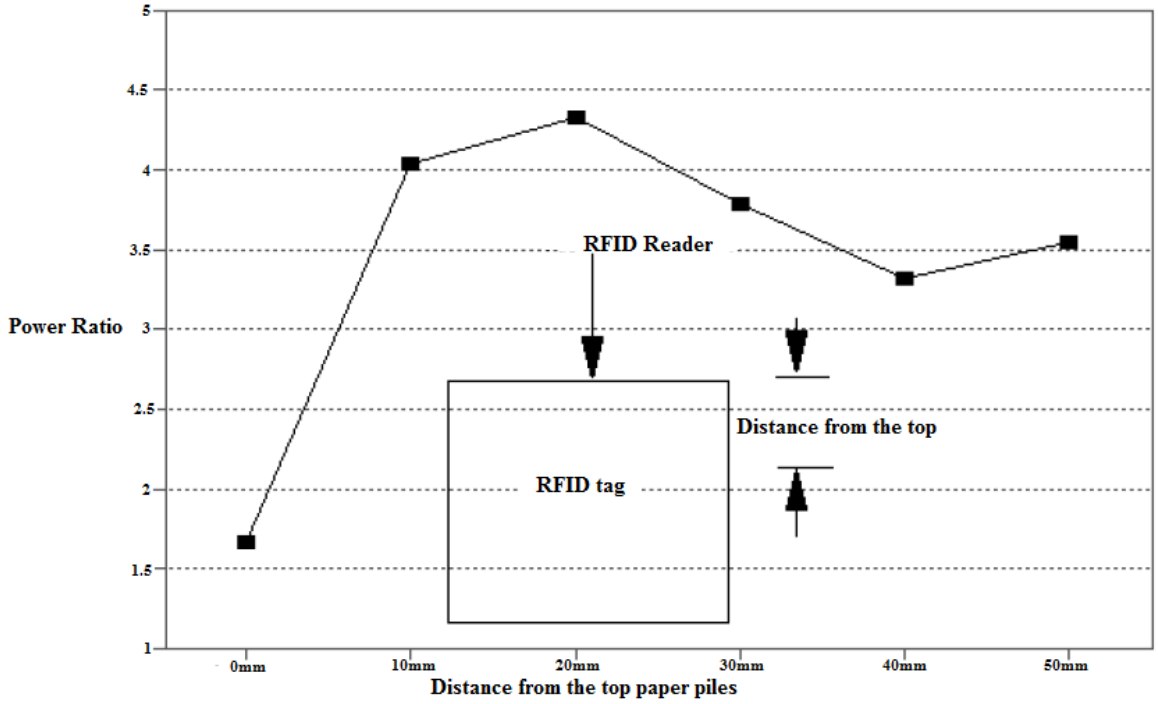

Figure 3.15: Tag performance on piled stack of papers [19]

The paper has a different dielectric constant from that of air meaning that at the interface between the paper and the air, energy will be lost as it will be reflected away. The energy would then travel through the paper to the tag. In Figure 3.15, we can compute this tag performance as if it is on air by attaching it on the paper. From then it is seen that, at about 10mm to 50mm below the surface of the paper piles, the energy goes between, 3.5 to 4.5 higher than that needed for the freely spaced tag.

3.2.8 RFID tag positioning in three dimensions

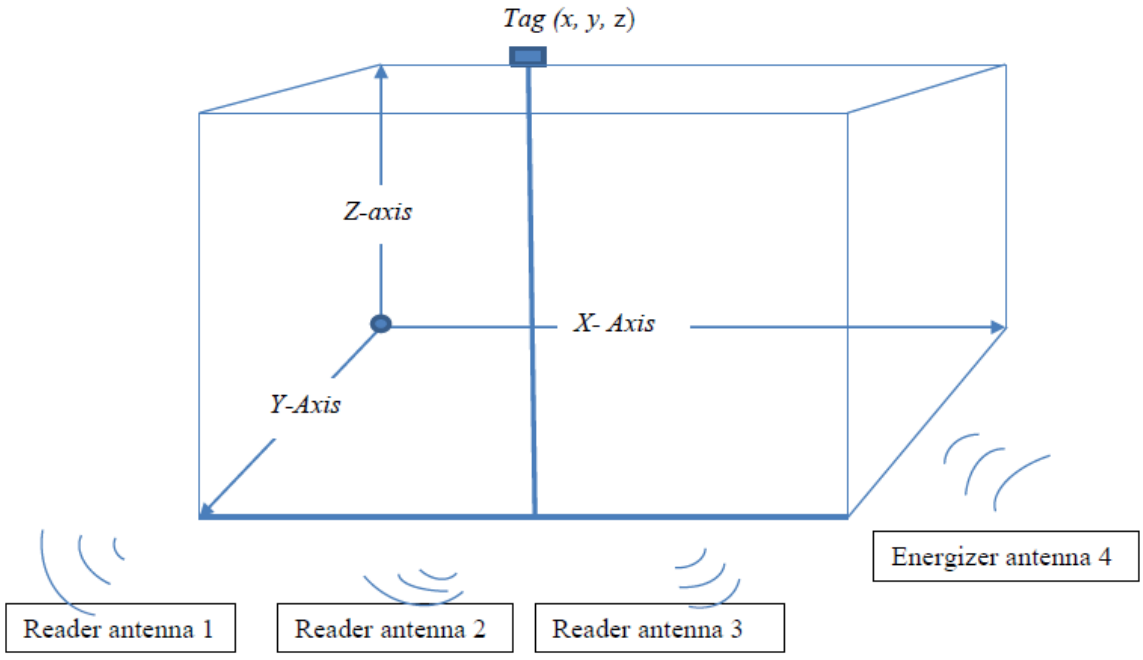

(a) Reader with three patch antennas and one energizer

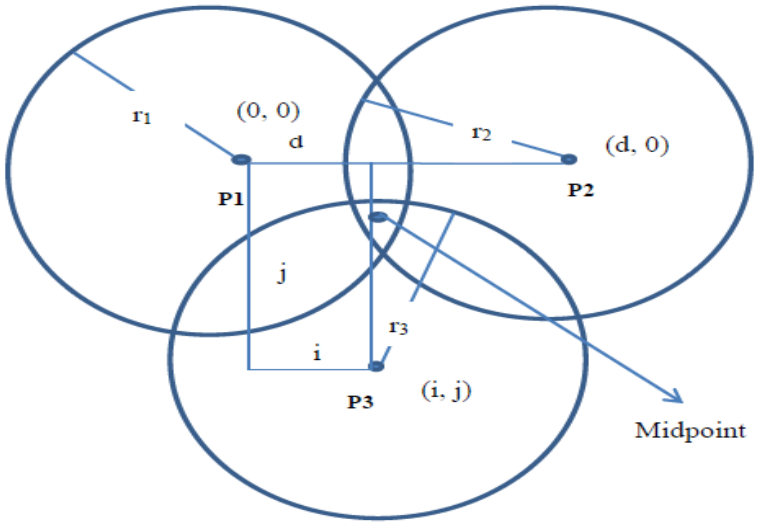

(b) Intersection of surface circles

Figure 3.16: Three dimension tag positioning

From Figure 3.16, the intersection of the three circles is found by formulating the equation for three surfaces and solving for the unknown variables of x y and z. From Figure 3.16 (a) we have x as the horizontal plane, y the vertical plane, and z the third dimension. The formation is in such that one point is at the origin and another point is on the x axis. To find the third dimension of the tag position, three receiving antenna are used. This process is simplified having the center of the circle placed on the $z = 0$ plane. The radius of the circle is denoted by r, the diameter d and P the circle. The first circle is represented by,

$$r_1^2 = x^2 + y^2 + z^2 \tag{3.56}$$

Establishing the second circle we have,

$$r_2^2 = (x-d)^2 + y^2 + z^2 \tag{3.57}$$

The radius of the third circle is then written in terms of the coordinates(i, j), i is the horizontal vector of P3 and j is the vertical vector of P3.

$$r_3^2 = (x-i)^2 + (y-j)^2 + z^2 \tag{3.58}$$

To obtain x we subtract equation (3.54) from (3.53),

$$x = \frac{r_1^2 - r_2^2 + d^2}{2d} \tag{3.59}$$

Assuming that the first circles intersect at more than one point then we have

$$d - r_1 < r_2 < d + r_1 \tag{3.60}$$

Substituting equation (3.56) in to (3.53), we have

$$y^2 + z^2 = r_1^2 - \frac{\left(r_1^2 - r_2^2 + d^2\right)^2}{4d^2} \tag{3.61}$$

Re-writing equating (3.53) in terms of z we have

$$z^2 = r_1^2 - x^2 - y^2 \tag{3.62}$$

Substituting (3.59) in to (3.55)

$$y = \frac{r_1^2 - r_3^2 - x^2 + (x-i)^2 + j^2}{2j} = \frac{r_1^2 - r_3^2 + i^2 + j^2}{2j} - \frac{i}{j}x \tag{3.63}$$

Having found x and y, the z-coordinate is found by rearranging the formula for the first circle.

$$z = \pm\sqrt{r_1^2 - x^2 - y^2} \tag{3.64}$$

3.2.9 Triangulation Method

Based on the accuracy features of the RFID radar system, i.e. low absolute accuracy but high relative accuracy, triangulation method is proposed making use of multi-station measurements. To reduce the cost, only a pair of receiving and sending antennas is needed. The receiver is moved to imitate multi-station radar system. Four measurements are made for positioning a tag. Complete 3D coordinates are calculated which high accuracy, which are valuable to evaluate the line to line and line to environment clearances. By detecting time of flight RFID radar has the ability to calculate the distance between the station and tags. For multi-station system the location of tags can be calculated by triangulation method. In fact, it is difficult for current technology to measure tiny time unit, such as picoseconds that the signal travelled between a station and a tag with ten meters distance. The time spent by individual tag to respond into the reader instruction is also different. Therefore the range measurement is not accurate. The method rely on the signal strength has the similar problem because the environment factors may affect the attenuation. RFID have significant when measure absolute distances (about half meter errors), however, may have much better accuracy (millimeter errors) for relative distance. According to this feature of RFID system, this research also detects the tag position by moving the reader for relative distance measurement and then using triangulation method to calculate the position.

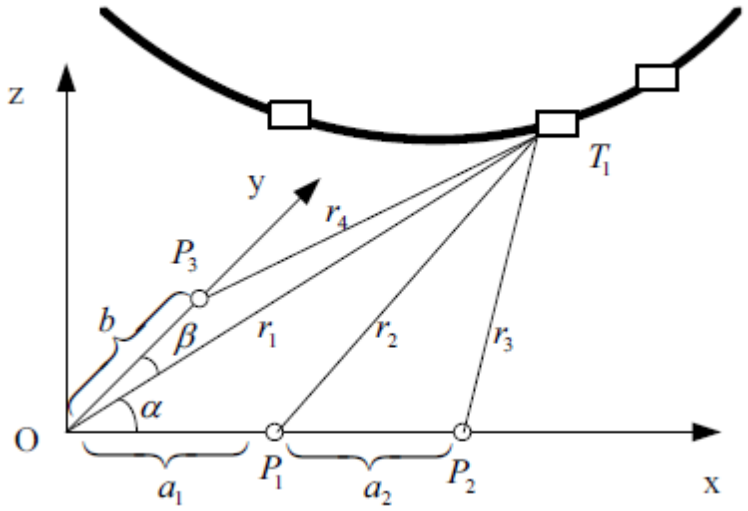

Figure 3.17: Triangulation of the proposed method

Figure 3.17, depicts the principle of the proposed method. In this method, tag T1 is stuck on a power line, the receiving antenna moves on ground points O, P1, P2 and P3. If assume O is the origin, then P1 and P2 are located on x-axis, P3 is on y-axis. The positions of P1, P2 and P3 can be exactly measured. The distances between T1 and these measures points are measured. According to the cosine theorem of triangles, in $\triangle T_1OP_1$, we have;

$$2r_1a_1\cos\alpha = r_1^2 + a_1^2 + r_2^2 \tag{3.65}$$

$$\cos\alpha = \frac{r_1^2 + a_1^2 + r_2^2}{2r_1a_1} \tag{3.66}$$

Considering triangle $\triangle T_1OP_2$

$$2r_1(a_1 + a_2)\cos\alpha = r_1^2 + (a_1 + a_2)^2 - r_3^2 \tag{3.67}$$

$$\cos\alpha = \frac{r_1^2 + (a_1 + a_2)^2 - r_3^2}{2r_1(a_1 + a_2)} \tag{3.68}$$

To be noted that the absolute values of r_1, r_2, r_3 and r_4 cannot be accurately measured. Fortunately the differences between them are much more reliable, such that:

$$\triangle r_1 = r_2 - r_1 \tag{3.69}$$

$$\triangle r_2 = r_3 - r_2 \tag{3.70}$$

$$\triangle r_4 = r_4 - r_1 \tag{3.71}$$

$$r_3 = r_1 + \triangle r_1 + \triangle r_2 \tag{3.72}$$

Substitute equation (3.67) to equation (3.65), one gets

$$\cos\alpha = \frac{r_1^2 + (a_1 + a_2)^2 - (r_1 + \triangle r_1 + \triangle r_2)^2}{2r_1(a_1 + a_2)} \tag{3.73}$$

From equation (3.63) and equation (3.73),

$$\frac{r_1^2 + a_1^2 + r_2^2}{2r_1a_1} = \frac{r_1^2 + (a_1 + a_2)^2 - (r_1 + \triangle r_1 + \triangle r_2)^2}{2r_1(a_1 + a_2)} \tag{3.74}$$

r_1 Can be derived as follows

$$r_1 = \frac{a_1a_2(a_1 + a_2) + a_2 \triangle r_1^2 - a_1 \triangle r_1(2\triangle r_1 + \triangle r_2)^2}{2(a_1 \triangle r_2 - a_2 \triangle r_1)} \tag{3.75}$$

$$\alpha = \arccos\left(\frac{r_1 + (a_1 + a_2)^2 - (r_1 + \triangle r_1 + \triangle r_2)^2}{2r_1(a_1 + a_2)} \right) \tag{3.76}$$

From Equation (3.68) we have

$$r_4 = r_1 + \triangle r_4 \tag{3.77}$$

In $\triangle T_1OP_3$

$$\cos\beta = \frac{r_1^2 + b^2 - r_4^2}{2r_1 b} \tag{3.78}$$

$$\beta = arc\cos\left(\frac{r_1^2 + b^2 - r_4^2}{2r_1 b}\right) \tag{3.79}$$

Since the Cartesian coordinates are convenient to calculate the distance to ground and the distances between power lines, the derived position is converted to $T_1(x, y, z)$ by the following equations.

$$x = r_1 \cos\alpha \tag{3.80}$$

$$y = r_1 \cos\beta \tag{3.81}$$

$$z = \sqrt{r_1^2 - x^2 - y^2} \tag{3.82}$$

z is the distance from the power line to ground. The tag stores the information of which phase power line it is sticking, so by the coordinates of tags it is easy to calculate the distances between the power lines. A trilateration simulation is tried with three tags at different positions in Figure 3.18.

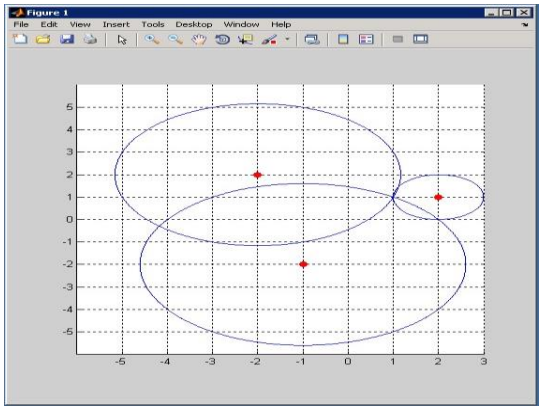

Figure 3.18: 2D trilateration simulation

Location of tag 1 on power
line; coordinates: [-2, 2]

Location of tag 2: [2, 1]
Location of tag 3: [-1, -2]

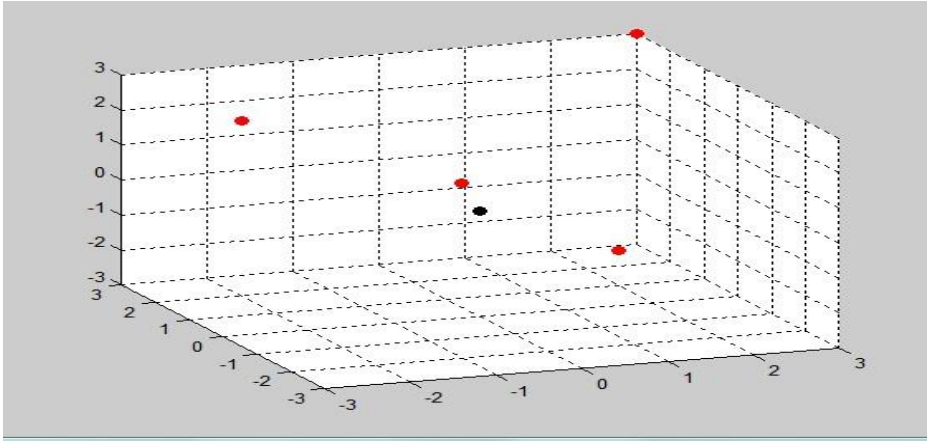

Figure 3.19: 3D trilateration simulation

Location of tag 1:

[-2, 2, 2]

Location of tag 2:

[2, 1, -1]

Location of tag 3:

[-1, -2, 2]

Location of tag 4:

[3, 3, 3]

Although tags are located at different heights, radar still identifies them correctly in both sides. Test 1 was viewed at the measurement of 7.5 meters. Test 2 at 1m, test 3 at 9m, and test 4 at approximately 5m. As Figure 3.20, depict the results are non- consistent yet some are closer to actual approximated measurable values. It can be seen that test 3 produce the most accurate

representation of distance compared to how far apart the tag and the radar can be. Test 4 also shows similar results.

The system was simulated at different lengths to also see how accurate the readings would be depending on the distance between the tag and the radar. This is one of the main reasons to why the distances vary each test. Another reason is to test the theory that at further distances, the readings would become more accurate rather than at closer distances. For this test, that theory was proven to be true.

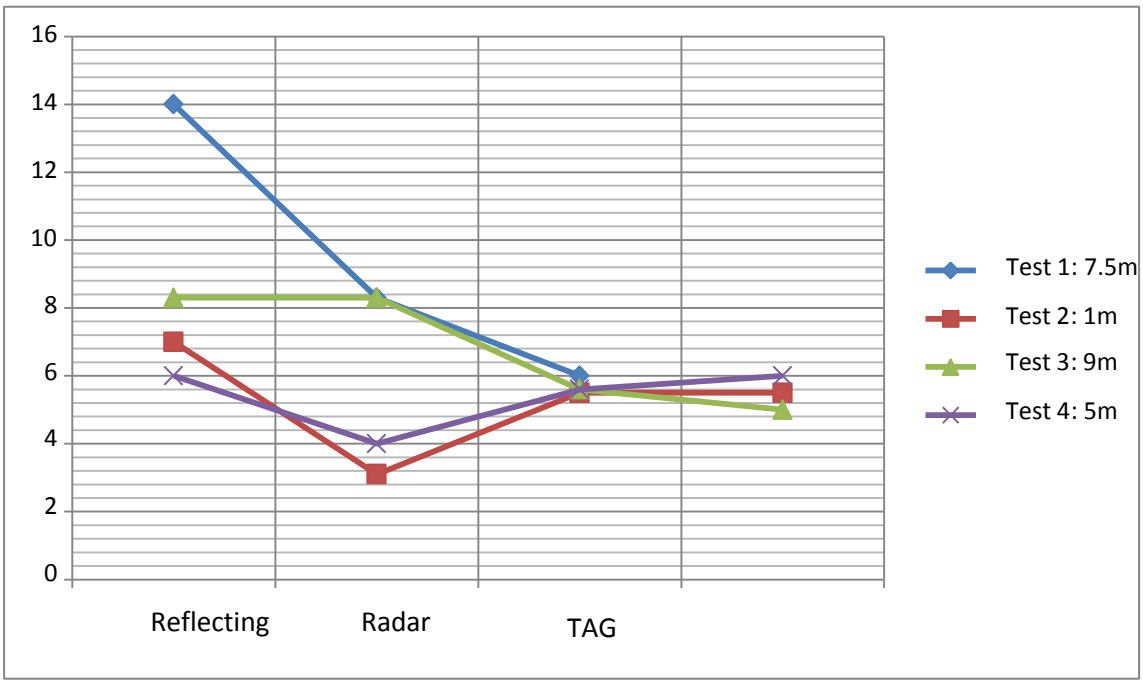

Figure 3.20: Varying distance between radar and tag

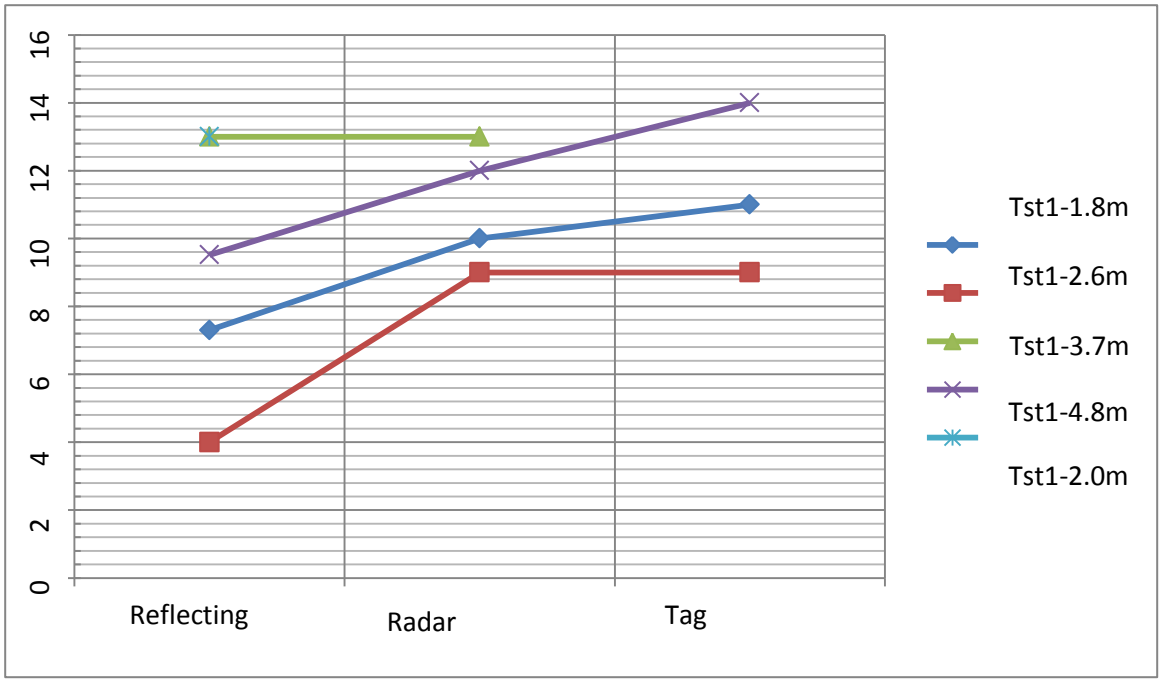

Figure 3.21: Distance between radar and tag

3.2.9.1 Summery of the proposed RFID sag monitoring system

The proposed system has the capability to monitor sag as long as the tag is present within the radar zone, by moving the antenna receivers up to 30 degrees. The performance of the system virtually depends on the amount of power a tag receives. This means that for a better performance battery assisted tags are needed. Although passive tags gain advantage over the active tags by their long life span, their drawback is that they are easily affected by most of environmental factors such as temperature, pressure, tension, and stress.

3.3 Evaluation of the proposed RFID sag monitoring system

The designed radar system can operate in different modes depending on the required data output. Acquisition mode is the method which we use to read tags in the reader field. There are two distinct methods for reading tags that is global scroll and inventory. The choice of one method over another depends on the application at hand.

Global scroll is the most primitive of tag identity (ID) reading operations. When a global scroll command is issued, the RFID Radar sends a single command over the air to each tag. This command is simply a request for any tag to immediately send back its ID to RFID reader.

There are advantages and disadvantages in this method. The command is very quick to execute as it involves only one round trip between the reader and the tag. However, because the command is so simple, problems arise if there is more than one tag in the field. At this point in time, multiple tags will all receive the same command and will all send back their ID's to the reader at virtually the same time all together. A situation such as this makes it difficult for the reader to discern individual ID's among the general noise of them all. Typically one or two of the closest tags will be decoded, but the majority will not be discerned due to collision.

On the other hand inventory command was examined. It is a full featured system for discerning the ID's of multiple tags in the field at the same time. This single high-level command transforms itself into a complex series of reader-tag interrogations that eventually resolve themselves into a single list of tags ID's seen by the RFID reader. This method of interrogation and evaluation of multiple tags seems to be opposite to the former hence anti-collision. These algorithms are far more complex than the global scroll algorithm, requiring many more readers' tags instructions.

Tag read mode was also examined in the research. There are two methods of reading the tags, interactive mode and autonomous mode. In what (Misic J., 2009), call inter-active mode, the controlling application issues a command to the reader to read the transponder. The command always immediately returns with a list of tags in the reader's field of view. On the other hand in the case of auto-nomous mode, the reader constantly reads tags, and may initiate a conversation with a network listener when certain events arise. Both methods are equally useful, although it is easier and require less coding to work in interactive mode.

A reader operating in autonomous mode moves between several states such as waiting, working, evaluation and notification. Movement from one state to the next may be initiated by an expiration of a timer, a triggered event on the digital input lines, or changes to the Tag list. Autonomous mode has a feature by which the tag list delivered has time stamps indicating the instants at which the tags were detected. These can then be used to correlate the tag ID's with the corresponding sensor data.

Antenna sequence technique provides the readers to invariably support the use of multiple antennas and allow selecting which antennas, in the order specified in the antenna sequence. The reader cycles through static systems or multi static systems. Mono-static system readers have the ability to transmit and receive RF signals on the same antenna port. Multi static system readers on the other hand transmit and receive RF signals on separate antennas providing significantly better sensitivity to weak tag backscatter signals. These readers may allow fixed antenna pairing scheme or more flexible arbitrary combinations of transmit/receive antennas, giving better RF coverage over a larger area in the front of the reader with fewer antennas.

4. ANALYSIS AND RESULTS

Comments on GPS

GPS is very different from RFID. While it also uses radio waves to transmit data, it does so using, global positioning system of 24 satellites, as opposed to radar system. Radio waves sent out from this system of satellites transmit their time and orbital data to receivers down on Earth. Using the data from multiple satellites, receivers can then triangulate their position relative to the satellites, and thus on the Earth's surface. GPS, thus, is best suited for tracking geographic position not sag detection. Because of the sheer distance of the satellites, the signal is weaker and is easier to jam, or even just not get a signal.

Comments on RFID

There are two types of RFID tags: active tags, which contain a battery and are constantly transmitting data such as vital signs, passive tags, which require radar to create a signal in an otherwise battery less device. There is a potential of battery assisted passive tag in future, which may function as a hybrid of the two in that an external source will be required to activate the battery function.

Efficiency of RFID

More efficiency is found in RFID. For a tag to receive power from the radar, the following link is followed:

$$P_{RF} = p_1 P_{RF} + p_2 P_{RF} \tag{4.1}$$

Where P_{RF} is the available output power from the antenna and p_1 and p_2 are the probabilities in time domain that tag chip is in mode *1* and mode *2* operation. The R_{ri} is the impedance radiation of the antennae and R_a is the antennae resistance. Therefore the total power reflected to the tag can be expressed as follows:

$$P_{bs} = \frac{v_0^2}{8R_a}\left[p_1(1-|p_1|^2) + p_2(1-|p_2|^2) \right] \tag{4.2}$$

$$P_{bs} = \frac{1}{8}|i_1 - i_2|^2 R_{ri} \tag{4.3}$$

Where P_{bs} is that total power reflection to tag.

RFID transmission system is modeled from Friis transmission equation as follows:

$$\frac{P_r}{P_t} = G_t G_r \left(\frac{\lambda}{4\pi R} \right)^2 \tag{4.4}$$

P_r is the power input and P_t is the power output to the transmitting antennae.

$$P_r = P_t + G_t + G_r + 20\log_{10}\left(\frac{\lambda}{4\pi R} \right) \tag{4.5}$$

G_t and G_r are the antennae gains and obviously lambda λ is the wave length

$$P_r = P_t\left(\frac{\lambda}{4\pi}\right)^2\left|G_0^{1/2}\frac{1}{r_0}\exp(-jkr_0)+G_i^{1/2}\sum_{i=1}^{n}\Gamma(\alpha_i)\frac{1}{r_i}\exp(-jkr_i)\right|^2 \quad (4.6)$$

G_0 is the direct pathway antennae gain G_i propagating antennae gain $\Gamma(\alpha_i)$ is the reflection coefficient. Table 4.1 shows the summery of comparison between RFID and GPS. Figure 4.1, depicts a simulation result of radar tag power received due to pole reflection.

<table>
<tr><th colspan="3">RFID</th><th>GPS</th></tr>
<tr><td rowspan="4">TAG has</td><td>CPU</td><td>I/O</td><td rowspan="4">Its purpose is to define geographic position on and above the earth surface. It consists of three segments namely: user segment, control segment and space segment.</td></tr>
<tr><td>RAM</td><td>ROM</td></tr>
<tr><td>RADIO</td><td>Tx/Rx</td></tr>
<tr><td colspan="2">Energizer</td></tr>
<tr><td colspan="3">Up to 96bit transmission</td><td>Transmitting power is only 50 watts or less</td></tr>
<tr><td colspan="3">Radar transmit power of 1Watt</td><td>Very high orbit at 1 revolution in approximately 12hrs</td></tr>
<tr><td colspan="3">Radar receiver sensitivity -80dBm</td><td>24 satellites with 55 degrees</td></tr>
<tr><td colspan="3">Radar antenna gain 1dBi-omini directional</td><td>Prone to errors and needs a secondary GPS namely DGPS</td></tr>
<tr><td colspan="3">Tag power required 100 microwatt</td><td>Broadcasting position and information on two frequencies</td></tr>
<tr><td colspan="3">Tag modular efficiency -20dB</td><td>Signal weaker because of sheer distance</td></tr>
<tr><td colspan="3">Method used to talk to the tag is modulated, message format, commands and anti-collision</td><td>Less power efficiency</td></tr>
<tr><td colspan="3">Radio wave transmission of data</td><td>Radio wave transmission of data</td></tr>
</table>

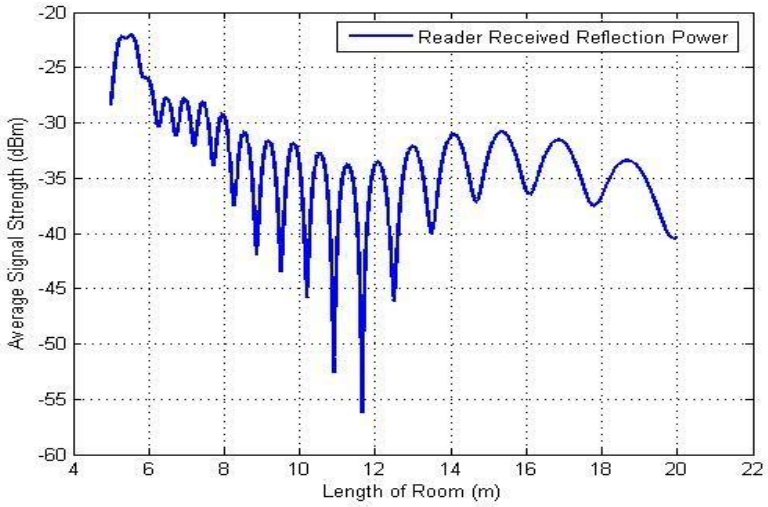

Figure 4.1: Radar received power

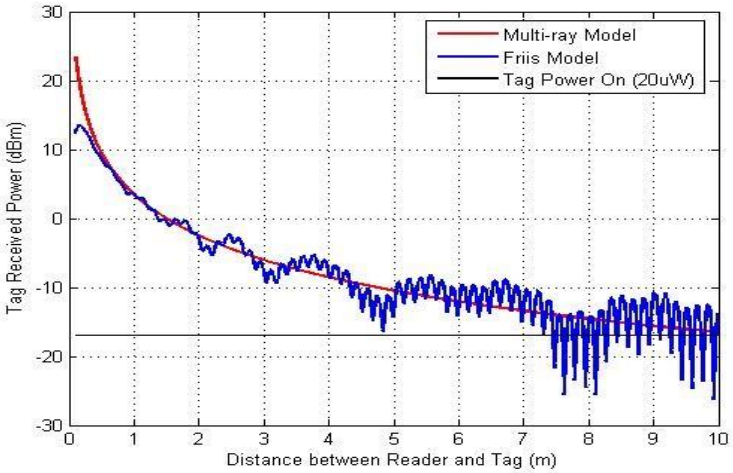

Figure 4.2: Tag received power

This concludes that the amount of signal power that the tag receives, after the command has

been send by the radar, become proportional to the wave-length, in that power tag is finally expressed as;

$$P_{i\_tag} = P_s \left(\frac{\lambda^2}{4\pi r} \right) .T\psi ri \tag{4.7}$$

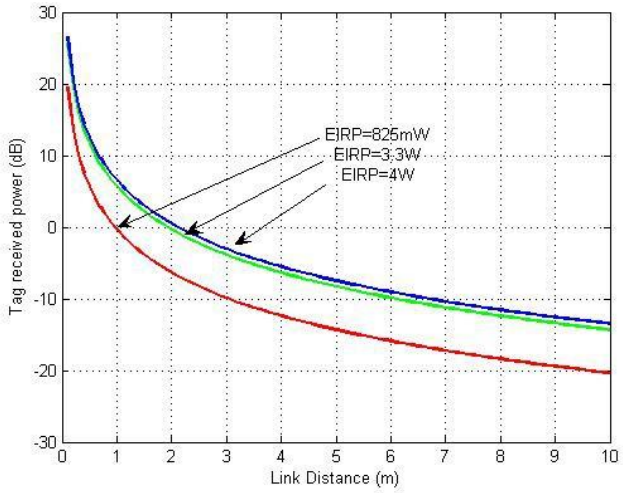

Figure 4.3: Radar to tag power transmission

The performance of patch antenna is then simulated for a number of fifty frequency points at most, to view the resonance and return loss.

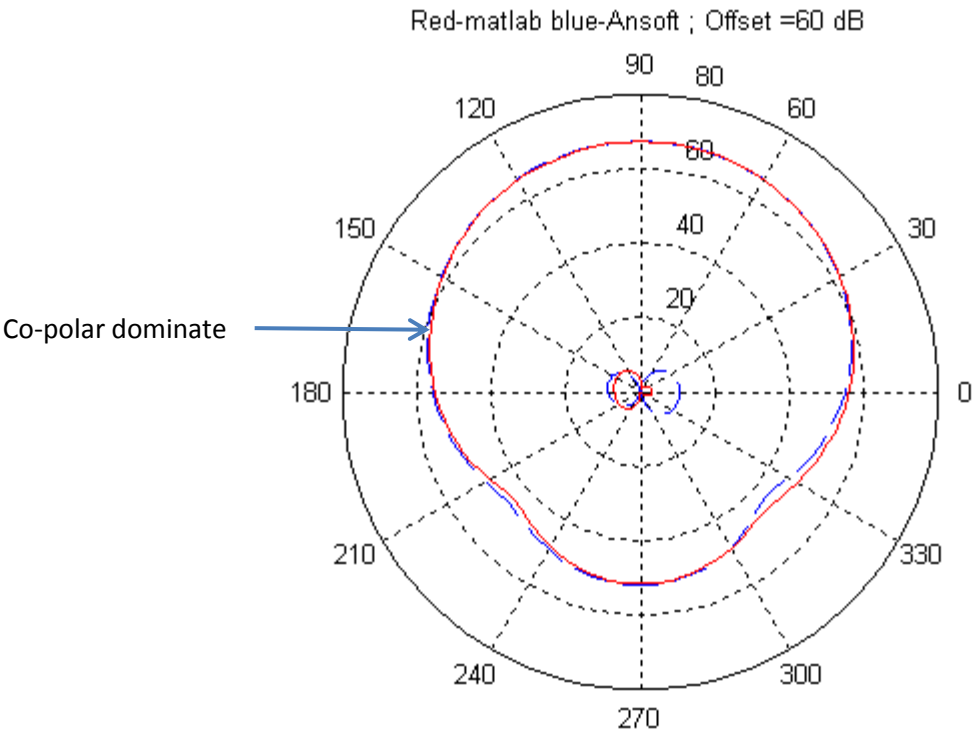

Figure 4.4: Front back ratio at 10dB

The front back ration is smaller at 10dB. The closer to resonance minimize the return loss. At figure 4.5 the current distribution is shown on a z-plane.

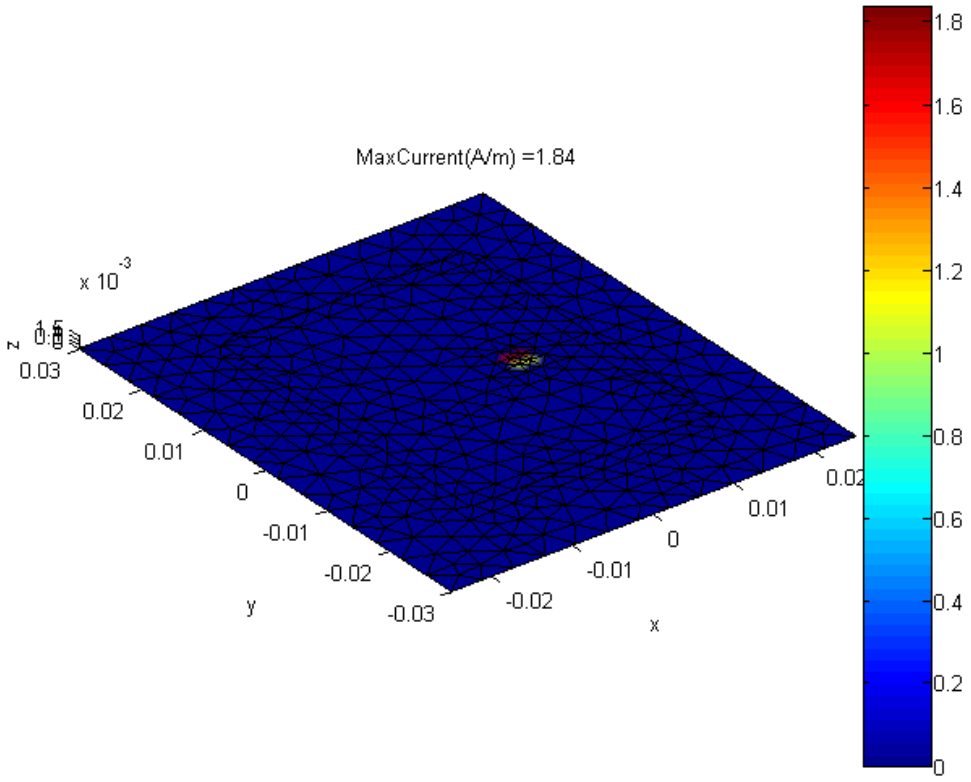

Figure 4.5: Current distribution on a z-plane

Although the distribution of current is visualized, it is possible for its value to be given zero at minimum, and either one or two because of the positive and negative root.

Figure 4.6, shows the relative range stability of the tag when using patch antenna.

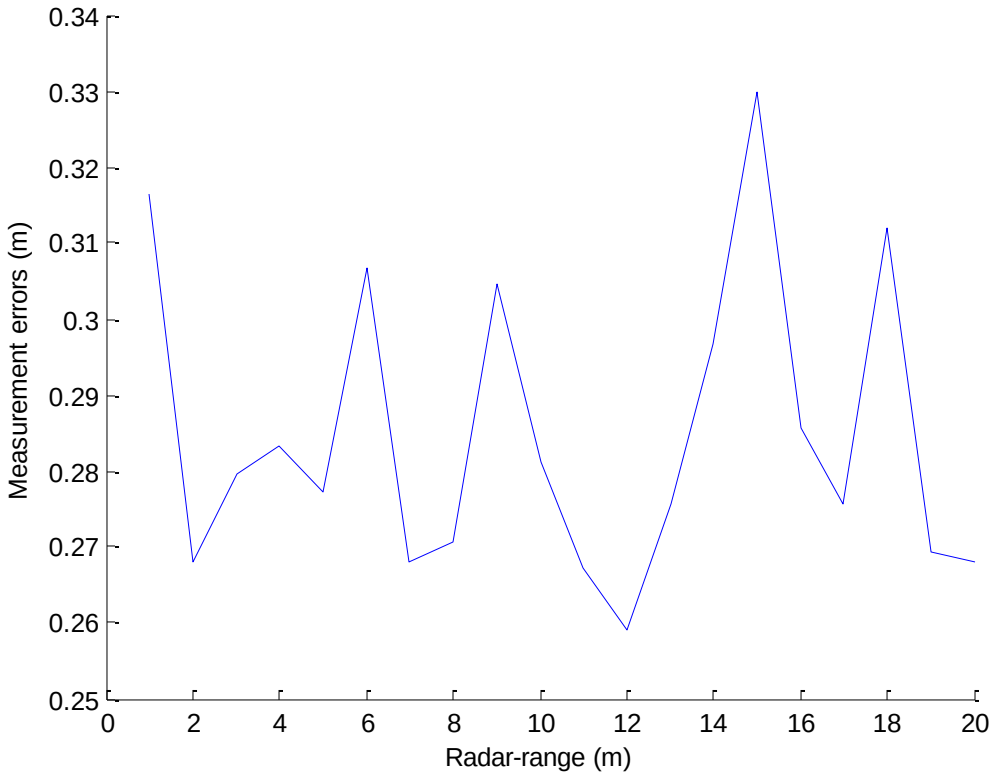

Figure 4.6: Relative range stability

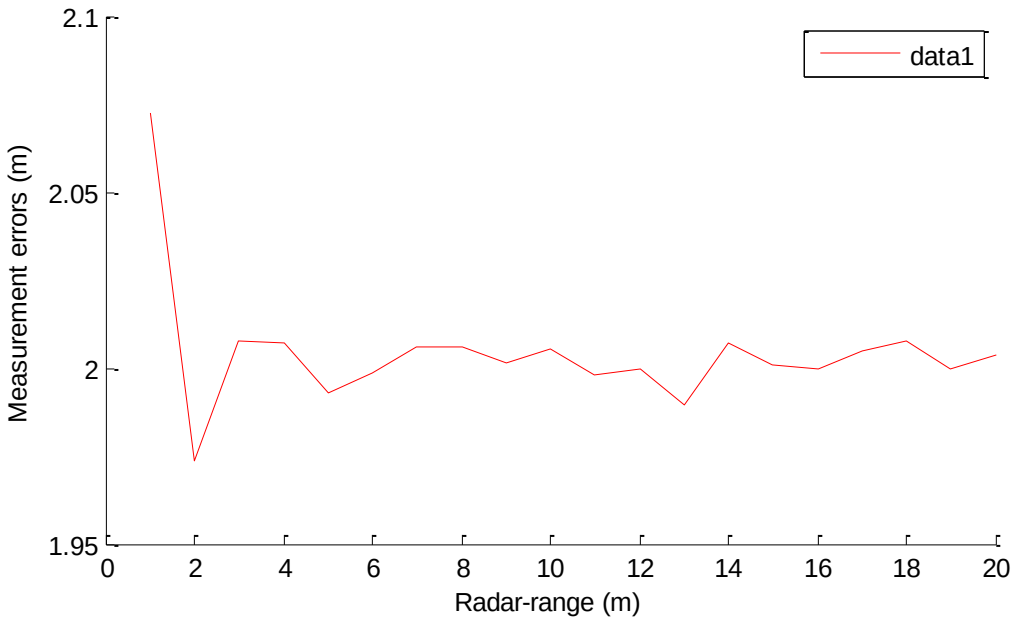

Figure 4.7: Relative range stability

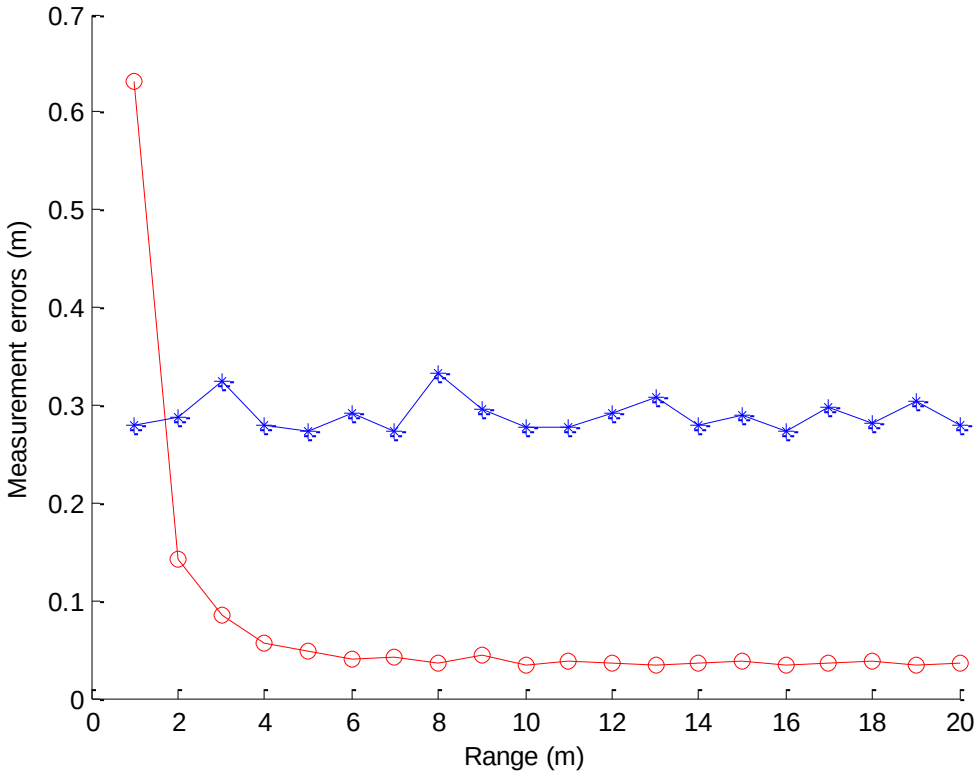

Figure 4.8: Detection errors

Due to the uncertainties of environment factors and the time spend by the tag to response the reader instructions; the measured ranges contain significant errors. Therefore the distance from the tag to ground calculated from the measured ranges has big errors. The blue stared curve denoted the detection error without using the proposed method, and the measurement errors of the proposed method are denoted as circle red curve. The performance is also seemed better at Figure 4.9., where the capacitance is of the line is smaller.

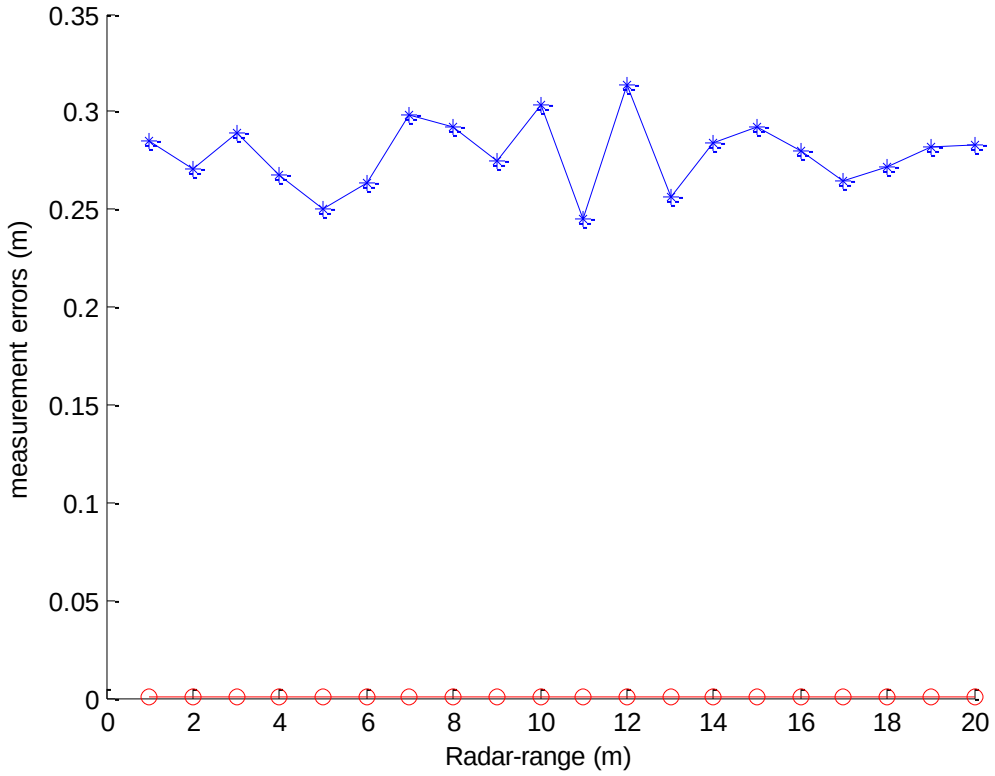

Figure 4.9: Detection errors

Assuming the voltage of the transmission line is varied on Figure 3.3 in chapter 3. The variation is done by injecting the pulse to the line from 0V to 8KV in simulation. The pulse shape was chosen because it incorporates three numbers that characterize any pulse.

Rise time (second)

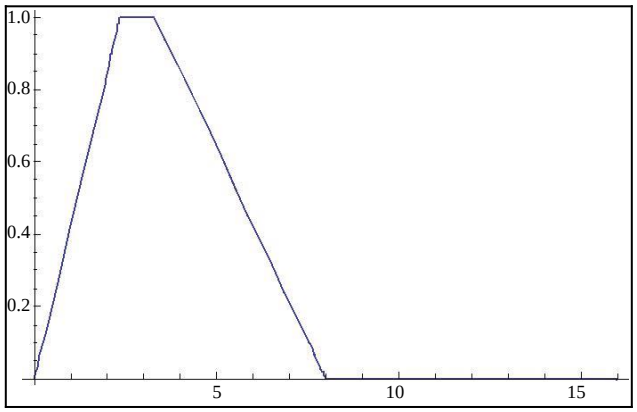

Voltage (Kv)

Figure 4.10: Rise time voltage pulse

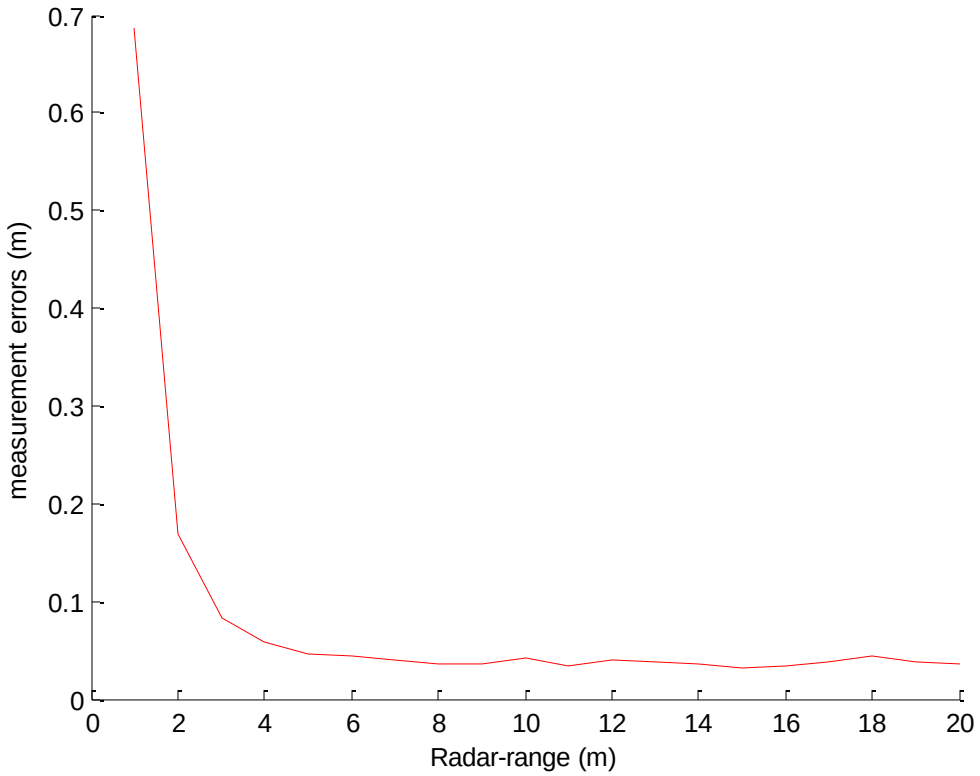

Figure 4.11: Radar detection errors

The transmission line response at 50 V signal, is of that of linear filter in nature whose total pulse length is at about 100 ns.

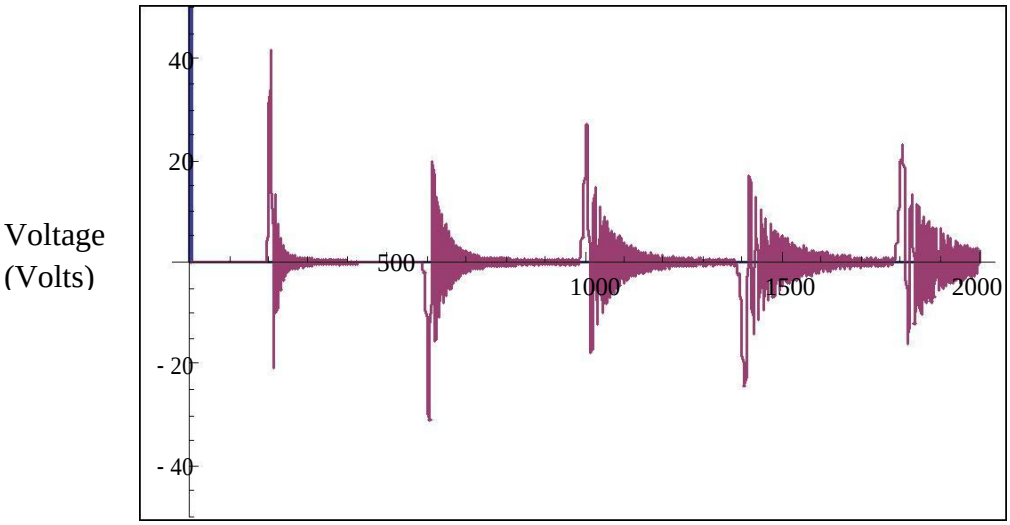

Figure 4.12: Transmission line response

When the pulse voltage is increased to 6KV, the response reveals almost the solid single outputs seen in Figure 4.10.

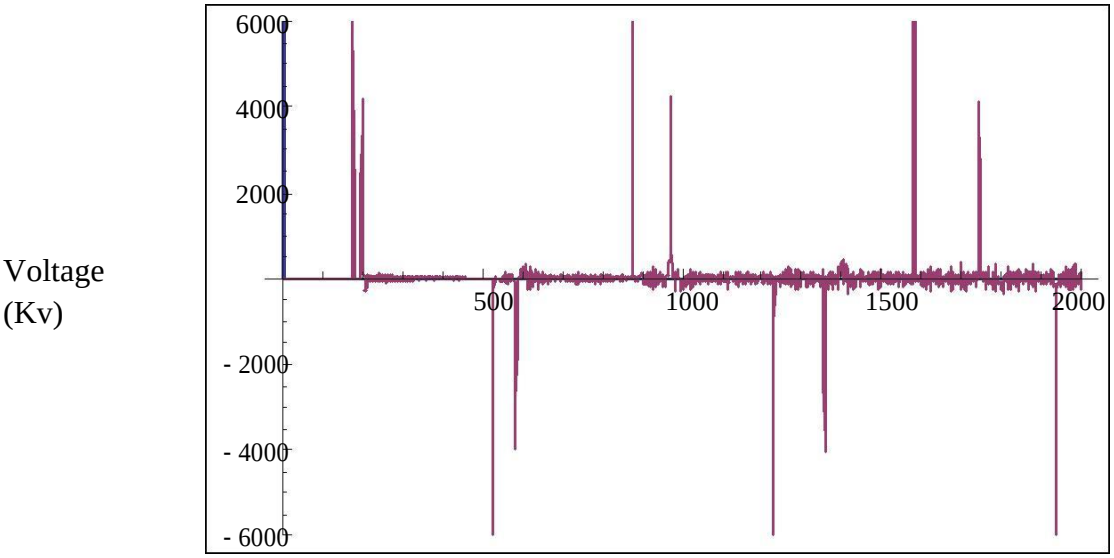

Figure 4.13: High Voltage injection response

As the same triangulation simulation is done superimposed with the line charge the pulse width period is now enlarged to 10millisecond and the injection voltage reduced to 50V.

Rise-time (seconds)

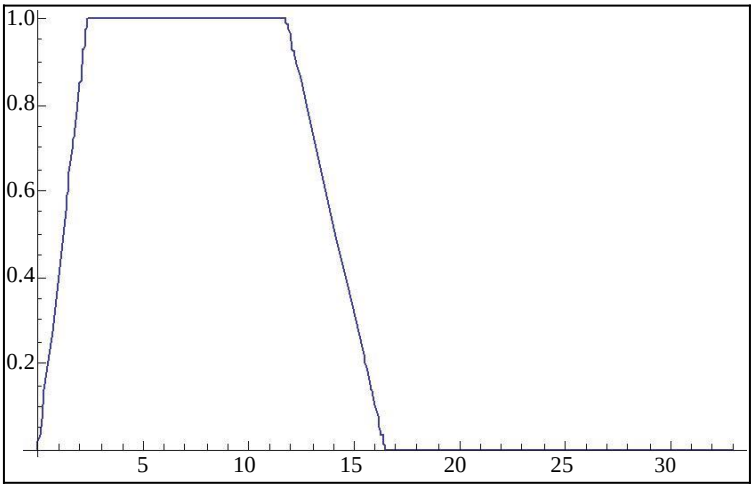

Voltage (V)

Figure 4.14: Increased pulse period

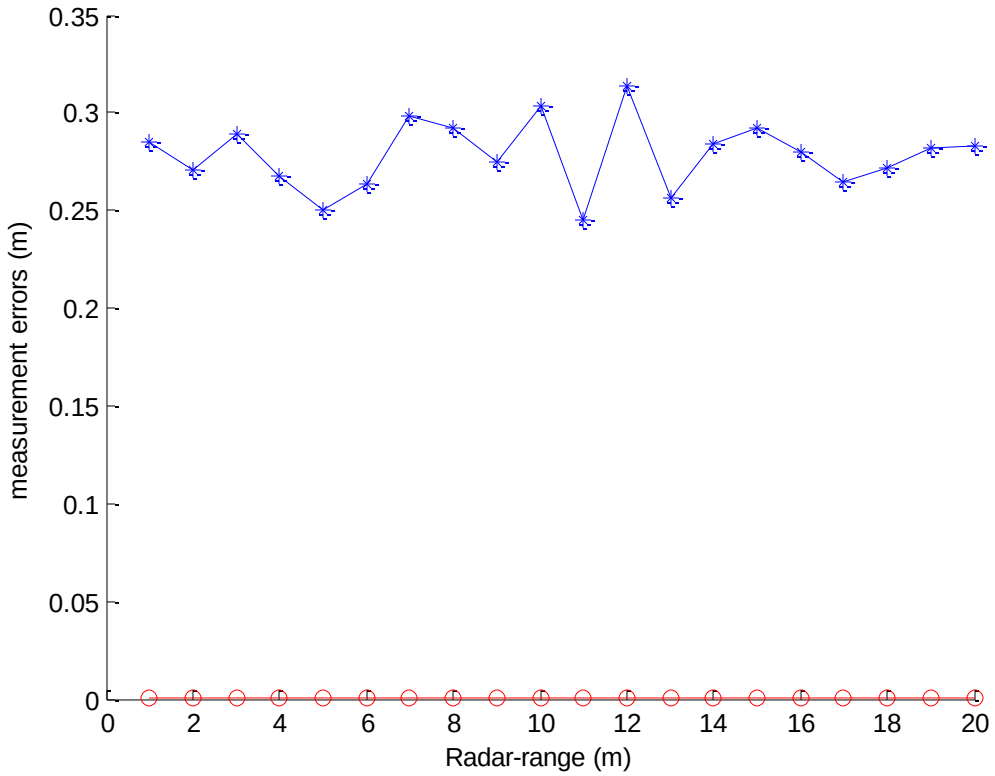

Figure 4.15: Better detection at low voltage

The voltage response is then seen in Figure 4.16, which is in linearity.

Voltage (V)

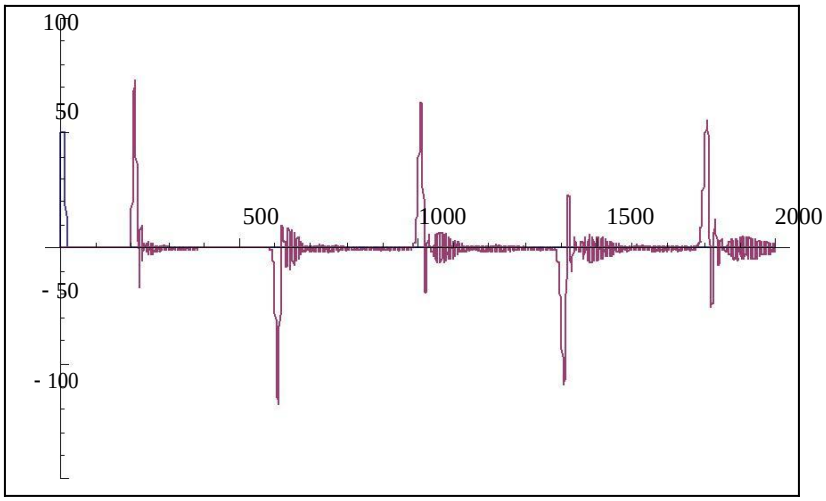

Period (Nano-seconds)

Figure 4.16: Voltage response at low injection

The rising of regions has been now clearly separated by the larger width of the period. Better performance is then recognized at low voltage.

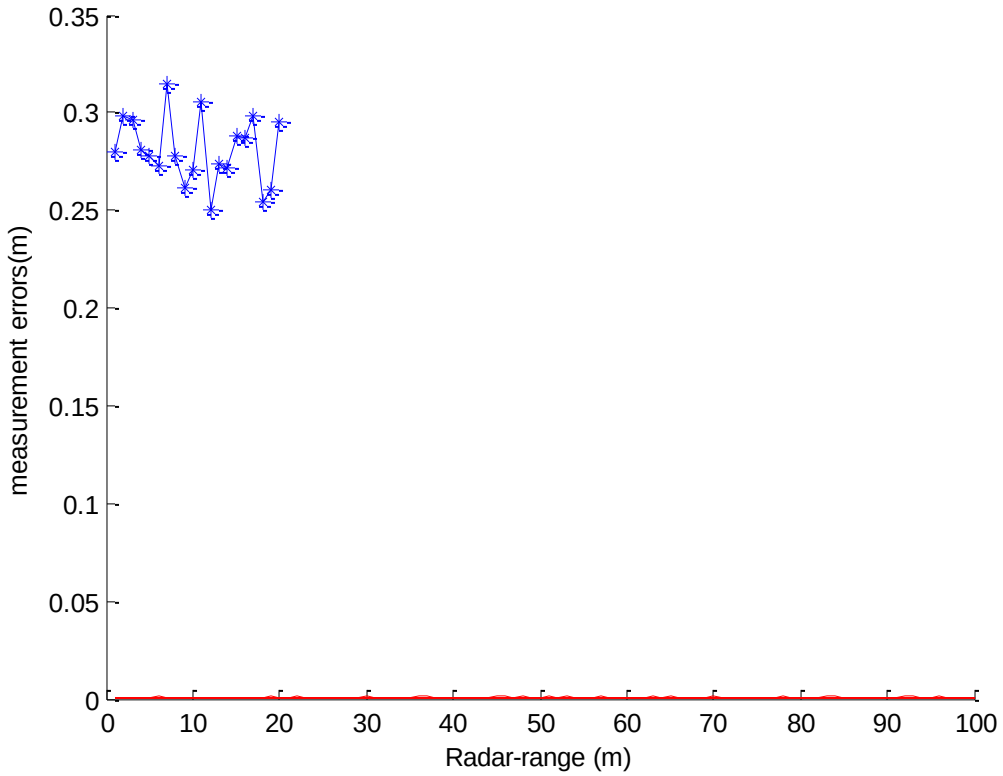

Figure 4.17: Detection errors

The position of the tag could be determined in three dimensions using three receiving patch antenna. High voltage spike could thwart the performance detection and therefore increase

errors. The line quantities such as capacitance, inductance and admittance strengthen the electric field and therefore play a major role in tag detection.

Detection Error correction attempt using Artificial Neural Network (ANN)

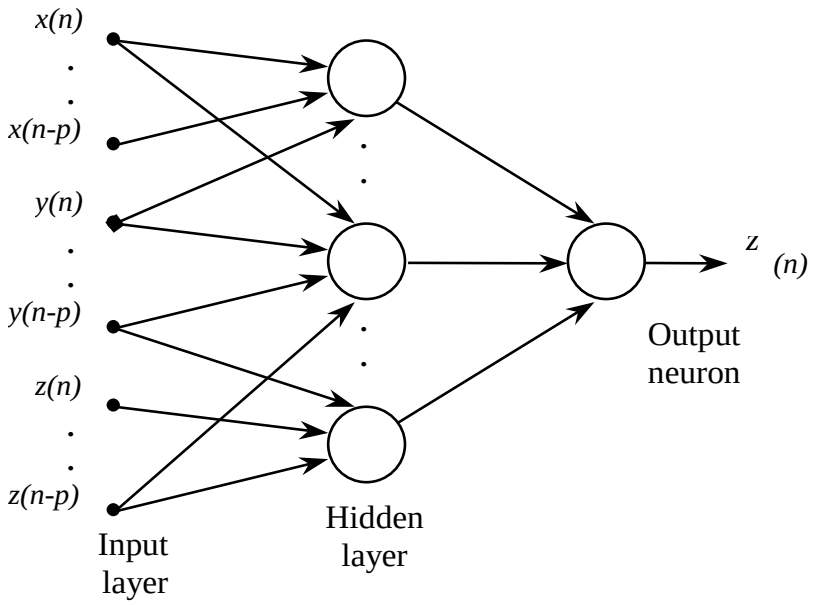

Figure 4.8: ANN error detection correction

The ANN estimator is applied using time lag feed forward network [63]. In this configuration, *p* previous readings of *x*, *y* and *z* are used to estimate *z*. Figure 4.18, depicts the RFID schematic of the network. A two-weighted layer network consisting of *h* neurons in the hidden layer and one output layer is used. The sigmoid function [63] is employed as the activation function of the hidden neurons but a linear function is applied for the output neurons. The optimum values

of p and h were determined by several trials in the training process. In this case good estimation result was attained for p = 9 previous data set and h = 4 neurons.

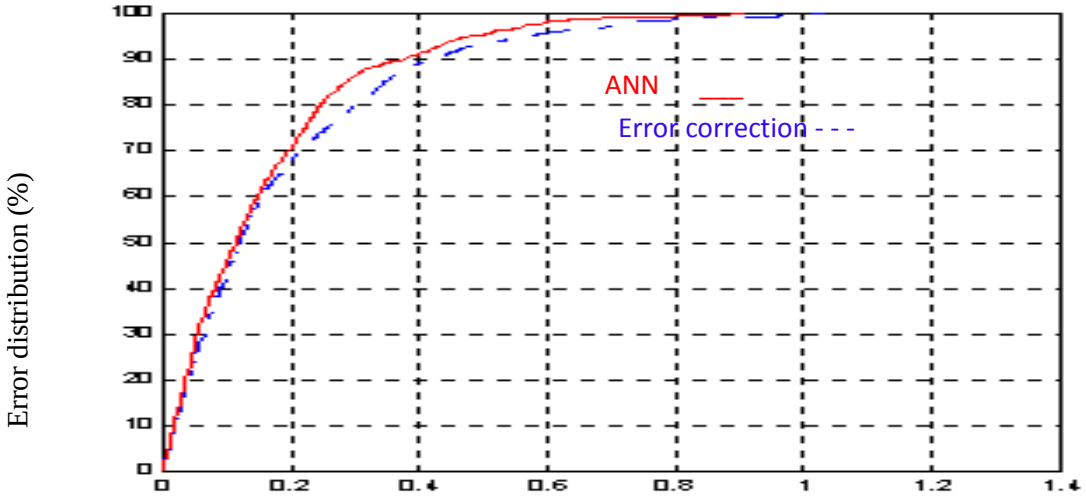

Strengths and weaknesses of RFID Sag detection system

Strengths of the method	• The concept is a more direct method in some ways as compared to GPS method. • Intermediate calculations or assumptions regarding ambient weather conditions, conductor temperature and tension measurements are not required. • Potentially accurate and cheaper cost • Capable of real time conductor sag detection • The accuracy of the proposed concept is achievable.
Weaknesses of the method	• Has not been tested directly on an energized physical High Voltage (HV) line. • Environmental uncertainties, lack of experience with the technique, and unstable performance in HV environment. • Influence to power reflection to tag due to environment need to be considered.

Table 4.2: Strengths and weakness of RFID

CHAPTER 5 DISCUSSION AND CONCLUSION

5.1 Discussion

In employing radio frequency identification for power transmission line conductor sag measurement different quantities of transmission line and external factors are taken in to consideration. On metal conductor, the tag sensitivity is better off seen from 8mm than that of a free space. This gives an additional range by lowering the power of the reader.

The reflection from the surface is not bigger in such that it requires much greater power for the tag that is close to the surface and at some instance at further distance they do not give sensitivity that are much better than that which we achieve in free space. The high water content body or flesh which is close to the tag, impacts the operation of the tag. It is observed that if the tag was wrapped, sensitivity approaching the free space would be recognized better.

It is seen that paper has a different dielectric constant from that of air meaning that at the interface between the paper and the air, energy will be lost as it will be reflected away. The energy would then travel through the paper to the tag. Capacitance of the transmission line as well as inductance is big internal factors since they cause non linearity and greater electric charge which affect tag performance.

5.2 Conclusion

The results obtained here support the hypothesis in that Radio Frequency Identification system has a potential of giving an accurate sag measurement in real time. The simulations validate that the positioning of the tag can be determined in 3D. Although there are some errors, high voltage varied to a low value to view error change and lastly a neural network was implemented to decrease the errors identified. With narrow bandwidth which allows RFID not to interfere with other communication systems, the angle of arrival measurement can virtually be used in conjunction with range from a single measuring location to determine sag. External and internal factors which have impact on the performance of the system such as Pole line obstruction or wall need to be carefully taken into consideration. Although transmission line and radio frequency identification theories are valid for designing, the system advances need to take place in future to improve the detection errors on the system.

Corona discharge effect in the transmission lines is a phenomenon in which ionization of the surrounding air of power conductors take place at voltages greater than critical break down voltage. When the potential between the power conductors o transmission lines high voltage lines goes further, increase in hissing noise is experienced which is followed by the violet glow and the production of ozone gas which finally brings about flash over and electrical break down. This phenomenon is complex and cannot be easily predicted. Future work will deal with this phenomenon.

Appendix A

List of publications obtained during the research

1. International conference in Electrical Engineering and Technology, (ICEET2013) 22-23 July 2013; Oslo, Norway ISSN 210 376X issued 79 page 1710. *Title "Radio Frequency Identification technology applied on high voltage transmission line for conductor-sag measurement"*

2. International journal of Engineering and Advanced technology (IJEAT) Peer reviewed ISO-9001:2008 ISSN 2249 – 8958 issue-1, volume-3, page 297-302 New Delhi, India. *Title "Real time Monitoring of High Voltage Power Transmission line: A review of a state-of-the-art" 25 October 2013*

Appendix B

3 D tag-radar positioning code in matlab

```
function [ x, y ] = two_tri(x1, x2, x3, y1, y2, y3, d1, d2, d3)
%2-D tri-function
%   Inputs: tags  1-3 (x,y) and Distances to Tag
%
% x_n1 = (d1^2 - d2^2)-(x1^2 - x2^2)-(y1^2 - y2^2)*2*(y3 - y1)
% x_n2 = 2*(y2 - y1)*(d1^2 - d3^2) - (x1^2 - x3^2) - (y1^2 - y3^2)
% x_d = 2*(x2 - x1)*2*(y3 - y1) - 2*(y2 - y1)*2*(x3-x1)
% x = (x_n1 - x_n2)/x_d
% y = 2;
%
x_n11 = (d1^2 - d2^2) - (x1^2 - x2^2) - (y1^2 - y2^2); x_n21 = (d1^2 - d3^2)
- (x1^2 - x3^2) - (y1^2 - y3^2); x_n12 = 2*(y2-y1);
x_n22 = 2*(y3-y1);

d11 = 2*(x2-x1); d21 = 2*(x3-x1); d12 = 2*(y2-y1); d22 = 2*(y3-y1);

x_n = [x_n11, x_n12; x_n21, x_n22]
d = [d11, d12; d21, d22]

x = x_n/d
x = det(x)
```

```
y_n11 = d11 y_n21 = d21 y_n12 = x_n11 y_n22 = x_n21

y_n = [y_n11, y_n12; y_n21, y_n22]
y = y_n/d
y = det(y)

end

Test2DD

%TAG 2-D Coordinates [x, y] Tag = [-2, 2; 2, 1; -1, -2];

%plot tag locations update 2015/07/01
scatter(getcolumn(tag(1:3,1:2),1),getcolumn(tag(1:3,1:2),2),
'MarkerEdgeColor', [1 0 0], 'MarkerFaceColor', [1 0 0]);figure(gcf)
%x = 0;0;0;
%y = 0;0;0;
%x = getcolumn(tag(1:3,1:2),1)
%y = getcolumn(tag(1:3,1:2),2)
%e = [1;1;1]
hold on
%errorbar(x,y, e, 'og', 'Marker', '+');
%axis([-5 5 -5 5]) %set axis for 2-D graphs set(gca, 'XTick', -5:1:5);
set(gca, 'YTick', -5:1:5);
grid on;

%distances to radar from tag(i)
%Distance = [2.82842715;2.236067977;2.236067977]; %(0, 0) radar
Distance = [3.16227766; 1; 3.60555127]; %(1, 1) radar

%error circles
circle([-2, 2],Distance(1), 1000,'-');figure(gcf)
circle([2, 1],Distance(2),1000, '-');figure(gcf)
circle([-1, -2],Distance(3), 1000, '-');figure(gcf)
pause;

x = 0;
y = 0;

%Tag(row, col)
[x, y] = two_tri(tag(1,1), tag(2, 1), tag(3,1), tag(1, 2), tag(2, 2), tag(3,
2), Distance(1), Distance(2), Distance(3));

%plot radar
scatter(x,y, 'MarkerEdgeColor', [0 0 0], 'MarkerFaceColor', [0 0
0]);figure(gcf)
circle([x, y],.5,1000,'-');figure(gcf)
pause;
clf;

3_three_tri.mou
function [x, y, z ] = three_tri( x1, y1, z1, d1, x2, y2, z2, d2, x3, y3, z3,
d3, x4, y4, z4, d4 )
```

```
%3-D tri_tri. 4 anchor nodes
%   x1 = x coordinate of tag 1
%   y1 = y coordinate of tag 1
%   z1 = z coordinate of tag 1
%   d1 = distance from radar to tag 1

%x_numerator elements
x_n11   =   (d1^2-d2^2) - (x1^2-x2^2)   - (y1^2-y2^2)   - (z1^2-z2^2);
%sigma
x_n21   =   (d1^2-d3^2) - (x1^2-x3^2)   - (y1^2-y3^2)   - (z1^2-z3^2);  %beta
x_n31   =   (d1^2-d4^2) - (x1^2-x4^2)   - (y1^2-y4^2)   - (z1^2-z4^2);  %phi
x_n12   =   2*(y2-y1);
x_n22   =   2*(y3-y1);
x_n32   =   2*(y4-y1);
x_n13   =   2*(z2-z1);
x_n23   =   2*(z3-z1);
x_n33   =   2*(z4-z1);

%all the individual
d11 =   2*(x2-x1);
d21 =   2*(x3-x1);
d31 =   2*(x4-x1);
d12 =   2*(y2-y1);
d22 =   2*(y3-y1);
d32 =   2*(y4-y1);
d13 =   2*(z2-z1);
d23 =   2*(z3-z1);
d33 =   2*(z4-z1);

%bringing M together into [3, 3] matrix
d = [d11, d12, d13; d21, d22, d23; d31, d32, d33];

%bringing numerator together for x
x_n = [x_n11, x_n12, x_n13; x_n21, x_n22, x_n23; x_n31, x_n32, x_n33];

%finding x by dividing matrix operation and then determinant x = x_n / d;
x = det(x);

%individual y elements y_n11 = 2*(x2-x1); y_n21 = 2*(x3-x1); y_n31 = 2*(x4-
x1); y_n12 = x_n11; %sigma y_n22 = x_n21; %beta y_n32 = x_n31; %phi y_n13 =
2*(z2-z1); y_n23 = 2*(z3-z1); y_n33 = 2*(z4-z1);

%bringing numerator together for y
y_n = [y_n11, y_n12, y_n13; y_n21, y_n22, y_n23; y_n31, y_n32, y_n33];

%finding y by dividing matrix operation and then determinant y = y_n / d;
y = det(y);

%individual z elements z_n11 = 2*(x2-x1); z_n21 = 2*(x3-x1); z_n31 = 2*(x4-
x1); z_n12 = 2*(y2-y1); z_n22 = 2*(y3-y1); z_n32 = 2*(y4-y1); z_n13 = x_n11;
%sigma z_n23 = x_n21; %beta z_n33 = x_n31; %phi

%bringing z numerator together
z_n = [z_n11, z_n12, z_n13; z_n21, z_n22, z_n23; z_n31, z_n32, z_n33];
```

```
%finding z by dividing matrix operation and then determinant z = z_n / d;
z = det(z);

end
```

Test3DD.mou

```
%prevents rounding off when fractions is long

%TAG 3-D Coordinates [x, y, z]
tag = [-2, 2, 2; 2, 1, -2; -1, -2, 2; 3, 3, 3];

%plot tag locations
scatter3(getcolumn(tag(1:4,1:3),1),getcolumn(tag(1:4,1:3),2),
getcolumn(tag(1:4,1:3),3), 'MarkerEdgeColor', [1 0 0], 'MarkerFaceColor', [1
0
0]);figure
%x = 0;0;0;
%y = 0;0;0;
%x = getcolumn(tag(1:3,1:2),1)
%y = getcolumn(tag(1:3,1:2),2)
%e = [1;1;1]
hold on
%errorbar(x,y, e, 'og', 'Marker', '+');
axis([-3 3 -3 3 -3 3]) %set axis for 2-D graphs set(gca, 'XTick', -3:1:3);
set(gca, 'YTick', -3:1:3); set(gca, 'ZTick', -3:1:3); grid on;

%distances to radar from tag(i)
%Distance = [2.82842715;2.236067977;2.236067977]; %(0, 0) radar
Distance = [3.464101615; 3; 3; 5.196152423]; %(0, 0 , 0) radar

%initialize variables x = 0;
y = 0;
z = 0;

[x, y, z] = three_tri(tag(1, 1), tag(1, 2), tag(1, 3), Distance(1), tag(2,
1), tag(2, 2), tag(2, 3), Distance(2), tag(3, 1), tag(3, 2), tag(3, 3),
Distance(3), tag(4, 1), tag(4, 2), tag(4, 3), Distance(4));

scatter3(x, y, z, 'MarkerEdgeColor', [1 1 0], 'MarkerFaceColor', [1 1
0]);figure(gcf)
```

Vuka.mou

```
%prevents format of decimals long

%super-node lower level nodes
%3-D coordinates [x, y, z]
Low tag = [-2, 2, 2; 1, 1, 2; -3, 0 , 2]; %all z-values must be the same

%x, y values must be same as lowtag values.
%Z values must be > lowtag values and equal to each other
hightag = [-2, 2, 4; 1, 1, 4; -3, 0, 4];
```

```
%radar x y z for testing purposes radar = [4; 5; 1];

low_d1 = sqrt((lowtag(1, 1)- radar(1))^2 + (lowtag(1, 2)- radar(2))^2 +
(lowtag(1, 3) - radar(3))^2);
low_d2 = sqrt((lowtag(2, 1)- tag(1))^2 + (lowtag(2, 2)- radar(2))^2 +
(lowtag(2, 3)- radar(3))^2);
low_d3 = sqrt((lowtag(3, 1)- radar(1))^2 + (lowtag(3, 2)- radar(2))^2 +
(lowtag(3, 3)- radar(3))^2);

%find distances for radar (0, 0, 0)
high_d1 = sqrt((hightag(1,1)- radar(1))^2 + (hightag(1, 2)- radar(2))^2 +
(hightag(1, 3)- radar(3))^2);
high_d2 = sqrt((hightag(2,1)- radar(1))^2 + (hightag(2, 2)- radar(2))^2 +
(hightag(2, 3)- radar(3))^2); STOPPED 07/07/15
high_d3 = sqrt((hightag(3,1)- radar(1))^2 + (hightag(3, 2)- radar(2))^2 +
(hightag(3, 3)- tag(3))^2);

lowDistances = [low_d1; low_d2; low_d3];
highDistances = [high_d1; high_d2; high_d3];

%height of radar
z = callHeight(lowtag, hightag, lowDistances, highDistances)
%array for 2-D trilateration distances = [0; 0; 0];
distances = findDistance(lowtag, hightag, lowDistances, highDistances);

[x, y] = two_tri(lowtag(1, 1), lowtag(2, 1), lowtag(3, 1), lowtag(1, 2),
lowtag(2, 2), lowtag(3, 2), distances(1), distances(2), distances(3))
```

```
Vuka_height.mou
function [ radarHeight ] = callHeight(lowtag, hightag, lowDistances,
highDistances)
%VukaHEIGHT Find height of tag
%   Using supernode distances, use trig to determine height of tag

heightDifference = hightag(1, 3) - lowtag(1, 3);

height = [0; 0; 0];

height(i) = hightag(i, 3) - ((highDistances(i)^2 - lowDistances(i)^2 +
heightDifference^2)/(2*heightDifference));
end

%set x = 0 for below x = 0;
%find average height found by the 3 super-nodes for more accurate results for
i = 1:3
x = x + height(i);
end
```

List of references

1. Glorver, B. & Bhatt, H. (2003) RFID Essentials. Research trends in radio frequency identification technology, 7(1), 22-25.
2. A. Cataliotti et al., "Characterization of current transformers in the presence of harmonic distortion, Presented at the*" IEEE Int. Instrum. Meas. Technol. Conf., Victoria, Vancouver Island, Canada, 2008.*
3. L. Fish, "Low Cost Sensors for Real Time Monitoring of Overhead Transmission Lines". Washington, DC: *Underground Systems Inc., 2006.*
4. February 5, 2010, Tension Monitor [online], available online http*://www.cat-1.com)*
5. G. Thomas Heydt, fellow, IEEE, "Application of the Global Positioning System to the Measurement of overhead Power Transmission Conductor Sag," *IEEE Trans. Power Del., Vol. 17 NO. 1, pp 273-278, January 2002.*
6. A. Edelstein, "Advances in magnetometry," *J.Phys., Cond. Matter,* vol. 19, pp. 165-217, Apr. 2007.
7. R.G. Olsen and K.S. Edward, "A new method for real-time monitoring of high-voltage transmission-line conductor sag," IEEE Trans, Power Del., vol.17 no.4 pp. 1142-1152, Oct. 2002.
8. C Mensah-Bonsu, "Novel application of Magnetoresisteve Sensors for High-Voltage Transmission-Line Monitoring," IEEE on Magnetics, Vol. 47 NO. 10 October 2011.
9. G. Ramon, IEEE Task Force Chairman, "Dynamic thermal line rating summary and status of the state-of-the-art technology," *IEEE Trans. Power Delivery,* vol. PWRD-2, pp. 851-856, July 1987.

10. S.W. Rienstra, “Nonlinear free vibration of coupled spans of overhead transmission lines,” in *proc. 3rd Eur. Conf. Math. Ind.,* 1988 pp 133-134.

11. R. G. Olsen and K.S. Edwards, “A new method for real-time monitoring of high voltage transmission line conductor sag,” *IEEE Trans. Power Del., vol.17, no. 4*pp 1142 – 1152, Oct. 2002.

12. Wernich de Villiers, and Arthur Burger, “Real-time sag monitoring system for high voltage transmission lines based on power-line carrier signal behavious” IEEE Trans. On power del., Vol.23, NO.1, January 2008.

13. Xignlong Zhu, and JipingShou, “An Autonomous Obstacles Negotiating Inspection Robot for Extra-High Voltage Power Transmission lines”.

14. Hectro Beltran San Sequndo, and Vicente Fuster, “Automated Inspection of Electric Transmission line: The power supply system”

15. Graham Hall “maxwell’s electromagnetic theory and special relativity” *Phil. Trans. R. Soc. A 2008, published 28 May 2008.*

16. Y.H Gu, and S Berlinjn, “Practical applications of automatic image analysis for overhead lines” 22nd Int. Conf. on Electricity distribution, Stockholm, Norway 10-13 June 2013.

17. A Martin and S Tosunoglu, “image processing technique for machine vision” univ. of florida.

18. MJ Tunstal et al., “State of the art of conductor galloping, 2002”

19. T.S Hlalele & S Du “Application of a Radio Frequency Identification Technology on High voltage Transmission Line for conductor sag measurement” ICEET2013 Conf. Proceedings, Norway 22-23 July 2013.

20. IEEE Std 1159-2009 IEEE Recommended Practice for Monitoring Electric Power Quality

21. DA Douglass & Ridley Trash “Sag and Tension of conductor” 2013

22. R.G. Olsen and K.S. Edwards, “A new method for real-time monitoring of high voltage transmission line conductor sag,” IEEE Trans. Power Del., vol.17, no. 4 pp 1142 – 1152, Oct. 2002.
23. Kern. C (1999), “ RFID technology – recent development and future requirements”, proceedings of the European Conference on Circuit Theory and Design ECCTD99, Stresa, vol.1 pp. 25-81, available at www.x.ident.com/pdf/develpment rfid.pdf.
24. 2006 MIT, American institute of Aeronautics’ and Astronautics Scientists, MA 02139 USA white paper IEEE 2006.
25. Information Technology Association of America (ITAA), “Radio Frequency Identification: RFID coming of Age,” White Paper, information Technology Association of America, Arlington, VA, June 2004. Available online: http:/www.itaa.org/rfid/docs/rfid.pdf.
26. SCIS 2007. The 2007 Symposium on Cryptography and information security sasebo, Japan, Jan 23 – 26, 2007 (The Electronics, information and communication Engineers).
27. K. Findenzeller, RFID Handbook: Fundamentals and Applications in Contac less smart cards and identification, New York: John Wiley and Sons, 2003.
28. S. M. Amin and B.F. Wollenberg, “Toward a smart grid: Power delivery for the 21st century,” *IEEE Power Energy Mag*., vol. 3 no. 5, pp.34-41, Sep. 2002
29. A Polycarpou, “Power Quality and Voltage Sag Indices in Electrical Power systems” Frederick University Cyprus, 2005 pp140-155.
30. M Bouc, D Simpiont and I Stojmenovic, “RFID Systems research trends and challenges” 2010 John Wiley & Sons Ltd., pp 57-90

31. Charles Mutigwe&FarhadAghdasi, “Research Trends in RFID Technology”, Presented at the *Central University of Technology, Free State. Annual Engineering seminar, Bloemfontein, 2008.*
32. Marrocco, G. (2008) “The art of UHF RFID antenna design: impedance-matching and size-reduction techniques”, *IEEE Antennas and Propagation Magazine,* 50(1): 66-79.
33. Bridgelall, R. (1999) UHF Tags – the answer to the ratail supply chanin’sprayres? *RF Innovations Magazine August.*
34. Bridgelall, R (2002) Bluetooth/802.11 protocol adaptation for RFID tags, *Proceedings of* the *4th European Wireless Conference, Feb. 28.*
35. Mandal. S and Sarpeshkar, R. (2007) Low-power CMOS rectifier design for RFID applications, *IEEE Transactions on Circuits and Sstems,* 54(6): 1177-1188
36. AA Smith,Jr, (1998) Radio Frequency Principles and Applications. New York: IEEE Press
37. P.R Gray, P.J Hurst, S.H Lewis, and R.G Meyer, (2001) *Analysis and Design of Analog Integrated Circuits*, 4thedn. New York: John Wiley & Sons, Ltd, pp. 127 – 128.
38. J. Misic , 2009 Recommended Wireless Network standard:*IEEE 802.11b and IEEE 802.15.4.*
39. B.Skalar, (1988*) Digital Communications Fundamentals and Applications’*. New jersey: Prentice Hall
40. EPC global Inc. (2005) *Radio Frequency Identification,* protocols Class-1 Generation-2 UHF RFID
41. U. Karthaus and M. Fischer (2003) “fully integrated passive UHF RFID transponder IC with 16.7-micro-Watt”.
42. Admirat, P., M. Maccagnan, and B. De Goncourt, 1988 ‘Influence of Joule effect and of climatic conditions on liquid water content of snow accreted on conductors’ *Proc. Of the 4th International Workshop on Atmospheric Icing of Structures, Paris.*

43. Chadha, J 1974b. ‘A dynamic Model Investigation of Conductor Galloping’ IEEE Winter power Meeting. Paper 74 59-2

44. Anjo, K., S. Yamasaki, Y. Matsubayshi, Y. Nakayama, A. Otsuki, and T. Fujimura. 1974. An Experimental Study of Bundle Galloping on the kasatory Yama Test lin for Bulk power Transmission. CIGRE report 22-04. Paris.

45. Bleviens, R.D 1990. ‘Flow Induced Vibration. ‘Van Nostrand Reinhold. New York. Second Edition.

46. Fujii,Y.,T.KoyamaandT.Sawamoto.1997.“Counter measures against Conductor Galloping.”Paper11.Colloquium on Environmental Impact of OHL inJapan.CIGRESC22.Sendai Meeting.

47. Gartshore,I.S. 1973. “*The effects of free stream turbulence on the drag of rectangular two-dimensional prisms*. “Boundary Layer Wind Tunnel Laboratory 4-73, University of Western Ontario.

48. Gurung, C.B., H.YamaguchiandT.Yukino.2002.“*Identification of large amplitude wind-induced vibration of ice- accreted transmission lines base on field observed data”* Engineering Structures,24,pp. 179-188.

49. Gurung, C.B., H.Yamaguchi, andT.Yukino.2003. “Identification and Characterization of Galloping of Tauranga Test Line Based on Multi-channel Modal Analysis of Field Data. *Journal of Wind Engineering & Industrial Aerodynamics*. Vol. 91, Issue7.June. Pp. 903-924.

50. Halsan, K.A., D.G. Havard, S. M. Fikke, andA. Gerezgiher. 1998. “Galloping Studies at Statnett Using Remote Monitoring.”CIGRESC22,WG11meeting.Graz, Austria. Paper No.22-98.

51. Harvard, D.G.1978. “Status of Conductor Galloping Research at Ontario Hydro. “Second

Canadian Workshop on Wind Engineering. IREQ Varennes, Quebec. September 28-29.

52. Harvard, D.G. and J.C. Pohlman.1979. "Field Testing of Detuning Pendulums for Controlling Galloping of Single and Bundle Conductors." Paper A79499-5.IEEESymposium on Mechanical Oscillations of Overhead Transmission Lines. Vancouver, Canada. July.
53. Harvard, D.G.1979a. "Detuning for Controlling Galloping of Single Conductor Transmission Lines."PaperA79500-0. IEEE Symposium on Mechanical Oscillations of Overhead Transmission Lines. Vancouver, Canada July.
54. Havard,D.G.1979b."DetuningPendulumsforControllingGallopingofBundleConductorTransmissionLines."Paper79 501-8. IEEE Symposium on Mechanical Oscillations of Overhead Transmission Lines. Vancouver, Canada. July.
55. Harvard, D.G.1979c.Galloping *Control by Detuning*. EPRI Research ProgramRP-1095.Progress Report No.2.Ontario
56. Havard,D.G.andJ C. Pohlman. 1981. "The Economics of Galloping Control." CEA International Symposium on overhead conductor dynamics. Toronto
57. Harvard, D.G. and J.C.Pohlman.1984."FiveYears'Field Trials of Detuning Pendulums for Galloping Control." *IEEE Transactions on Power Apparatus and Systems*. Vol. PAS-103,No 2.pp.318-327.February.
58. Havard,D.G. and C.J.Pon.1990. "Use of Detuning Pendulums for Control of Galloping of Single Conductor and Two- and Four-Conductor Bundle Lines." Fifth International Workshop on Atmospheric Icing of Structures. Tokyo.
59. Harvard,D.G.1996."FifteenYears Field Trials of Galloping Controls for Overhead Power Lines."IWAIS'95.7th international workshop on atmospheric Icing of structures. Chicoutimi, Canada. June 3-6

60. Harvard, D.G.1997."Analysis of Field Data on Galloping of Single and Bundle Conductors with and without Control Devices." Paper16, International Seminar on **C**able Dynamics. Tokyo. October 1997.

61. Hillier,R. and R.J.Cherry. 1981. "The effect of stream turbulence on separation bubbles. *"Journal of Wind Engineering and Industrial Aerodynamics*, v. 8,pp. 49-58.

62. Hoerner,S.F. 1965."Fluid dynamic drag," published by the author, New York, pp. 415.

63. M. A. El-Sharkawi, D. Niebur, 1996 "A Tutorial Course on Artificial Neural Networks with Applications to Power systems", IEEE Power Engineering Society, IEEE Catalogue Number: TP 112-0, New York.